UNIVERSITAT POLITÈCNICA DE VALÈNCIA

DEPARTAMENTO DE INGENIERÍA HIDRÁULICA Y MEDIO AMBIENTE

PROGRAMA DE DOCTORADO DE INGENIERÍA DEL AGUA Y MEDIOAMBIENTAL

PHD THESIS

COMPARISON OF PARSIMONIOUS DYNAMIC VEGETATION MODELLING APPROACHES FOR SEMIARID CLIMATES

BY

MARTA PASQUATO

SUPERVISORS

DR. FÉLIX FRANCÉS GARCÍA

DR. CHIARA MEDICI

VALENCIA, NOVEMBER 2013

Acknowledgements

The research leading to this thesis was conducted in the Institute for Water and Environmental Engineering at the Universitat Politècnica de València, in collaboration with the Geography Department at the University of Cambridge. It has received funding from the Spanish Ministry of Economy and Competitiveness through the research projects FLOOD-MED (ref. CGL2008-06474-C02-02), SCARCE-CONSOLIDER (ref. CSD2009-00065) and ECO-TETIS (ref. CGL2011-28776-C02-01).

I am very grateful to Prof. Dr. Félix Francés García for his support, guidance and for giving me the opportunity to work in this interesting field.

I owe my sincere gratitude to Dr. Chiara Medici for countless fruitful discussions, for her time and support in decision-making and for being a true friend.

I wish to thank Dr. Andrew D. Friend for his advice and expertise, which helped considerably improving this thesis quality.

Many thanks to Alicia, Giamba, Camilo, Ismael, Mario, Jesús, Sergio and to all and each fellow PhD-student at the Research Group of Hydrological and Environmental Modelling (GIMHA), for all the help during these years, and for the moments and coffee breaks shared.

My gratitude goes to my mother Bruna, my father Silvio, my sister Ester and my brother Flavio, for supporting me and helping me becoming who I am.

Thanks also to my in-laws, for being proud of me and always sharing my joys.

Finally, I want to express my deep gratitude to my husband Davide, for being so attentive to me, for helping and encouraging me whenever needed. It would have been so much harder without your support. Thank you!

Table of contents

Abstract

A large portion of Earth's terrestrial surface is subject to arid climatic water stress. As in these regions the hydrological cycle and the vegetation dynamics are tightly interconnected, a coupled modeling of these two systems is needed to fully reproduce the ecosystems' behavior over time and to predict possible future responses to climate change.

In this thesis, the performance of three parsimonious dynamic vegetation models, suitable for inclusion in an operational ecohydrological model, are tested in a semi-arid Aleppo pine forest area in the south-east of Spain. The first model considered, HORAS (Quevedo & Francés, 2008), simulates growth as a function of plant transpiration (T), evaluating environmental restraints through the transpiration-reference evapotranspiration ratio. The state variable related to vegetation is R, relative foliar biomass, which is equivalent to FAO crop coefficient (Allen *et al.*, 1998), but not fixed in time. The HORAS model was then abandoned because of its unsatisfactory results, probably due to a poor simulation of evaporation and transpiration processes. As for the other two models, WUE-model and LUE-model, the state variable is the leaf biomass (B_l, kg dry mass m^{-2} vegetation cover). Both models simulate gross primary production (GPP), in the first case as a function of transpiration and water use efficiency (WUE), in the second case as a function of absorbed photosynthetically active radiation (APAR) and light use efficiency (LUE). Net primary production (NPP) is then calculated taking into account respiration. The modelling is focused particularly on simulating foliar biomass, which is obtained from NPP through an allocation equation based on the maximum leaf area index (LAI) sustainable by the system, and considering turnover.

An analysis of the information offered by MODIS EVI, NDVI, and LAI products was also performed, in order to investigate vegetation dynamics in the study site and to select the best indices to be used as

observational verification for models. MODIS EVI is reported in literature (Huete *et al*., 2002) to be highly correlated with leaf biomass. In accordance with the phenological cycle timing described for the Aleppo pine in similar climates (Muñoz *et al*., 2003), the EVI showed maximum values in spring and minimum values in winter. Similar results were found applying the aforementioned WUE- and LUE- models to the study area. Contrasting simulated LAI with the EVI series, the correlation coefficients r_{WUE} = 0.45 and r_{LUE} = 0.57 were found for the WUE-model and LUE-model respectively. Concerning NDVI, its own definition links this index to the "greenness" of the target, so that it appears highly linked to chlorophyll content and vegetation condition, but only indirectly related to LAI. Photosynthetic pigment concentrations are reported to be sensitive to water stress in Aleppo pine (Baquedano and Castillo, 2006) so, to compare the models' results with NDVI, the simulated LAI was corrected by plant water-stress. The resulting correlation coefficients were r_{WUE} = 0.62 and r_{LUE} = 0.59. Lastly, MODIS LAI and ET were found to be unreliable in the study area because very low compared to field data and to values reported in literature (e.g. Molina & del Campo, 2012) for the same species in similar climatic conditions. The performance of both WUE- and LUE- models in this semi-arid region is found to be reasonable. However, the LUE-model presents the advantages of a better performance, the possibility to be used in a wider range of climates and to have been extensively tested in literature.

Resumen

Una porción significativa de la superficie terrestre está sometida a estrés hídrico debido a su clima árido o semiárido. En estas zonas, los ecosistemas vegetales están controlados principalmente por la disponibilidad de agua, así que se instaura una profunda interconexión entre el ciclo hidrológico y las dinámicas de la vegetación. Por lo tanto, para reproducir adecuadamente el comportamiento de estos ecosistemas es imprescindible modelar conjuntamente la vegetación y el ciclo hidrológico.

En esta tesis se han probado tres modelos dinámicos de vegetación, elegidos por ser "parsimoniosos" y aptos para ser incluidos en un modelo conceptual eco-hidrológico. El análisis se ha efectuado para una zona semiárida del sureste de España, con cubierta vegetal de pino Carrasco. El primer modelo considerado, HORAS (Quevedo & Francés, 2008), simula el crecimiento vegetal como función de la transpiración (T), evaluando las restricciones ambientales considerando el ratio entre T y la evapotranspiración de referencia. La variable de estado relativa a la vegetación es R, biomasa foliar relativa, que es equivalente al coeficiente de cultivo de la FAO (Allen *et al.*, 1998), sin estar fijo en el tiempo. El modelo HORAS se ha posteriormente abandonado debido a los resultados poco satisfactorios, probablemente causados por una descripción demasiado aproximada de los procesos de evaporación y transpiración. Por lo que se refiere a los restantes dos modelos, WUE- model y LUE-model, la variable de estado es la biomasa foliar (B_l, kg material seca m^{-2} cobertura vegetal). Ambos modelos simulan la productividad primaria bruta (GPP, por su sigla en inglés), en el primer caso calculándola como función de la transpiración y de la eficiencia en el uso del agua (WUE), y en el segundo caso calculándola como función de la radiación fotosintéticamente activa absorbida (APAR) y de la eficiencia en el uso de la luz (LUE). La productividad primaria neta (NPP) se calcula teniendo en cuenta la respiración de mantenimiento. La modelación se centra en particular en

la simulación de la biomasa foliar, obtenida de la NPP a través de una ecuación de asignación de recursos que se basa en el máximo índice de área foliar (LAI) sostenible por el sistema.

El trabajo comprende el análisis de la información proporcionada por los productos EVI, NDVI y LAI de los satélites MODIS, con el objetivo de evidenciar las dinámicas de la vegetación en el área de estudio y para seleccionar los índices mejores a la hora de evaluar los resultados de un modelo eco-hidrológico. En literatura (Huete *et al.*, 2002) se demuestra que el EVI es sensible a la estructura del follaje, y en particular al LAI. En acuerdo con el ritmo fenológico descrito para el pino Carrasco en zonas con clima similar al área de estudio (Muñoz *et al.*, 2003), el EVI presenta valores máximos en primavera y mínimos en invierno. Resultados similares se obtuvieron aplicando los modelos WUE-model y LUE-model en la zona de estudio. Comparando el LAI simulado con la serie de EVI, los coeficientes de correlación encontrados fueron r_{WUE} = 0.45 and r_{LUE} = 0.57 para los modelos WUE-model y LUE-model respectivamente. Por lo que se refiere al NDVI, su propia definición relaciona este índice con la presencia del color verde en el espectro registrado por los sensores remotos, así que resulta dependiente del contenido de clorofila en las hojas y de las condiciones de la vegetación, reflejando solo indirectamente las variaciones de LAI. La concentración de pigmentos fotosintéticos es sensible al estrés hídrico en el pino Carrasco (Baquedano & Castillo, 2006) así que, para poder comparar los resultados de los modelos con el NDVI, se corrigió el LAI simulado por el estrés hídrico de las plantas. Los coeficiente de correlación que resultan son r_{WUE} = 0.62 and r_{LUE} = 0.59. Finalmente, el LAI derivado de los datos satelitales no ha sido tenido en cuenta por sus valores excesivamente bajos con respecto a los los valores que se pueden encontrar en literatura para la misma especie y en condiciones climáticas similares (p. ej. Molina & del Campo, 2012). El comportamiento en climas semiáridos de ambos modelos, basados en WUE y LUE, resulta razonable. Sin embargo, el LUE-model presenta las ventajas de unos resultados mejores, la posibilidad de ser usado en un abanico de climas diferentes y que ha sido probado extensamente en literatura.

Resum

Una porció significativa de la superfície terrestre està sotmesa a estrés hídric a causa del seu clima àrid o semiàrid. En aquestes zones, els ecosistemes vegetals estan controlats principalment per la disponibilitat d'aigua, així per això s'estableix una ferma interconnexió entre el cicle hidrològic i les dinàmiques de la vegetació. Per tant, per a reproduir adequadament el comportament d'estos ecosistemes és imprescindible modelizar conjuntament la vegetació i el cicle hidrològic. En esta tesi s'han provat tres models dinàmics de vegetació, triats per ser "parsimoniosos" i aptes per a ser inclosos en un model conceptual eco-hidrològic. L'anàlisi s'ha efectuat per a una zona semiàrida del sud-est d'Espanya, amb coberta vegetal de Pi Blanc.

El primer model considerat, HORES (Quevedo i Francés, 2008) , simula el creixement vegetal com a funció de la transpiració (T), avaluant les restriccions ambientals considerant el ràtio entre T i l'evapotranspiració de referència. La variable d'estat relativa a la vegetació és R, biomassa foliar relativa, que és equivalent al coeficient de cultiu de la FAO (Allen et al., 1998) , sense estar fix en el temps. El model HORES fou posteriorment abandonat a causa dels resultats poc satisfactoris, probablement causats per una descripció massa aproximada dels processos d'evaporació i transpiració. Pel que es referix als restants dos models, WUE- model i LUE-model, la variable d'estat és la biomassa foliar (Bl, kg material seca m^2 cobertura vegetal). Ambdós models simulen la productivitat primària bruta (GPP, per la seua sigla en anglés) , en el primer cas calculant-la com a funció de la transpiració i de l'eficiència en l'ús de l'aigua (WUE) , i en el segon cas calculant-la com a funció de la radiació fotosintèticament activa absorbida (APAR) i de l'eficiència en l'ús de la llum (LUE) . La productivitat primària neta (NPP) es calcula, a continuació, tenint en compte la respiració de manteniment. La modelització se centra en particular en la simulació de la biomassa foliar, obtinguda de la NPP a

través d'una equació d'assignació de recursos que es basa en el màxim índex d'àrea foliar (LAI) sostenible pel sistema.

El treball comprèn, a més, l'anàlisi de la informació proporcionada pels productes EVI, NDVI i LAI dels satèl·lits MODIS, amb l'objectiu d'evidenciar les dinàmiques de la vegetació en l'àrea d'estudi i per a seleccionar els índexs millors a l'hora d'avaluar els resultats d'un model eco-hidrològic. En la literatura (Huete et al., 2002) es demostra que l'EVI és sensible a l'estructura del fullatge, i en particular al LAI. D'acord amb el ritme fenològic descrit per al Pi Blanc en zones amb clima semblant a l'àrea d'estudi (Muñoz et al., 2003), l'EVI presenta valors màxims a la primavera i mínims a l'hivern. Resultats semblants es van obtindre aplicant els models WUE-model i LUE-model en la zona d'estudi. Comparant el LAI simulat amb la sèrie d'EVI, els coeficients de correlació trobats van ser r_{WUE} = 0.45 and r_{LUE} = 0.57 per als models WUE-model i LUE-model respectivament. Pel que es refereix al NDVI, la seua pròpia definició relaciona aquest índex amb la presència del color verd en l'espectre registrat pels sensors remots, així que resulta dependent del contingut de clorofil·la en els fulls i de les condicions de la vegetació, reflectint només indirectament les variacions de LAI. La concentració de pigments fotosintètics és sensible a l'estrés hídric en el Pi Blanc (Baquedano & Castillo, 2006) així que, per a poder comparar els resultats dels models amb el NDVI, es va corregir el LAI simulat per l'estrés hídric de les plantes. Els coeficient de correlació que resulten són r_{WUE} = 0.62 and r_{LUE} = 0.59. Finalment, el LAI derivat de les dades satel·litàries no ha sigut tingut en compte pels seus valors excessivament baixos respecte a les dades mesurades en camp i als valors que es poden trobar en literatura per a la mateixa espècie i en condicions climàtiques semblants (p. ex. Molina & del Camp, 2012).

1 Introduction

A large portion of Earth's terrestrial surface is covered by arid and semi-arid biomes (Renard *et al.*, 1993). These water-controlled ecosystems are complex and their dynamics depend on multiple interconnections between climate, soil and vegetation (Rodriguez-Iturbe *et al.*, 2001). Projections of the IPCC (IPCC, 2007) indicate the high probability of an increase in the area of drought-affected regions and a decrease in water resources in many semi-arid areas. The potential adverse impacts on sectors such as agriculture or water supply makes an in-depth knowledge of the dynamics of these environments vital (Cayrol *et al.*, 2000).

In the last few years there has been an increasing awareness of the critical role of vegetation in soil moisture dynamics (Scanlon *et al.*, 2005; Teuling & Troch, 2005) and ground water resources (Le Maitre *et al.*, 1999; Scanlon *et al.*, 2006). For this reason, a great deal of effort has been made by ecohydrologists in modelling vegetation dynamics along with the hydrological cycle. In order to be suitably coupled with operational hydrological models, vegetation models need to be simple and only requiring information commonly available in practical hydrological applications (Arora, 2002; Montaldo *et al.*, 2005).

A first group of models that can be identified simulates gross primary production (GPP) as a function of plant transpiration (T), based on the

fact that, even though transpiration is not directly responsible for plant growth, in arid and semi-arid environments water is the scarcest resource and, hence, its availability controls every other process in plants. Transpiration is either related to the potential transpiration to evaluate the environmental restraints (Quevedo & Francés, 2008) or linked to primary production through an ecosystem water use efficiency (WUE), which is the amount of carbon gained for unit of water loss (Williams & Albertson, 2005; Istanbulluoglu *et al.*, 2012).

A second group of models that can be identified in literature, and that is applicable to a wider range of plant environment, simulates GPP as a function of intercepted light and light use efficiency (LUE), the ratio between the unstressed canopy carbon assimilation rate and the photosynthetically active radiation absorbed by the canopy (APAR) (Arora, 2002; Polley *et al.*, 2011).

The research presented in this document focuses on the comparison between these modelling approaches and with collocated satellite data. MODIS remote sensing products are evaluated in order to ascertain the value of the information that can be extrapolated from remote sensing data, taking into account the fact that external conditions (e.g. soil moisture, soil colour) and the structure of vegetation canopy can alter the computed vegetation indices values (Jackson & Huete, 1991). Satellite data information is contrasted with published observations regarding LAI's reference values and seasonality in Mediterranean forests.

1.1 Objectives

The following questions are addressed in this thesis.

(1) Which of the proposed approaches to vegetation modelling performs best in a semi-arid environment, and hence should be recommended in a coupling process with a conceptual hydrological model? In order to answer this question, the three models are first of all thoroughly described, underlying the characteristics of each conceptualization, and characterizing variables and parameters. The models are applied to a semi-arid Aleppo pine region. Once discarded

the first model (HORAS) for poorly behaving, uncertainty bands are obtained through the GLUE method for the remaining two models. This analysis is useful to trace the range of possible solutions for the models, identifying the general strengths and weakness of the models themselves. As a final step, calibrations and comparisons with satellite data and between models are performed.

(2) Which satellite data sets are most suitable to evaluate vegetation dynamics in semi-arid environments and can be used to assess models' performance? This second research question is answered through a prior literature review regarding the characteristics of vegetation structural components and their interactions with different wavelengths of the electromagnetic spectrum. This description leads to the identification of remote-sensing vegetation indices and other satellite products, potentially useful to assess vegetation characteristics and their development in time. Finally, the designated satellite data, made available for the semi-arid study site, are compared and contrasted with documented Aleppo pine phenological features and literature values of a characterising index as leaf area index. This analysis leads to the evaluation of the reliability of available vegetation-related satellite data sets in the study site, allowing to broaden, to some extent, conclusions, doubts and intuitions to satellite products for semi-arid environments in general.

1.2 Document structure

This thesis is structured as follows. Chapter 1 sets the basis for the research, defining the research scene and identifying the basic questions that will be addressed in the thesis. Chapters 2 and 3 are intended as an overview of the most relevant features of vegetation and remote sensing, respectively, in view of the research questions previously defined. In chapter 4, three dynamic vegetation models are presented: HORAS (Quevedo & Francés, 2008; Pasquato, 2011) and WUE-model (after Williams & Albertson, 2005), both basing GPP modelling on plant transpiration, and LUE-model (e.g. Ruimy *et al.*, 1999), which use the fact that in unstressed canopy the carbon assimilation to APAR ratio is constant. The study area is described in

chapter 5, while in chapter 6 the MODIS satellite data relative to the research site are analysed. Following, in chapter 7, the results of the 3 models are presented and discussed. Chapter 8 and 9 are focused on conclusions and future research lines.

2 Vegetation

The term vegetation refers to the ground cover provided by plants. It is a general denomination that does not refer specifically to any botanical or geographic characteristics.

This chapter is meant as an overview of vegetation characteristics that are significant for the development of the research presented in this thesis.

2.1 Variability in space and time

As any living system, plant communities are dynamic both in time and in space. Variability is expressed with changes in vegetation structure and species distribution.

In relation to temporal dynamics, they can be classified into two major groups: abrupt changes, and gradual changes (Glenn-Lewin & Van der Maarel, 1992). Abrupt changes are caused by disturbances like wildfires, strong storms, landslides and floods, which induce a sudden, remarkable and long-lasting change in the involved ecosystem. It is common, for the great majority of terrestrial ecosystems, to be subjected to recurring disturbance events that form an integral part of long term systems equilibrium. On the other hand, gradual changes take place

slowly and continuously in any vegetation system, leading, on the long period, to the ecological succession process. Succession is the progressive change in vegetation structure and species composition caused by the alteration of the ecosystem characteristics (among others light, water and nutrient levels) induced by the impact of vegetation itself on the ecosystem in which it lives (Bazzaz, 1979). Succession begins either after the formation of a new unoccupied habitat, or as a consequence of a disturbance. The community starts with a relatively simple structure and reduced set of species, increasing over time both complexity and number of coexisting species, until reaching a stable state called climax, or until a disturbance event occurs. On the shorter time (months/years), vegetation responds to the variability in environmental conditions with changes in growth rate, lushness and reproductive allocation.

As to the heterogeneity in space, it depends mainly on two factors. Firstly, the environmental variability, which includes among others differences in climate (Woodward & Williams, 1987), soil, nutrients (Robertson *et al.*, 1988) and topography (Dufour *et al.*, 2006), leads to different habitats, and therefore, different communities. Secondly, the specific history of disturbances influences the succession stage, and consequently the composition, of each local community (McIntyre *et al.*, 1995).

2.2 Processes in plants and growth

When referring to vegetation, growth is defined as that process by which plants increase the number and the size of their foliage and stems. The energy required is supplied by the sun, and it is made available to growth through photosynthesis: solar radiation is intercepted by leaf pigments and, thanks to the absorbed energy, water and carbon dioxide molecules react to form molecular oxygen and simple sugars. In turn, simple sugars are transformed to produce complex sugars and starch, which are used as energy reserve or structural components. In the next paragraphs, the main processes occurring in plants are described. Unless otherwise stated, information was taken from “Plants in action”, book edited by Atwell et al. (2003).

2.2.1 Leaf structure

Leaves are those organs of higher plants that are specialised for photosynthesis. Evolution has led to a large variety of shapes, sizes and superficial or internal features. They all share, though, the same functions that are to intercept sunlight and absorb CO_2, while limiting water loss.

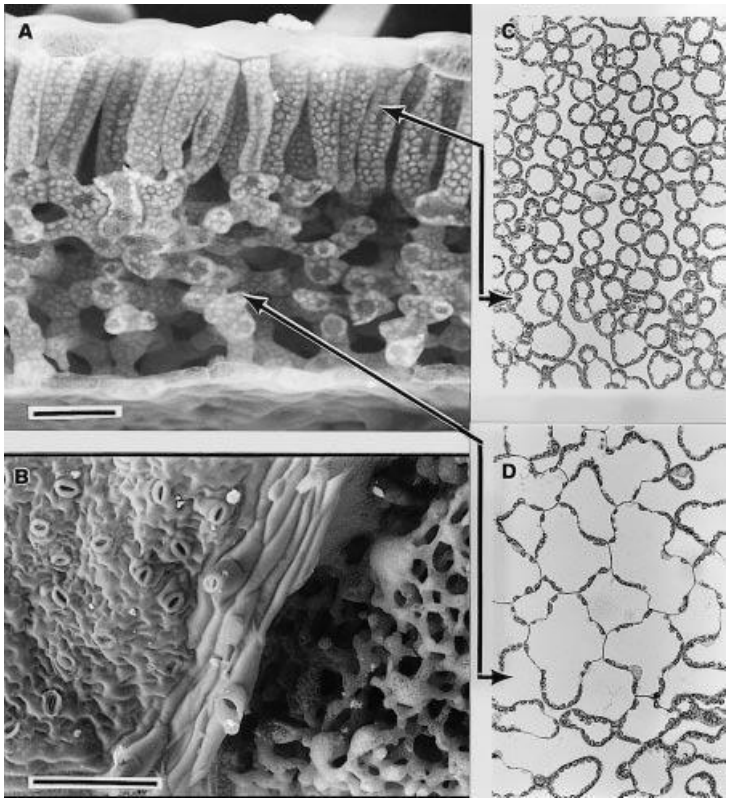

Figure 1: A scanning electron micrograph of a piece of tobacco leaf fractured in (A) to reveal palisade mesophyll cells beneath the upper leaf surface and spongy mesophyll in the lower half. Chloroplasts can be seen covering the inner faces of cell walls. Looking onto the lower surface (B), the epidermis and stomata are present on the left side of the vein, whereas the epidermis is fractured away on the right side, revealing spongy mesophyll tissue. Light micrographs (C, D) of sections cut parallel to the leaf surface are shown for palisade (C) and spongy mesophyll (D) with solid lines showing where the paradermal sections align with (A). Scale bar in (A) = 50 µm and in (B) = 200 µm. Magnification given in (A) also applies to (C) and (D) **(source: Evans, 1999)**.

Three types of tissues can be identified in leaves (Evans, 1999): epidermis, which cover the external surfaces; vascular tissue, divided into xylem that supplies water for photosynthesis, and phloem that move nutrients produced by photosynthesis to the parts of plants where they are needed; and mesophyll, the internal part of the leaf, which in turn is divided into palisade and spongy mesophyll (Figure 1). The palisade, located beneath the upper epidermis, is composed by vertically packed, elongated cells. They are slightly separated from each other to permit the absorption of CO_2, and they contain a high number of chloroplasts, organelles accountable for photosynthesis. Below the palisade layer, the spongy layer is composed by globular cells, containing a lower number of chloroplasts with respect to palisade cells, and separated by large intercellular spaces that connect to the substomatal chambers, located proximal to the stomata. Stomata are pores on the epidermis of leaves that permit the gaseous exchange (carbon dioxide and water vapour) with the external atmosphere. Commonly, leaf epidermis is covered by small hairs (trichome) that can serve a wide range of functions.

2.2.2 Photosynthesis

Photosynthesis is that process by which solar radiant energy is transformed into chemical energy, stored in the bonds of the produced sugars.

Two parts of the process can be identified: the light reaction and the dark reaction (Whitmarsh & Govindjee, 1999). The light reaction, as its name indicates, involves light that is absorbed by pigments in chloroplasts; its energy is harvested and stored by forming a chemical compound called ATP (adenosine triphosphate). The dark reaction, on the other hand, involves the Calvin cycle, through which CO_2 and water are converted into sugar. This process is also known as carbon fixation. The RuBisCO enzyme catalyses this reaction, and the ATP produced in the light reaction is used as energy source to make the process possible.

Three different metabolic pathways for carbon fixation have been identified in nature: C3, C4 and CAM. C3 plants are the most widespread, representing approximately 95% of total vegetation

biomass. C4 and CAM plants, on the other hand, developed as an adaptation to high-radiation and dry climates: water use efficiency is improved and photosynthesis under high light intensity is enhanced. Photosynthetic capacity depends therefore on carbon fixation mechanism, varying also with light, water and nutrient availability, and being linked to RuBisCO content.

2.2.3 Light absorption

Pigments in chloroplasts are responsible for the absorption of solar radiation in the blue (~ 700 nm) and red (~ 470 nm) wavelengths of the visible spectrum. On the contrary, radiation in the green region (~ 530 nm) is reflected, commonly giving to leaves their characteristic green colour.

Light absorption pattern is very complex because of sieve-effect and scattering (Evans, 1999). The sieve-effect is linked to the fact that pigments are packed into discrete units, the chloroplasts, being the rest of foliar tissue transparent to light. As palisade cells are organised parallel to each other, if chloroplast are vertically aligned a great percentage of radiation can penetrate deeply into the leaf tissues. Once in the spongy layer, which is composed by irregularly-shaped cells, light is scattered because of the multiple water-air interfaces encountered on its path, substances that present different refractive indices. This phenomenon greatly increment the path of light through the leaf, increasing the probability of absorption.

Radiation penetrating into leaf tissues is attenuated logarithmically following Beer's law, a general law that relates the transmission of light to the properties of the substance through which light is travelling.

2.2.4 Carbon dioxide intake and assimilation

Leaf epidermis forms a barrier that prevents water loss, impeding at the same time CO_2 intake. This gas, necessary for photosynthesis, is absorbed through the stomata, openings that are found on the lower (abaxial) surface of leaves and, not rarely, also on the upper (adaxial) surface, depending on the species. As intercellular air spaces are

saturated in water vapour, the opening of stomata results in a double gaseous flux: from one side an inward flux of CO_2, and from the other side an outward flux of water vapour (transpiration). To regulate this loss (transpiration) that can ultimately lead to dehydration, plants regulate the stomata opening through a complex mechanism triggered by changes in soil and plant water potentials. The outward flux of H_2O is also controlled by the thickness of the boundary layer of still air adjacent to the leaf surface, which depends on wind speed and on the presence of external structures (e.g. hair) on the leaf.

The inward flux of CO_2 is similarly controlled by the boundary layer and by the stomata opening, but other restrictions are encountered before the gas enters the energy production process: after penetrating in the substomatal cavities, it has to diffuse throughout the mesophyll, dissolve into cell walls, enter the cytosol (intracellular fluid) and diffuse into chloroplasts through a double membrane. These processes are eased by the highly extended area for diffusion developed internally by leaves, and by the fact that chloroplasts tend to concentrate adjoining the cell walls that face air intercellular spaces (see Figure 1D).

2.2.5 Evapotranspiration

Evaporation is the process by which liquid water is converted to water vapour from soil surface or water-bodies. Transpiration is the evaporation of liquid water from plant tissues through leaf stomata. These two processes occur simultaneously and, being hard to separate the contributions of the two phenomena, they are often jointly referred to as evapotranspiration (ET).

ET is affected by weather parameters, vegetation characteristics and environmental constraints (Allen *et al.*, 1998). Weather parameters, namely radiation, air temperature, humidity and wind speed, determine the evaporation power of the atmosphere that is expressed by the reference evapotranspiration (ET_0). ET_0 is the evapotranspiration rate from a reference surface, as defined by Allen et al. (1998), with no water deficit. Vegetation type and development stage also influence evapotranspiration. For this reason the FAO introduced the vegetation factor (k_c) that, multiplying ET_0, leads to ET_c, crop evapotranspiration

under standard conditions. Finally, environmental conditions like soil salinity, low land fertility, the presence of pests or water stress should be taken into consideration when determining actual ET.

2.2.6 Respiration

Respiration is the set of catabolic reactions by which the high-energy bonds, present in large molecules (sugars), are broken to release usable energy. Depending on how the plant uses this freed energy, respiration can be distinguished between maintenance and growth respiration.

Maintenance respiration is that metabolic process that is needed to keep a plant healthy and alive. Energy is used to re-synthesise all those cellular component that undergo turnover, to maintain the physiological ionic and metabolitic gradients across cellular membranes, to support the processes of adaptation to changes in the plant's external environment, and to repair the damages caused by stress conditions.

In growth respiration, the released energy is used to support the processes that lead to an increase in plant biomass.

2.3 Vegetation indices

When assessing and modelling vegetation properties, the use of vegetation indices can be useful. As far as this research is concerned, the most important indices are as follow:

LAI

The leaf area index (LAI) is a dimensionless quantity defined as the total one-sided area of photosynthetic tissue per unit ground surface area (e.g. Gobron, 2008). It represents the amount of leaf biomass in an ecosystem.

WUE

Water use efficiency (WUE; kg C kg^{-1} H_2O) is an index that measures the production of biomass or the quantity of carbon fixed by

plants, normalized by the amount of water used in the process (e.g. Whifield, 1999). Its definition depends on the context in which the concept is discussed, particularly on the time scale over which the efficiency is measured. In this sense, it is possible to define a photosynthetic WUE, the instantaneous ratio between carbon gain in photosynthesis and water loss in transpiration, and a long-term WUE, obtained comparing GPP and transpiration losses at daily, monthly or annual time scale..

LUE

Light use efficiency (LUE; kg C MJ^{-1} APAR) is defined as the ratio between carbon fixed by plants during photosynthesis and the absorbed photosynthetically active radiation (APAR) used in the process, in ideal conditions (e.g. Turner *et al.*, 2003). LUE vary with plant species.

2.4 Ecophysiology

Ecophysiology is defined as the study of the physiology of organisms with respect to their adaptation to the environment (Collins English Dictionary - Complete & Unabridged, 2009). The next paragraphs are meant as an overview of the responses of vegetation to different environmental conditions and stress sources. Depending on the site-specific characteristics, these limitations can acquire more or less importance.

2.4.1 Sunlight

Plants have evolved to adapt to environments characterized by extremely diverse solar radiation levels: from deeply shaded places like the understory of rainforests, to high-radiation environments like deserts. To do so, mechanisms to optimize the use of limited radiation or to protect the plant from excessive radiation have been developed. Some species also present a considerable ability to adapt to variable sunlight levels (Robinson, 1999).

A way to regulate light interception is to change the leaf magnitude. In shaded environments, leaves tend to be large, to maximize the interception surface. Similarly, the leaf orientation and angle affect light absorption: a vertical position facilitates interception when the incoming radiation is weak (early morning and late afternoon), limiting absorption at noon when the radiation levels are highest. On the contrary, the horizontal position maximizes radiation interception when the incoming radiation is highest.

Another possibility for plants to regulate light interception is to change leaf surface properties: hair, wax or salt crystals are used to coat leaves with a reflective layer. The structure of epidermal cells can, on the contrary, increase the interception of light when shaped to act like lens.

At mesophyll level, radiation absorption can be regulated by the position of photosynthetic tissues (equally distributed on both sides of leaves or concentrated on one side) and by the distribution of chloroplasts (alignment on vertical palisade cell walls reduces absorption). Allocation of resources to photosynthetic pigments and to RuBisCO, which is involved in CO_2 fixation, varies depending on the average light availability in each plant environment.

CO_2 fixation itself depends on the instantaneous light availability. At low radiance the increase in photosynthetic rate can be considered linearly dependent on the increase in radiation; at higher radiance levels, the linearity is lost and the assimilation rate increases progressively less with increasing radiation, till reaching a plateau where further increase in light intensity does not affect fixation levels and light saturation is reached (Smith, 1936). This plateau depends on RuBisCO maximum activity and differences between photosynthetic capacity of leaves is related to RuBisCO content. High radiation adapted plants develop higher levels of RuBisCO, leading to higher photosynthetic capacity, with respect to shade species.

Absorption of excessive radiation can lead to tissue damage, to prevent which, plants have developed a complex system of photoprotective mechanisms that include thermal dissipation, non-assimilatory photochemistry (i.e. energy consumption by processes that

do not involve CO_2 fixation) and chlorophyll fluorescence. When excessive radiation exposure is combined with other sources of stress, such as high temperatures, drought or nutrients deficiency, plants can incur more easily in photodamage (Solovchenko, 2010).

2.4.2 Water

The soil-plant-atmosphere continuum is the path followed by water in its journey from soil to atmosphere. Plants play an active role in this process, thanks to the fact that their roots occupy the upper layers of the soil, while their trunks, branches and leaves occupy the lowest layers of the atmosphere (Philip, 1966). To fully understand the plant-water relations it is essential to consider the entire soil-plant-atmosphere system because of the deeply interconnected water and energy transfer mechanisms that occur between the three domains.

Water potential (Ψ) is the potential energy of water subjected to external forces (pressure, osmotic, gravitational and matrix effects), with respect to pure water in reference state. Differences in water potential control the movements of water through the soil-plant-atmosphere continuum, which will tend to migrate from areas of higher to areas of lower water potential. Canopy transpiration lowers leaf water potential, causing water to move from the soil to the plant tissues, along the stem and branches, till reaching the atmosphere through the stomata (Eamus, 1999).

Transpiration is a consequence of stomata opening, which is needed to acquire CO_2 from the atmosphere. Plants can regulate stomata opening, depending on ambient light, CO_2 intercellular partial pressure and cellular turgor. Particularly, partial or total stomatal closure is a fundamental protection mechanism of plants against desiccation when soil water is scarce.

Plants adapted to arid and semi-arid climates have evolved different strategies to cope with water restrictions: escape, tolerance and avoidance (Levitt, 1980; Lo Gullo & Salleo, 1988). Drought-escape mechanisms involve rapid plant life cycles, centred in the periods of soil moisture availability. Drought-tolerant species, on the other hand, have

developed structural adjustments that include different carbon fixation pathways (C4 and CAM, as opposed to C3), the adaptation of stomata and roots, and the presence of succulent and water-filled tissues. Finally, drought avoidance is obtained through two different strategies (McDowell *et al.*, 2008): isohydric species (water-saver species) maintain a relatively constant midday leaf water potential regardless of drought conditions, thanks to early stomata closure; anisohydric species (water-spender species), on the contrary, allow a decrease in midday leaf water potential that facilitates the extraction of soil moisture to compensate water loss experienced due to high transpiration rates.

2.4.3 Other environmental variables

Temperature

Temperature greatly influences plant development stages, that is its phenology (e.g. Post & Stenseth, 1999). Also, at each development stage, a minimum and a maximum temperature define the range within which the plant will survive. A sub-interval of optimal temperature range is identifiable as the one in which growth is at its maximum rate. Sensitivity to temperature varies with plant tissues and physiological processes on one side, and with plant species and acclimation characteristics on the other side. Enzymes play a major role in the response of plants to temperature, because temperature greatly influences enzymes activity; in fact, plant acclimation can lead to changes in enzyme concentration.

Temperature primarily influences the following plant processes: photosynthesis, water and nutrient uptake by roots, assimilate transport, growth and development, plant form (Wardlaw, 1999).

Particularly, CO_2-assimilation relation to temperature considerably varies with photosynthetic path, C3 or C4: while C3 plants show minor changes in CO_2 fixation with temperature within optimum range, C4 plants respond favourably to temperature increase, showing also higher optima with respect to C3 species. The latter, in fact, have to deal with increased photorespiration at high temperatures.

As for water and nutrient uptake by roots, the major control of temperature regards the stomatal conductance and transpirational water demand. In addition, the root permeability is affected by low temperatures, while for many species increased soil temperature facilitates nutrient uptake.

Carbon dioxide

The rise in atmospheric carbon dioxide concentration over the last 50 years has urged scientists towards a research effort in order to increase the understanding of plant response to CO_2 enriched atmosphere. Despite the countless experiments conducted in the past years, and particularly since the 1990s (Leuzinger & Hättenschwiler, 2013), the issue remains critical and largely unresolved.

Nutrients

Plant growth depends on the availability of nutrients in the soil. Nutrients can be classified into two groups, macronutrients and micronutrients, basing on the quantity required (Marshner, 2012). The first group includes, from higher to lower % in dry mass, Nitrogen, Potassium, Magnesium, Phosphorous, Calcium and Sulphur. Micronutrients are Sodium, Chlorine, Iron, Boron, Manganese, Zinc, Copper, Nickel and Molybdenum.

Salt

Soil salinity inhibits growth in plants other than halophytes, species adapted to this type of environment, because salt both reduces soil moisture uptake and becomes toxic at high concentrations (Borowitzka & Colmer, 1999).

Soil salinization is a major worldwide soil degradation problem. The main source of salts is the primary minerals that, once exposed to chemical weathering, release salts. These salts are transported by surface and soil water, undergoing concentration when moving to more arid areas. In this process, concentration may become sufficient as to lead to precipitation of salts in low soluble forms (Abrol *et al.*, 1988).

Poor soil practices as irrigation with saline water or overgrazing, which induces erosion and may lead to exposure of saline subsoil, have been deeply affecting soil properties in the last decades.

Fire

Fire is one of the most common abrupt disruptions that may initiate a succession process, damaging the previously existing environment through heat and gas emissions.

The response of the ecosystem depends on the fire regime that is related to fire intensity, fire frequency, seasonality of fire and whether it is an above or below ground fire (Gill & Allan, 2009). Plant communities in areas frequently subjected to wildfires tend to present a range of fire-tolerant responses that involve stimulation by fire of seed release from woody capsules, germination of soil-stored seeds, bud development and flowering (Pate, 1999).

Reduced competition for nutrients and water from plants killed by the fire benefit fire-tolerant species development. Moreover, ashes derived from burnt biomass supply a substrate rich in inorganic nutrients that foster new plant growth (Renbuss *et al.*, 1973).

2.5 Pinus halepensis Mill.

The research conducted in this study focused particularly on a site where the species Pinus halepensis Mill. is dominant (Figure 2).

Pinus halepensis, also named Aleppo pine after the largest city of Syria, is a pine native to the Mediterranean area. It is generally found at low altitudes, up to 200 m a.s.l., but it can grow at altitudes of 1000 m in the south of Spain, and up to 1700 m in Morocco, Algeria and Tunisia (Farjon, 2005).

Pinus halepensis is a medium-size tree, which reaches a height of 22 m when growing in favourable conditions. The bark is hash-grey or silver on the young trunk and on the branches, becoming orange-red, thick and deeply fissured in mature trees, particularly at the base of the trunk. The crown, at first globe-like and pointed or pyramidal, when

approximately 20 years old stretches and opens taking a lobed and irregular outline. It remains light and thin because of the little amount of foliage. The needles are slender, 6 – 12 cm long and 0.5 -0.8 mm wide, light green and generally produced in pairs (Figure 2). They persist on the tree for approximately 2 years (Ceballos & Ruiz de la Torre, 1979) and needle shedding occurs mostly during summer droughts (García-Plé *et al.*, 1995; Borghetti *et al.*, 1998; Calatayud *et al.*, 2000). Shoot maximum elongation rate is registered in spring (Weinstein, 1989; Borghetti *et al.*, 1998; Pardos *et al.*, 2003).

Figure 2: Aleppo pine trees in Valdeinfierno catchment, south-east of Spain.

Florescence (Figure 3) occurs from March to May, depending on location. In protected regions, where winters are mild, can bloom in February. Male cones are oblong and yellowish, 5 – 8 mm long and 3 – 4 mm wide, grouped in cylindrical spikes. Female cones are 6 -12 cm long, green at first, becoming red-brown after a 24 months ripening

process, and opening slowly over the next few years. The seeds are 5 – 7 mm long, with a wing three times their length, and are wind-dispersed.

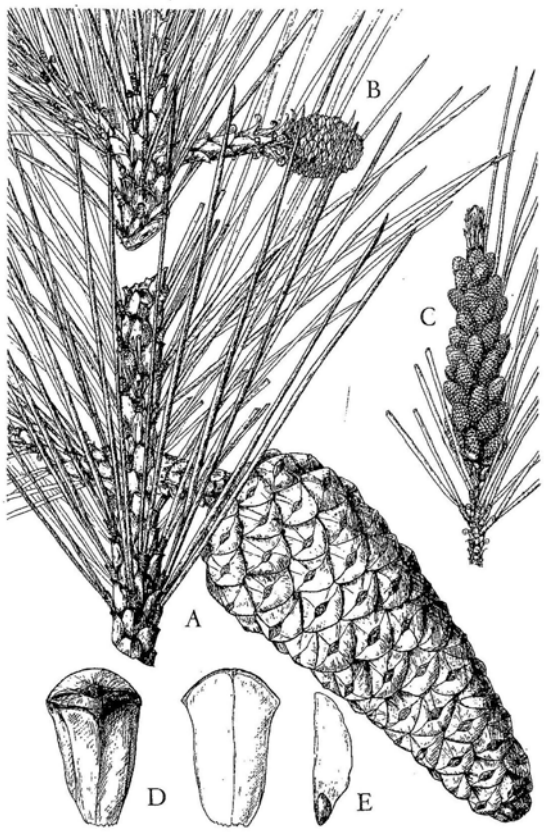

Figure 3: Aleppo pine tree's elements. A - Branch with a ripe female cone. B – Branch with developing cone. C – Branch with male inflorescence. D – Cone scale, front and back. E – Winged seed. (source: Ceballos & Ruiz de la Torre, 1979)

Basing on its ecological behaviour, it can be described as thermophilous, xerophilous, basiphilous. It does not well tolerate saline substrate and prefers basic and clayey soils (Ceballos & Ruiz de la Torre, 1979).

The Aleppo pine stands out because of its good drought tolerance. The average annual precipitation typical of its habitat is higher than 250 mm, while the rainfall occurring between May and September is lower than 300 mm. Average temperatures in January are higher than 0 ºC, while in August the average values usually stay between 18 and 26 ºC. For those regions where summer temperatures are higher, watering is often necessary (Ceballos & Ruiz de la Torre, 1979).

3 Remote sensing of vegetation

Remote sensing is the acquisition of information regarding the Earth's surface, oceans and atmosphere, performed without a direct contact with the targets of the measurements, and using instruments usually mounted on aircrafts or satellites. This result is obtained by sensing and recording the radiation originated from the targets of the analysis.

Two different types of remote sensing can be identified: passive and active remote sensing. In passive collection, the natural radiation emitted or reflected by the targets is recorded. Reflected sunlight is the typical source of radiation used by passive sensors (e.g. photographic equipment, spectroradiometers). Active sensing (e.g. with Radar or Lidar), on the contrary, involves an artificial source that emits a signal. The signal hits the target, is reflected or backscattered and is then measured by the sensor.

Remote sensing permits to gather information about inaccessible sites and to replace costly and time consuming data collection on the ground, while leaving the area of investigation undisturbed. In the case of satellite multispectral scanners, many years of worldwide data are available: Landsat program, for example, has been active since the 70's. This makes possible long term and retrospective analysis of the phenomena or areas of interest (e.g. Vicente-Serrano *et al.*, 2010).

Satellite-based remote sensing has been widely used, over the last 20-30 years, for monitoring activities related to vegetation. This application requires the knowledge of the structures and functions of vegetation and its reflectance properties. Thanks to this knowledge, it is possible to link the vegetative states and structures of a certain ecological system of interest to their reflectance behaviour. Applications, among others, include Net Primary Production (NPP) estimation, drought evaluation, phenological variability measurement and fire risk assessment.

3.1 Solar reflected optical spectrum

The Sun's electromagnetic emission is close to that of a black body with a temperature of about 5800 K: the solar radiation spectrum striking the terrestrial outer atmosphere spans a wavelength range of approximately 100 nm to 4000 nm (Figure 4). In the process of crossing the atmosphere, the radiation undergoes reflection, scattering and absorption due to the presence of gases and suspended particles. Absorption, in particular, is attributable to the presence of water vapour, carbon dioxide and ozone in the atmosphere (Figure 5).

Once reflected by the Earth's surface, the radiation spectrum encompasses the range of 400 nm to 2500 nm. This reflected optical spectrum can be divided into three distinct wavelength ranges: visible (VIS: 400 - 700 nm) (Figure 6), near infra-red (NIR: 700 – 1300 nm) and shortwave infra-red (SWIR: 1300 – 2500 nm). The 400 nm to 2500 nm region is routinely measured using a variety of passive remote sensors ranging from multispectral (e.g. Landsat TM, Modis) to hyperspectral (e.g. AVIRIS). The reflected spectrum highly depends on the material and structure of the reflecting surface. The knowledge of the characteristics of the specific spectral signatures of different targets allows, therefore, retrieving of information from the remote sensing data on the nature and characteristics of the targets themselves.

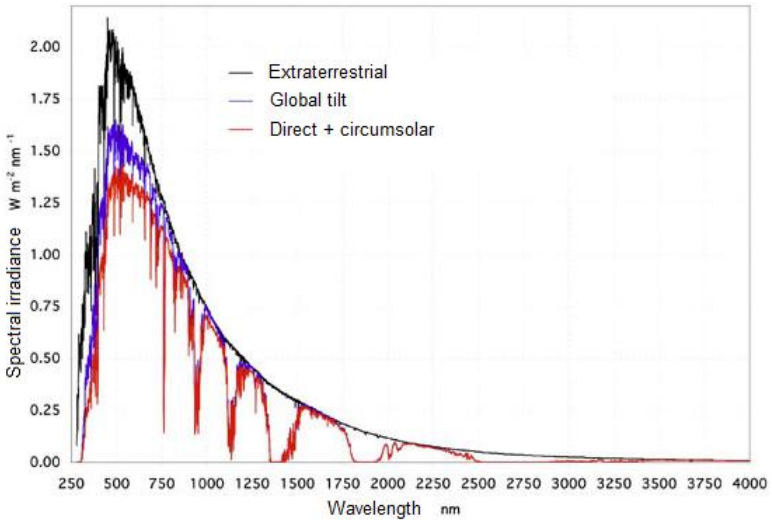

Figure 4: Solar spectrum at top of atmosphere at mean Earth-Sun distance (black); Spectral radiation from solar disk plus sky diffuse and diffuse reflected from ground on south facing surface tilted 37 deg from horizontal (blue); nearly parallel radiation on surface with surface normal pointing to the sun, excluding scattered sky and reflected ground radiation (Direct) + spectral radiance within +/- 2.5 degree field of view centred on the 0.5 deg diameter solar disk, but excluding the radiation from the disk (Circumsolar) (red). (source: American Society for Testing and Materials, 2003).

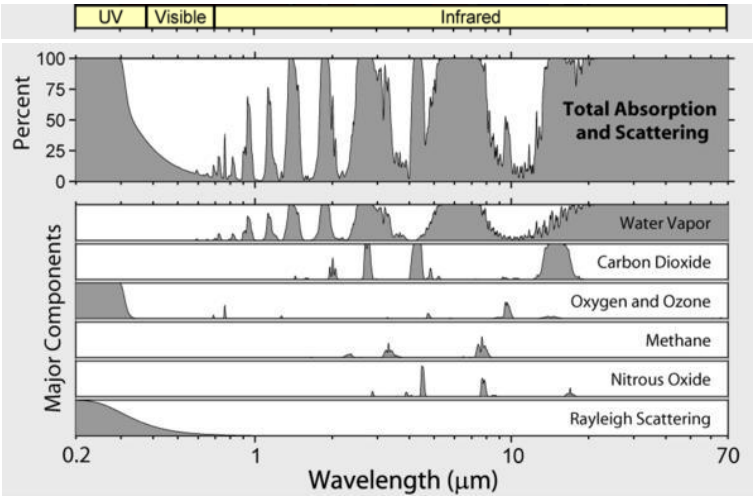

Figure 5: Absorption bands of the radiatively active species in the Earth's atmosphere (after Rohde, 2007).

Figure 6: Visible spectrum. (after Spiggest, 2010). The visible colours, from shortest to longest wavelength, are: violet (400 nm), indigo (445 nm), blue (475 nm), green (510 nm), yellow (570 nm), orange (590 nm), and red (650 nm).

3.2 Vegetation reflectance properties

Plant foliage reflectance properties are determined by their chemical composition. The most important leaf components that affect their spectral properties are pigments, water, carbon and nitrogen. Other components, such as phosphorus and calcium, are significant to plant function, but they do not contribute to the spectral properties of leaves, thus cannot be directly measured using remotely sensed data.

Reflectance is also influenced by the canopy structure, the presence of senescent or dead vegetal material and the soil colour.

3.2.1 Pigments

Pigments are substances that absorb energy in the visible spectrum, serving a variety of purposes and being critical to the function and health of vegetation. There are three main categories of leaf pigments in plants: chlorophylls, carotenoids, and anthocyanins.

Chlorophylls, -a and -b, are vital for photosynthesis. They absorb violet, blue, orange and red ranges, and reflect green light. For this reason, they appear green to our eyes. More precisely, and due to the slightly different absorption spectra, chlorophyll-a looks bluish-green, while chlorophyll-b looks yellowish-green (Figure 7). Chlorophyll-a's absorption peaks occur at 435, 670-680 and 740 nm while chlorophyll-b's peaks are centred on 480 and 650 nm (Zwiggelaar, 1998).

Carotenoids assist the process of light absorption for photosynthetic purposes and help protect plants from the noxious effects of very high radiation conditions. They are generally found in high concentration in leaves that are stressed, senescent or dead. Carotenoids absorb light from violet into the greenish-blue range, appearing yellow-orange to our

eyes (Figure 7). Absorption peaks are at 420, 440 and 470 nm for α-carotenoid; at 425, 450 and 480 nm for β-carotenoid (Zwiggelaar, 1998).

Lastly anthocyanins, unlike the chlorophylls and carotenoids, do not participate in photosynthesis. They give colour to flowers and to leaves, helping to protect them from the damages excessive sunlight could cause, and are found abundant both in newly forming and senescent leaves. Anthocyanins absorb light mainly in the green wavelengths, appearing red, purple or blue.

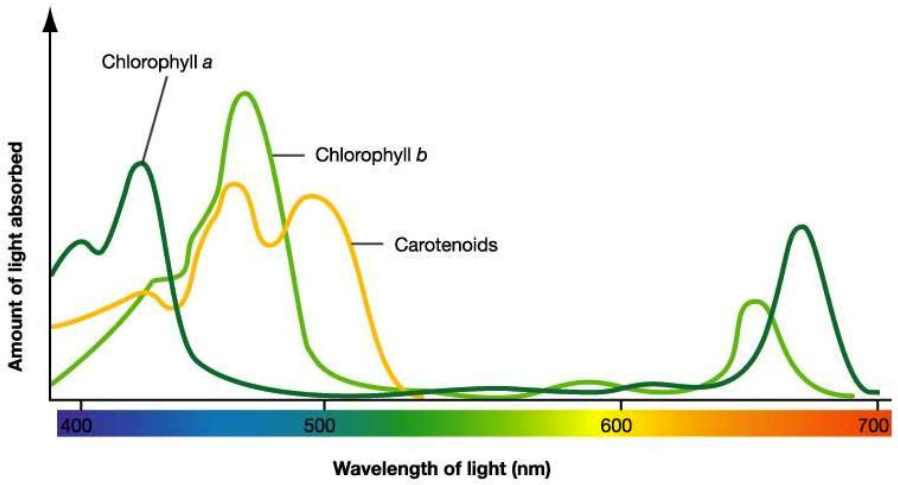

Figure 7: Absorption spectra of Chlorophyll a, Chlorophyll b and Carotenoids (after AgSpecific, 2012).

3.2.2 Water

Leaf water affects plant reflectance in the shortwave infrared regions of the spectrum (Tucker, 1980). In fact, the absorption spectra of leaves over the 1400 – 2500 nm is not statistically different from that of pure water (Allen *et al.*, 1970). As this absorption depends only on water's characteristics, it may be considered a *primary* effect of water content on leaf reflectance spectrum (Asner, 1998). The absorption of radiation by water tends to decrease reflectance, so that a decrease in leaf water content determines an increase in shortwave infrared reflectance (Figure 8). In particular, the wavelengths 1530 nm and 1720 nm appear to be

the most suitable to evaluate the leaf water content from satellite remote sensing data (Fourty & Baret, 1997).

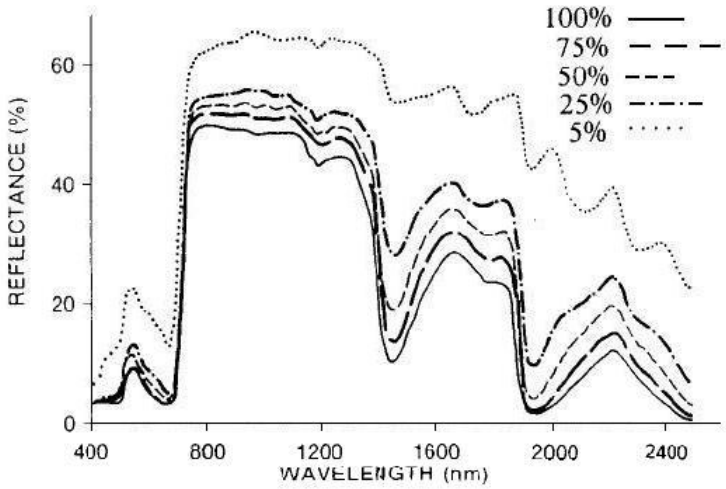

Figure 8: Leaf reflectance spectra for decreasing leaf water content (LWC = 100%; 75%; 50%; 25%; 5%) (after Carter, 1991)

Between 400 and 1300 nm, absorption by pure water is relatively weak (Woolley, 1971; Curcio & Petty, 1951). Nevertheless, reflectance was reported to increase also in the visible and near-infrared range when leaf water content decreased (Hunt & Rock, 1989; Woolley, 1971). This phenomenon can be explained by secondary effects of leaf water content, particularly by the decrease of absorption by substances other than water for decreasing water content (Carter, 1991). Baquedano and Castillo (2006) described a decrease of both total chlorophyll and total carotenoids induced by water deficit in the three analyzed Mediterranean species: Pinus halepensis, Quercus coccifera and Quercus ilex. An increase of the reflectance in the red-infrared transition region (680 -760 nm), subsequent to dehydration and to other stress conditions, has also been reported in literature (Carter, 1993). This phenomenon is referred to as “blue shift” (Figure 9), because this reflection increase could be seen as a shift of the near infra-red reflectance plateau towards the blue part of the spectrum (Rock *et al.*, 1988). Another secondary effect of

decreased water content, particularly noticeable in the 700 – 1300 nm wavelength range because tends to be masked in the rest of the optical spectrum, is the multiple refraction of light crossing cell walls-air interfaces (Sinclair *et al.*, 1973). As water is lost from leaves, intercellular air increases and so does the number of interfaces between cell walls and intercellular air, leading to a higher probability that the refracted radiation is directed back and measured as reflection.

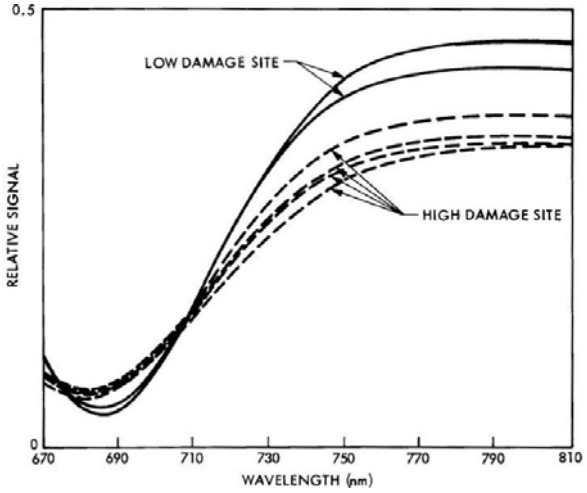

Figure 9: "Blue shift" of the red-near infrared edge, observed in the spectrum of a damaged forest site (source: Rock *et al.*, 1988).

3.2.3 Carbon

Plants contain carbon in many forms, including sugars, cellulose, and lignin. Sugars are products of photosynthesis; they are used by the plants to produce more complex molecules such as cellulose and lignin. Cellulose is primarily used in cell walls while lignin forms the most structurally robust portions of plants. The possibility of the analysis of these substances through remote sensing is related to the absorption characteristics of different molecular bonds: C-H aromatic, C-H, O-H and O-H C-O combination (Martin & Aber, 1997). The 1200 – 2500 nm region appears to be the most suitable to analyse cellulose and lignin plant content (Raymond & Schimleck, 2002; Martin & Aber, 1997).

Absorption appears to be directly related to dry matter density in the near-infrared and shortwave-infrared spectrum (Figure 10).

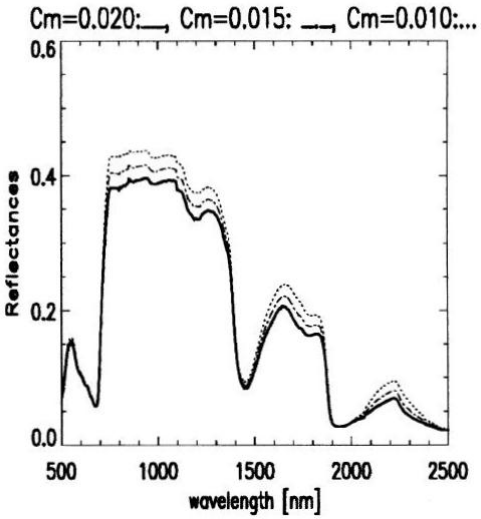

Figure 10: Response of leaf reflectance to decreased leaf dry matter content (C_m = 0.02; 0.015; 0.01 g/cm^2) (source: Ceccato *et al.*, 2001).

3.2.4 Nitrogen

Leaves contain nitrogen bound in molecules as chlorophyll pigments and proteins. For this reason, nitrogen leaf content can be assessed analysing the regions of the spectrum influenced by these substances. For example, nitrogen content predictors based on the reflectance in the transition region between red and near-infrared (700 – 720 nm), linked therefore to chlorophyll content, proved to perform well (Lee *et al.*, 2011; Zhao *et al.*, 2005).

3.2.5 Canopies

At canopy level, in addition to the chemical constituents of leaves, some structural characteristics of plants influence the reflectance properties, particularly leaf area index (LAI) and leaf angle distribution (LAD).

LAI variations produce the most pronounced effects in the NIR region, and the least strong effects in the VIS region (Figure 11). This is because vegetation strongly reflects light in the near-infrared portion of the spectrum, while highly absorbing photons in the visible and in the SWIR ranges (particularly in the 1900 – 2500 region). This results in a deep penetration of photons into the canopy in the NIR wavelengths thanks to multiple reflections that make it possible a downward transmission of the light, so that the radiation that is finally reflected by the canopy conveys information of various layers of leaves (Huete *et al.*, 1985). VIS and SWIR reflected spectrum is, on the contrary, mainly sensitive to upper-canopy conditions because multiple reflections are extremely rare. The incremental importance of the increase of reflectance in the NIR region, concurrent with a LAI increase, diminishes as LAI increases (Asner, 1998). A deepening of the two water absorption features within the NIR (~1000 nm and 1200 nm) also occurs as LAI increases, because of enhanced radiation absorption due to increased leaf surface.

The LAD describes the variety of directions in which the plant leaves are oriented and it is often simplified by specifying the mean leaf angle (MLA), which is the average of the angles of leaves in the canopy with respect to the horizontal. The decrease of MLA produces an increase in reflectance, particularly in the NIR region, but with an important effect also on the SWIR wavelengths (Figure 11).

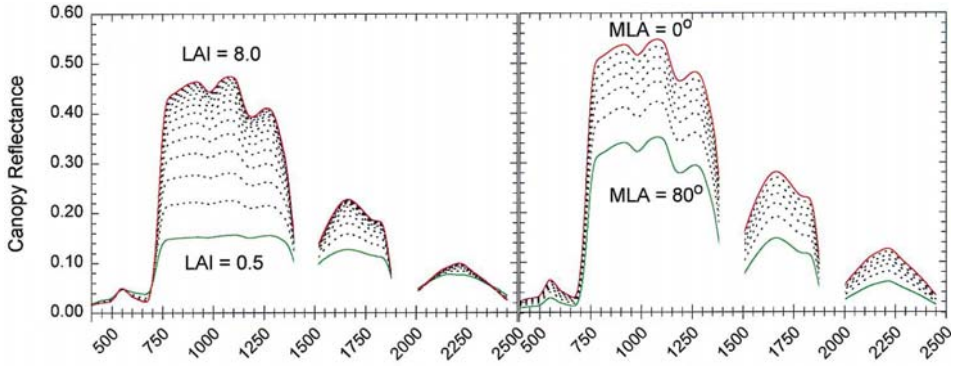

Figure 11: Effect of increasing LAI on canopy reflectance, for MLA = 45º (left); effect of decreasing MLA on canopy reflectance, for LAI = 5 (right) (source: Asner, 1998).

The departure from horizontal orientation allows multiple scatterings that permit photons to penetrate deeper into the canopy and cause greater signal attenuation. Leaf inclination does not alter significantly the shape of the reflectance signal (Asner, 1998).

3.2.6 Non-photosynthetic vegetation

The majority of ecosystems, in addition to green vegetation, contain senescent or dead vegetation and woody structure. This material is often referred to as non-photosynthetic vegetation (NPV) because it does not directly participate in the photosynthetic process.

When considering the contribution of woody stem material to tree and shrubs canopy reflectance, it has been reported (Asner, 1998) that an increase of stem surface decreases the magnitude of the NIR plateau and elevates the SWIR reflection. Again, the effects of stem material are intensified in the NIR because photons penetrate and exit the canopy more efficiently in this region, highly interacting with woody surfaces. The overall effect will depend on the position of woody stems within the canopy and, ultimately, on the level of interaction between these materials and the radiation exiting the canopy.

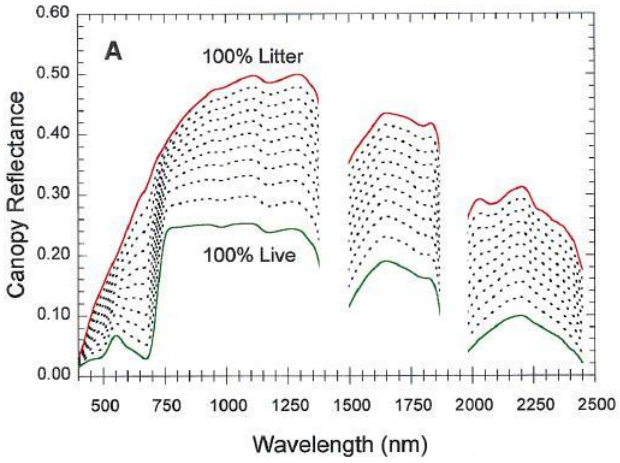

Figure 12: Influence of fraction of litter on the reflectance properties of grassland (source: Asner, 1998).

As for standing litter, it was shown to have greater impact on grass canopy reflectance compared to tree one (Asner, 1998). The increase of litter causes an increase of reflectance throughout the entire shortwave spectrum, with a deterioration of pigment absorption features and NIR plateau, and a flattening of the red edge (Figure 12).

3.3 Soil reflectance

When using remotely sensed datasets to assess vegetation characteristics, an important factor to be taken into account is the soil background reflectance spectrum, particularly significant when vegetation is not very dense.

The contribution of soil signal to total reflected spectrum varies as a consequence of several factors, among which soil type, organic matter content, surface roughness, shading, spectral irradiance (which depends on sun angle and canopy extinction properties) and soil moisture content (Huete & Jackson, 1988). In particular, soils tend to become darker when wet (Figure 13), primarily because the change in the medium surrounding the soil particles, from air to water, decreases their relative reflectance index, increasing therefore the “forwardness” of scatter. Accordingly, incident photons have to be scattered more times to be reflected and are, therefore, exposed to a greater probability of being absorbed (Twomey *et al.*, 1986). The changes in reflectance, consequent to soil moisture variations, are shown to be well explained by exponential functions, when water content is expressed on a volumetric basis (Lobell & Asner, 2002). The SWIR region appears to be more responsive to moisture variations than the VIS and NIR ones (Figure 14). In fact, a saturation occurs for visible wavelengths when soil moisture exceed 20%, while SWIR responds to water content variations up to 50%.

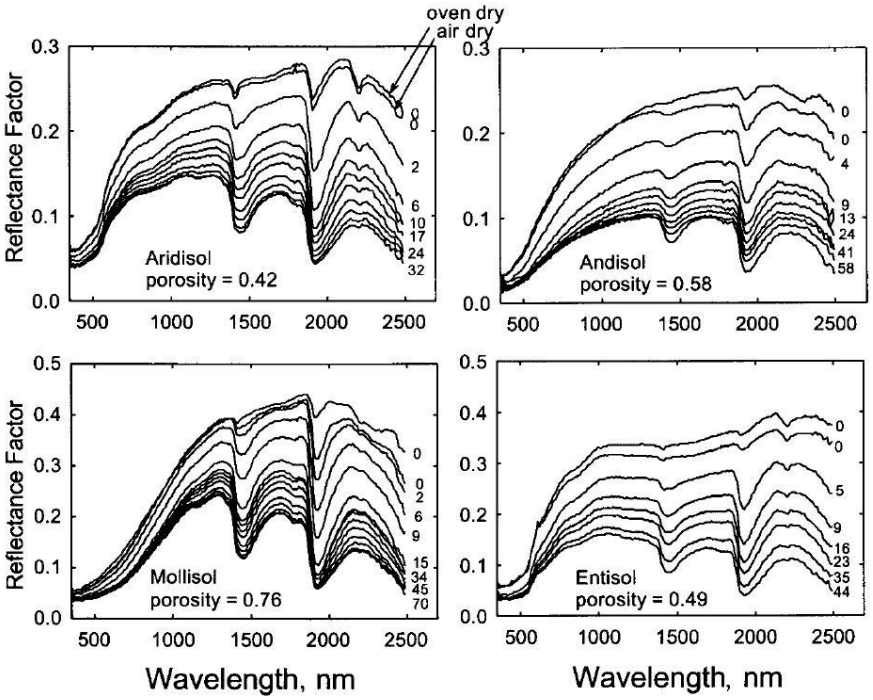

Figure 13: Four soil spectra at different volumetric water content (θ). The values of θ, in percentages by volume, are indicated next to each spectrum (source: Lobell & Asner, 2002).

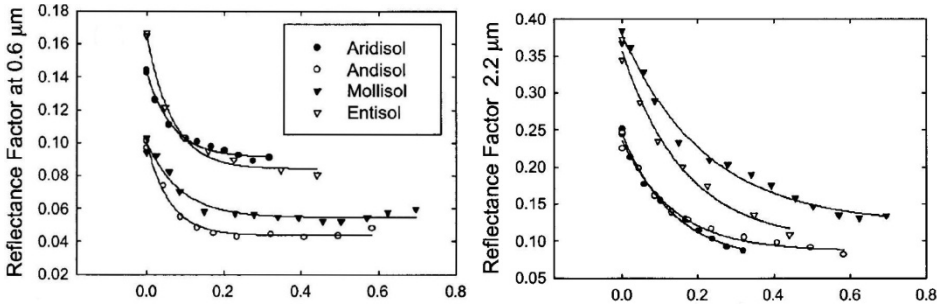

Figure 14: Changes in reflectance due to volumetric water content variations for four different soils at 600 nm (left) and 2200 nm (right), along with best fit exponential model (after Lobell & Asner, 2002)

The analysis of vegetation from remote sensors frequently passes through the use of vegetation indices (VIs; cf. section 3.6). It is therefore

important to understand the effects of background soil on these indices. Huete and Jackson (1988), for example, report an increase in NDVI values with “darker” soils under a constant amount of vegetation. The importance of this effect depends on the vegetation density, which controls the exposed fraction of bare soil, but, contrary to what might be expected, soil brightness influences intensify with increased vegetation densities up to 60% green cover (Huete *et al.*, 1985). The explanation lies on the different penetration of red and NIR radiations, wavelengths used to calculate “greenness indices”, through the vegetation canopy. While NIR can be transmitted through canopy, crossing for example up to 8 layers of cotton leaves, reflected red radiation results almost unaffected by background spectrum (Allen & Richardson, 1968; Gao *et al.*, 2000), as shown in Figure 15.

Various indices have been developed to minimize soil background effects. Most of these VIs assume that bare soil reflectance lies on a line, the so called soil line, in the space generated by the wavelength bands used to calculate the VIs. The indices are then often calculated determining the deviation with respect to this line, either as a linear or an angular distance (Baret *et al.*, 1993). Even though a mean soil line can be determined for a range of different soil classes, the identification of specific soil lines for individual soil types greatly improves the evaluation of background effects on the reflected spectra (Huete *et al.*, 1984).

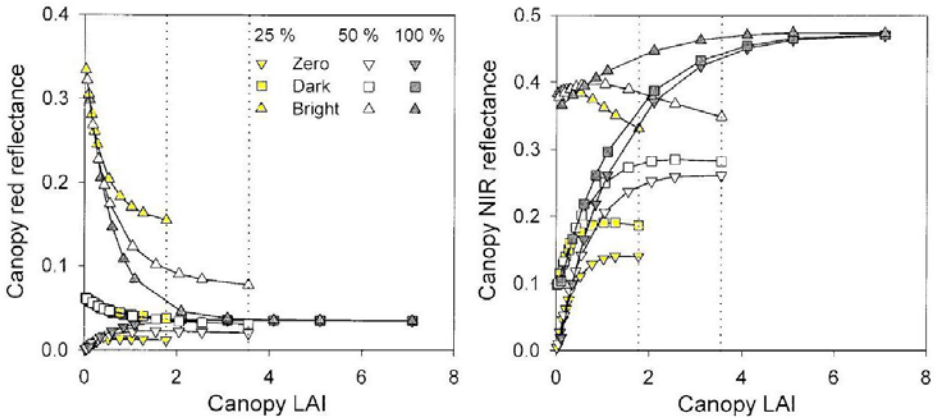

Figure 15: Relationship between canopy LAI and canopy red (620 – 670 nm) and NIR (841 – 876 nm) reflectance (after Gao *et al.*, 2000).

3.4 Atmospheric noise

The signal registered by remote sensing sensors is perturbed by the atmosphere through the absorption and scattering processes performed by the constituent particles of the atmosphere.

Absorption, on the one hand, converts the radiation into molecular excitation energy, reducing the solar radiance within the absorption bands of the atmospheric gases. As the reflected radiance is also attenuated when passing through the atmosphere, and being this attenuation wavelength-dependent, the atmospheric absorption alter the apparent spectral signature of the observed target. Scattering, on the other hand, redistributes the VIS and NIR incident energy to all directions. The consequences are haziness of the resulting image and the so called “adjacent effect”, where the reflected radiances of two regions with different brightness interfere one with the other, causing an increase in the apparent brightness of the darker region, while diminishing the apparent brightness of the brighter region.

In order, for the sensor-recorded data, to be useful to analyse the vegetation properties, the relationship between top-of-atmosphere (TOA) signal and top-of-canopy (TOC) or ground-level signal has to be established through a radiative transfer equation. The process required in the conversion from TOA to TOC signal is referred to as atmospheric correction or atmospheric compensation (Jiménez-Muñoz *et al.*, 2010).

3.5 Satellite sensors

Since the launch of Landsat 4 in 1982, sensors have been installed on board several satellites, with the objective of studying the terrestrial surface, and particularly vegetation.

Landsat satellites are equipped with Thematic Mapper sensors (TM). They perform at high spatial resolution (30 m; 120 m for thermal band) with the drawback of low temporal resolution (16 days). Data are captured in 7 spectral bands, ranging between 0.45 and 12.5 μm.

The low temporal resolution with which data are gathered may become a problem when dealing with relatively rapidly changing

processes undergone by vegetation, such as spring sprouting, particularly in regions/seasons with frequent cloud coverage. For this reason, medium spatial resolution (≥ 250 m) sensors with higher temporal resolution (1 – 2 days) are generally preferred to investigate temporal progression of seasonal vegetation development.

It is, for example, the case of Moderate-Resolution Imaging Spectroradiometer (MODIS) onboard the Terra (EOS AM) and Aqua (EOS PM) NASA satellites. The instruments collect data every 1 to 2 days in 36 spectral bands, within the spectral range 0.4 – 14.4 μm, and with spatial resolution that depends on the bands (250, 500, 1000 m).

Daily global coverage is also guaranteed by Advanced Very High Resolution Radiometer (AVHRR) and Vegetation sensors. The AVHRR sensors are found on board the NOAA family of Polar Orbiting Platforms (POES) and the EUMETSAT Met-op. The spatial resolution is 1.1 km and reflectances are registered in 5 bands, centred on 0.6, 0.9, 3.5, 11 and 12 μm. Vegetation sensors, on the other hand, are installed on SPOT satellites. The instruments measure Earth's reflectance in 4 bands, within the spectral range 0.43 – 1.75 μm. Spatial resolution is 1 km.

3.6 Remote-sensing vegetation indices

The vegetation indices (VIs) are designed to highlight specific characteristics of vegetation, combining surface reflectance at two or more wavelengths in the solar-reflected optical spectrum, and using the reflectance characteristics of leaf components and canopy structures. The majority of VIs compares red and NIR reflectances, taking advantage of the highly different response of green vegetation in these two spectral regions. VIs have been shown to be relatable to many biophysical parameters of interest, including LAI (e.g. Tucker, 1979), fractional vegetation cover (e.g. Purevdorj *et al.*, 1998), primary production (e.g. Tucker & Sellers, 1986), green leaf biomass (e.g. Gitelson *et al.*, 2003), fraction of absorbed photosynthetically active radiation (fPAR) (e.g. Myneni *et al.*, 1997), and photosynthetic activity (e.g. Gamon *et al.*, 1995).

The vegetation indices can be divided into two general classes: ratios and linear combinations. VIs may therefore be, on one hand, the simple ratio of two spectral bands or the ratio of sums, differences or products of bands and, on the other hand, the linear combination of two or more bands (Jackson & Huete, 1991). The choice of using a set of indices rather than another depends on the objective of the research and on the characteristics of the study site.

Some of the most common VIs will be discussed in the next paragraphs.

3.6.1 Simple Ratio index

First described by Jordan (1969), the Simple Ratio index (SR) is one of the most widely calculated index. It is formed by dividing the NIR radiance by the red radiance:

$$SR = \frac{NIR}{red} \qquad [1]$$

The value of this index can range from 0 to more than 30. As red reflectance decreases, the SR index increases unbounded. For this reason, a considerable precision is needed in the measurement of reflected red light, in order to obtain plausible values of the index. When reflectances are measured with adequate precision, the SR is rather sensitive to vegetation changes during the periods of maximum growth. However, the Simple Ratio index is not very responsive when vegetation is sparse (Jackson & Huete, 1991).

SR value for bare soil is usually around 1, meaning that NIR and red bands show similar reflectances. The common range for green vegetation is 2 to 8.

3.6.2 Normalized Difference Vegetation Index

The Normalized Difference Vegetation Index (NDVI) is another old, well known and highly used VI. Jackson and Huete (1991) report that Deering (1978) found that this index, equivalent to ratioing the difference between SR and 1 to the sum of SR and 1, improves the behaviour of the SR when vegetation is sparse. In terms of NIR and red band reflectance, the NDVI is calculated as:

$$NDVI = \frac{NIR - red}{NIR + red} \qquad [2]$$

This index varies between -1 and 1. Bare soils are generally characterised by very low, positive NDVI values; vegetated areas tend to show positive values, with increasing index as vegetation canopy becomes denser. Free standing water results in very low positive or even slightly negative NDVI values, while clouds and snow fields are characterized by negative values of this index.

NDVI is sensitive to green leaf biomass so that it can be primarily employed to monitor the photosynthetically active biomass of plant canopies (Tucker, 1979). The relationships between NDVI and LAI have also been studied. A nonlinear dependence and a tendency towards saturation at dense vegetation levels can be observed (Figure 16).

This relation can be expressed by Beer's general equation as in Lacaze and Hill (1996) and Gigante *et al*. (2009):

$$LAI_{NDVI} = -\frac{1}{k}\ln\frac{NDVI_{can} - NDVI}{NDVI_{can} - NDVI_{back}} \qquad [3]$$

where $NDVI_{can}$ (canopy) is the value to which NDVI tends at high vegetation density, $NDVI_{back}$ (background) is the NDVI value corresponding to very low vegetated soil and k is the extinction

coefficient. $NDVI_{can}$ and $NDVI_{back}$ may be retrieved from the NDVI images, considering the maximum and minimum values registered during the observation period (Anselmi *et al.*, 2004).

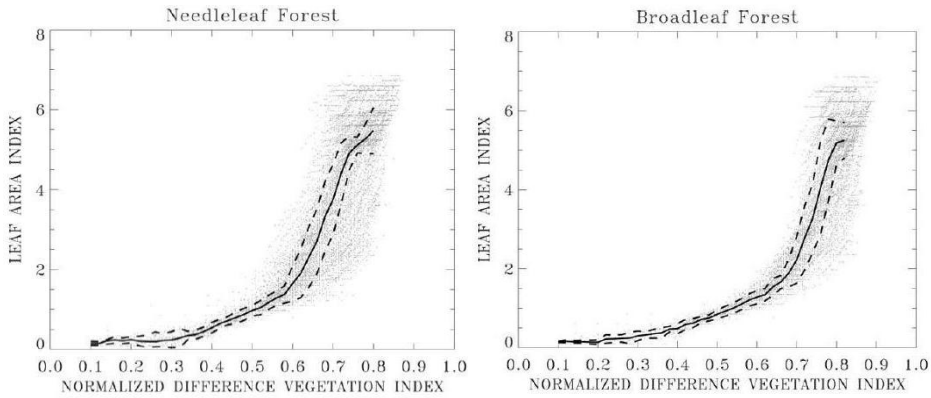

Figure 16: Scatterplot of the NDVI-LAI relationship for broadleaf and needleleaf canopies. Solid lines are regression curves that represent the mean values of a Gaussian fit for each 0.02 NDVI interval. The regression curve is the best possible prediction of LAI and also minimizes the expected squared error of the prediction of LAI given a realized value of NDVI. The upper and lower sigma boundaries are shown as dashed lines (source: Buermann *et al.*, 2002).

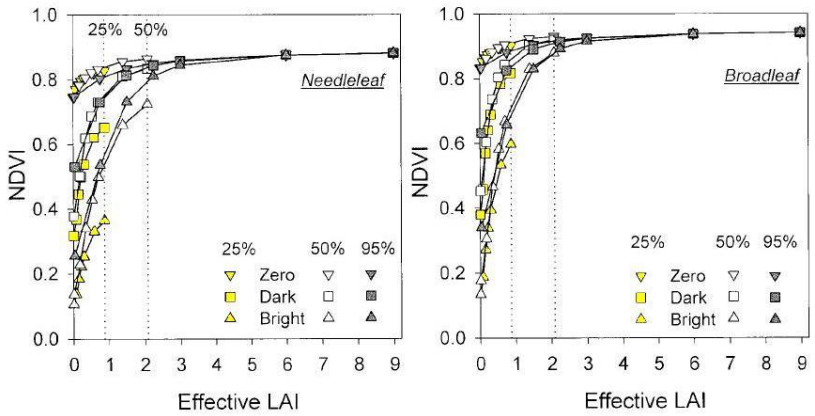

Figure 17: Relationship between effective LAI and NDVI for "zero", dark and bright soil backgrounds for needleleaf and broadleaf forest with 25%, 50% and 95% crown cover (after Gao *et al.*, 2000).

NDVI is influenced by the background soil brightness (Figure 17; see also section 3.3) while it is insensitive to the canopy structure, responding similarly to needleleaf and broadleaf forests (Huete *et al.*, 2002).

3.6.3 Enhanced Vegetation Index

The Enhanced Vegetation Index (EVI) was developed to improve the NDVI by enhancing the vegetation signal through the use of the blue band reflectance. In this way, a correction for soil background signals is performed, together with a reduction in atmospheric influences, including aerosol scattering, and an improvement in the sensitivity at high biomass concentrations. EVI is computed as follows:

$$EVI = G \cdot \frac{\left(NIR - red \right)}{\left(NIR + C1 \cdot red - C2 \cdot blue + L \right)} \qquad [4]$$

where L, C1, C2 and G are parameters that, in the MODIS-EVI algorithm, assume the values: 1; 6; 7.5; and 2.5 respectively. The value of this index ranges from -1 to 1. EVI has been found to be highly responsive to both LAI and canopy type (Gao *et al.*, 2000; Huete *et al.*, 2002).

3.6.4 Soil-Adjusted Vegetation Index

The Soil-Adjusted Vegetation Index (SAVI) was first introduced by Huete (1988) as a modification of NDVI, to correct for the influence of background soil brightness when vegetation is sparse. This correction is particularly important when comparisons are to be made across different soil types that may show different reflectance in the red and near infrared wavelengths.

SAVI is defined as:

$$SAVI = \frac{NIR - red}{NIR + red + L} \cdot (1 + L) \qquad [5]$$

where L is the soil brightness correction factor, which ranges from 0 for very high vegetation cover to 1 for very low vegetation cover. Typically, a value of 0.5 is used, suitable for intermediate vegetation cover. When L is 0, SAVI and NDVI coincide. The range of variation of this index is between -1 and 1.

As for the case of EVI, SAVI is insensitive to soil background brightness, while SAVI vs. effective LAI relationships are highly canopy structure dependent, i.e. needleleaf vs. broadleaf (Figure 18).

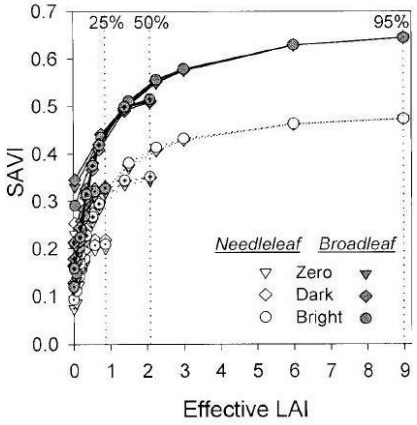

Figure 18 Relationship between effective LAI and SAVI for "zero", dark and bright soil backgrounds for needleleaf and broadleaf forest with 25%, 50% and 95% crown cover (after Gao *et al.*, 2000). The authors report that similar results were found when considering the EVI.

3.6.5 Atmospherically Resistant Vegetation Index

The Atmospherically Resistant Vegetation Index (ARVI) was developed by Kaufman and Tanre (1992). It uses the reflectance in the blue band to correct the red reflectance for atmospheric scattering and is defined as:

$$ARVI = \frac{NIR - rb}{NIR + rb} \qquad [6]$$

where $rb = red - \gamma \cdot (red - blue)$ and γ is usually equal to 1.

ARVI values' range is -1 to 1. The substitution of *red* for *rb* in any of the ratio-based indices (e.g. SAVI) gives the atmospherically resistant version of the considered index.

3.7 Other satellite products

Based on the satellite recorded reflectances, and by means of specific algorithms, the estimations of some biophysical land properties, linked to vegetation, have been made available to the scientific community. Among these, it is worth to mention the Leaf Area Index (LAI), the Fraction of Photosynthetically Active Radiation (FPAR) and the Evapotranspiration (ET) products, obtained from the MODIS observed reflectances.

3.7.1 Leaf Area Index and Fraction of Photosynthetically Active Radiation

The MODIS LAI/FPAR datasets are estimated by an algorithm that exploits the spectral information content of MODIS surface reflectances at up to 7 spectral bands, requiring at the same time a land cover classification (Myneni *et al.*, 2003). Therefore, the algorithm has interfaces with the MODIS Surface Reflectance Product (MODAGAGG) and the MODIS Land Cover Product (MOD12Q1). A three-dimensional formulation of the LAI/FPAR inverse problem underlies this procedure: observed and modelled Bidirectional Reflectance Distribution Functions (BRDFs) are compared for a suite of canopy structures and soil patterns. If modelled and observed BDRFs are not significantly different, the correspondent LAI and FPAR are accepted as true. If the main algorithm

fails, a back-up algorithm is triggered to estimate LAI and FPAR from vegetation indices.

3.7.2 Evapotranspiration

MODIS Global Evapotranspiration (ET) product (MOD16) is an estimate of global terrestrial actual evapotranspiration from earth land surface, obtained using satellite remote sensing data. The evaluation is performed using Mu et al.'s algorithm (2011) which is based on the Penman-Monteith equation (Monteith, 1965). Land cover classification, albedo, LAI and FPAR information, necessary for the calculations, are obtained from the MODIS Land Cover Product (MOD12Q1), the MODIS Land Surface Albedo Product (MOD43B3) and the MODIS LAI and FPAR Product (MOD15A2) respectively. Meteorological inputs (i.e. air pressure, air temperature, radiation and humidity) are also used by the algorithm.

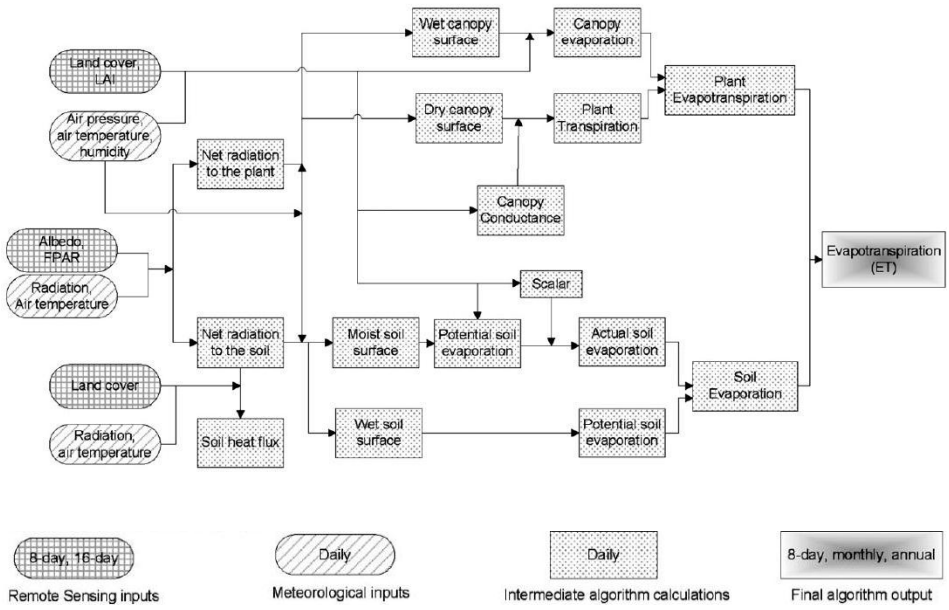

Figure 19: Flowchart of the MODIS Evapotranspiration (ET) algorithm. LAI: leaf area index; FPAR: fraction of photosynthetically active radiation (source: Mu *et al.*, 2011).

4 Description of the implemented vegetation models

Eykhoff (1974) defined a model as "...a representation of the essential aspects of an existing system (or a system to be constructed) which presents knowledge of that system in a usable form". A mathematical model is therefore a simplified representation of reality, which describes a system through a set of equations, parameters and state variables. In particular, a vegetation model is a mathematical model that aims to reproduce some characteristics of plant development and behaviour. Depending on the purpose of the modelling, the hypothesis made, the physiological processes considered and the modelling scale (both spatial and temporal) will be different. The hydrological models, on the other hand, are designed to reproduce the hydrological cycle within a catchment. Considering the tight interconnection between the water cycle and the vegetation processes, particularly in water controlled ecosystems, the coupling of vegetation and hydrological models might be essential for an adequate reproduction of the vegetation state at basin scale.

4.1 Simple versus complex models

When building a mathematical model to be representative of a system of interest, the first impulse is to include as many details as possible, in order to improve the description of the processes involved, and to obtain this way a better representation of the system. The tendency is therefore towards complex models. But while complex models have the advantage of relying on the best up-to-date knowledge of the considered system, the risk is to try to build a full-scale map of the World[1]. Complex models tend to be difficult to be implemented and imply a considerable computational burden (e.g. Cayrol *et al.*, 2000; Montaldo *et al.*, 2005). Also, the high number of parameters included in the models, which has to be estimated, requires high amounts of field data, rarely available particularly in natural science investigations (e.g. Montaldo *et al.*, 2003). Finally, the fact that these models are so detailed tends to give the impression that results are absolutely reliable, dozing off the user's critical spirit.

Simple models, on the other hand, are usually quicker to build and easier to implement, interpret and update. Their relative transparency allows the user to adapt them to the particular characteristics of the considered system and parameters are fewer and of easier estimation. Undoubtedly, the risk is to simplify processes too much, so that instead of a simple model, a simplistic and completely unreliable model is implemented. To avoid this chance, it is essential that the most important processes of the system are identified and reproduced satisfactorily.

In this regard, Montaldo et al. (2005) analysed five variants of a vegetation dynamics model (VDM) included in a land surface model

[1] "Del rigor en la ciencia", Jorge Luis Borges

En aquel Imperio, el Arte de la Cartografía logró tal Perfección que el Mapa de una sola Provincia ocupaba toda una Ciudad, y el Mapa del Imperio, toda una Provincia. Con el tiempo, estos Mapas Desmesurados no satisficieron y los Colegios de Cartógrafos levantaron un Mapa del Imperio, que tenía el Tamaño del Imperio y coincidía puntualmente con él. Menos adictas al Estudio de la Cartografía, las Generaciones Siguientes entendieron que ese dilatado Mapa era Inútil y no sin Impiedad lo entregaron a las Inclemencias del Sol y los Inviernos. En los Desiertos del Oeste perduran despedazadas Ruinas del Mapa, habitadas por Animales y por Mendigos; en todo el País no hay otra reliquia de las Disciplinas Geográficas.

Suárez Miranda: *Viajes de varones prudentes*, Libro cuarto, cap. XLV, Lérida, 1658.

(LSM), starting with the most complex one and gradually reducing the VDM complexity and parameterization. The five variants are as follows:

a) CVM, the complete VDM, which simulates three compartments of biomass (i.e. green aboveground, living root and standing dead). The number of parameters is 20, including 7 from the LSM;

b) SVM1, a simplified version of CVM (also with 20 parameters), which simulates the three biomass compartments but uses a simplified equation for photosynthesis computation;

c) SVM2, a simplified version of SVM1, which does not explicitly treat root biomass. The number of parameters is 15, of which 6 from LSM;

d) SVM3, a simplified version of SVM2, which only simulates green biomass. It has 13 parameters, including 6 from the LSM;

e) SVM4, a simplified version of SVM3, in which both senescence and respiration biomass loss terms are comprised into a single term, linearly related to biomass. The total number of parameters is 10 (6 from the LSM).

The comparison between the results of the five model versions and field data revealed that the complete model and the simplified models from number 1 to number 3 performed well and similarly. The SVM4, on the other hand, failed to capture plant respiration dynamics and therefore appeared to have an oversimplified structure. The authors concluded that SVM3 is a good compromise reconciling a low number of parameters with a satisfactory simulation of LAI dynamics and land surface fluxes.

Commonly, vegetation and hydrological models are either physically based or conceptual. A physically based model, or deterministic model, is based on complex physical theory and requires a large amount of data and computational time (Jajarmizadeh *et al.*, 2012). Conceptual models, instead, are composed by a number of conceptual elements which are simple representations of a reference system. When dealing with highly complex systems, like water-vegetation ones in semi-arid climates, the poor level of understanding and/or observation of the processes involved makes conceptual modelling powerful, while the frequently limited available information requires a parsimonious approach.

Keeping in mind these needs, HORAS (Quevedo & Francés, 2008; Quevedo, 2010), a conceptual parsimonious vegetation model, was developed by the Research Group of Hydrological and Environmental Modelling at Universitat Politècnica de València. Considering the not entirely satisfactory results obtained by HORAS, the model was at first modified (Pasquato, 2011) and subsequently abandoned in favour of a modelling approach that, despite the fact of being founded on a conceptual scheme, maintains a certain connection with physiological processes. Two approaches to dynamic vegetation modelling were finally compared, to evaluate their ability to simulate the evolution of carbon and water exchange processes in a semi-arid region.

4.2 HORAS

4.2.1 General conceptualization

HORAS is a conceptual tank-type model. The water balance is determined at each time step considering a system of two-storage tanks, representative, on the one hand, of canopy-intercepted water, and on the other hand of water accumulated in the effective root soil depth (Figure 20). Simulations are performed with a daily time step, on a per unit ground area basis, and the dynamics of vegetation biomass are modelled through a mass balance. Equations are solved with finite difference approximations, using at each time step the variable values calculated at the previous time step. Considering that in semi-arid climates vegetation processes are mainly controlled by water availability, vegetation growth is linked to the ratio between transpiration and possible maximum transpiration, while leaf shedding depends on water stress and on the seasonal cycle when deciduous species are involved.

Soil moisture in the effective root zone (H) is the result of the balance between incoming precipitation (P) minus canopy interception (I) and the losses produced by evaporation from bare soil (E), transpiration (T), and excess water (leakage plus runoff, L) (Figure 20).

The effective root soil depth is implicated in the processes of bare soil evaporation and root transpiration. Actual evapotranspiration is

based on potential rate (ET_o), corrected by a water stress function. The model is forced by daily inputs, namely precipitation and ET_o.

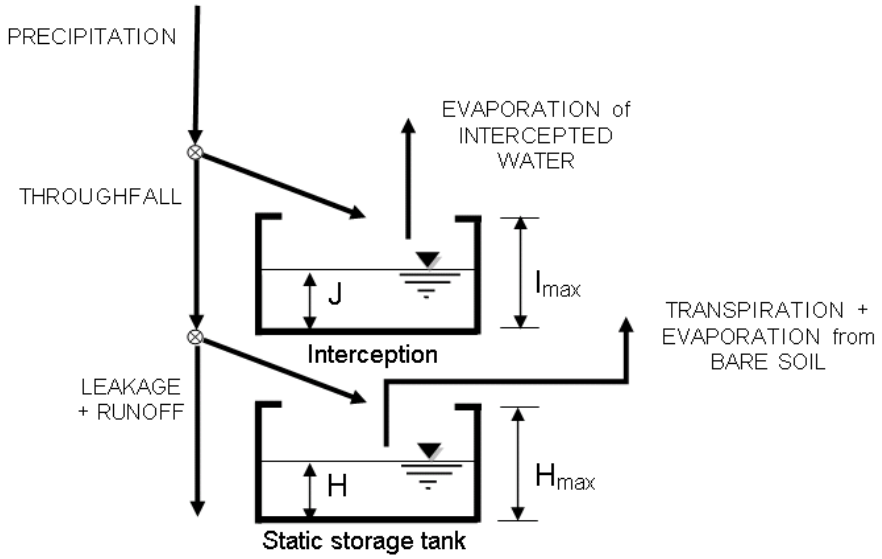

Figure 20: HORAS model general structure.

4.2.2 Vegetation dynamics

The modelled state variable is R, relative foliar biomass, whose value spans from 0 to 1. When no vegetation is present on the area, R is equal to 0 and soil moisture is completely available to bare soil evaporation processes. R's value is 1 when vegetation has reached its maximum possible development: there is no bare soil evaporation and transpiration is as high as soil moisture and ET_o permit. R is equivalent to FAO's crop coefficient (Allen *et al.*, 1998), but instead of being purely a function of the plant development stage, it is a state variable. R's dynamics are controlled by:

$$\frac{dR}{dt} = \frac{A_{n,mx}}{B_{pot}} \left(\frac{T}{T_{mx}} \right)^{c} - k_{se} \cdot R - k_{ws} \cdot R \cdot \zeta \qquad [7]$$

where $A_{n,mx}$ is the maximum net carbon assimilation (kg C m^{-2} d^{-1}), B_{pot} is the potential foliar biomass (kg C m^{-2}), T is transpiration (mm d^{-1}), T_{mx} is maximum transpiration (mm d^{-1}) and depends on vegetation type, c (-) is a shape exponent, k_{se} is the season-dependent leaf shedding coefficient, k_{ws} is the water stress–dependent leaf shedding coefficient and ζ (-) is the water stress (see section 4.2.3).

4.2.3 Water balance terms

Water balance is performed daily for the two tanks representing the canopy water interception and the effective root zone moisture storage. The amount of intercepted water is referred to as I (mm H_2O), while the water depth accumulated in the static tank is H (mm H_2O):

$$\frac{dH}{dt} = \left(P - I\right) - L - E - T \qquad [8]$$

where t is time (d), P is precipitation, I is canopy interception, L is leakage and runoff, E is bare soil evaporation, and T is plant transpiration, all with units of mm d^{-1} per unit of ground area. Ponding is not considered because the research area is sufficiently sloping as to avoid the accumulation of water on the surface while the presence of trees facilitates infiltration. A distributed hydrological simulation with Tetis model (Francés *et al.*, 2007) showed that in the study area these two processes are negligible (unpublished data).

Interception follows:

$$I = \min\left(P \cdot R, I_{\max} \cdot R - J\right) \qquad [9]$$

where I_{max} is the maximum possible leaf water interception (mm d^{-1}), R is the relative foliar biomass and J (mm) is the interception storage:

$$\frac{dJ}{dt} = I - \min\left(ET_o \cdot R, J\right) \qquad [10]$$

Leakage + runoff (*L*) is calculated as an "overflow" from the soil compartment, as in the cascading bucket models: when water depth of the soil layer exceeds the maximum storage capacity for that zone (H_{max}), the excess of water either percolates out of the effective root depth or is transformed in runoff.

Plant transpiration (*T*) is modelled taking into account the reduction of available energy due to evaporation of intercepted water (E_i):

$$T = \min\left(ET_o \cdot R \cdot \beta_t, ET_o - E_i, H\right) \qquad [11]$$

where β_t is the water limitation function for trees. The soil water limitation function is (Figure 21):

$$\beta\left(H\right) = \begin{cases} 1 & \text{for } H \geq H_{cr} \\ \left(\dfrac{H - H_{\lim}}{H_{cr} - H_{\lim}}\right)^q & \text{for } H_{\lim} < H < H_{cr} \\ 0 & \text{for } H \leq H_{\lim} \end{cases} \qquad [12]$$

where H_{lim} and H_{cr} are the water storages (mm) corresponding respectively to the wilting point and the critical point, below which transpiration is limited (Laio *et al.*, 2001); *q* is a measure of the nonlinearity of the effects of soil moisture deficit on plant condition (Porporato *et al.*, 2001) and differs by species and might vary even among individuals (Rodriguez-Iturbe *et al.*, 1999). As an example, in drought tolerant species that adopt a water-saving strategy (e.g. Pinus halepensis Mill.), stomata opening is reduced before leaf water potential

suffers any change (Baquedano & Castillo, 2006), generating a nonlinearity in the plant response to soil moisture shortage. In that case, a value of 3 for the parameter *q* is considered appropriate.

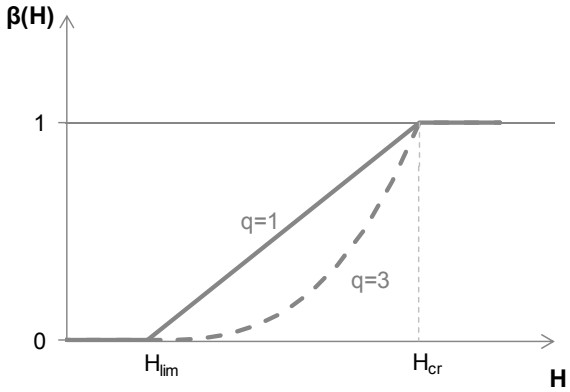

Figure 21: Soil water limitation function for two values of nonlinearity parameter values (q = 1and q = 3).

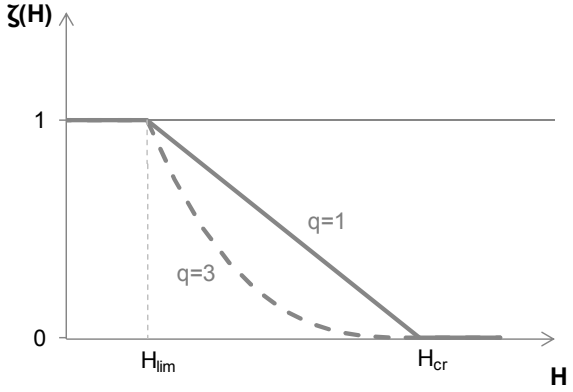

Figure 22: Water stress function for two values of nonlinearity parameter values (q = 1and q = 3).

Similarly, the water stress function (Figure 22) is defined as (Porporato *et al.*, 2001):

$$\zeta(H)=\begin{cases} 0 & \text{for } H \geq H_{cr} \\ \left(\dfrac{H_{cr}-H}{H_{cr}-H_{\lim}}\right)^{q} & \text{for } H_{\lim} < H < H_{cr} \\ 1 & \text{for } H \leq H_{\lim} \end{cases} \quad [13]$$

The power function proposed by Clapp and Horberger (1978) is used to obtain soil water content at specific soil states (typically at wilting point and critical point):

$$\psi = \psi_{ae} \cdot \left(\frac{n}{H}\right)^{b} \quad [14]$$

where Ψ (MPa) is the matric potential at the analyzed state, Ψ_{ae} (MPa) is the air entry matric potential, n is porosity, b is an index related to porosity distribution and H is the soil water content (mm). The representative hydraulic parameters values for each soil texture are reported in Table 1. For limit and critical points, Ψ assumes the values 3 and 0.03 MPa respectively (Laio *et al.*, 2001).

The choice of the Ψ_{cr} value was particularly controversial as different and contrasting values are reported in literature. Some authors have directly measured the soil water potential at critical point (e.g. Gollan *et al.*, 1986; Hensley & Deputy, 1999), others have reported the percentages of available soil moisture in correspondence of a decline in plant transpiration (e.g. Bates & Hall, 1981; Dingman, 2008), or estimated xylem and leaf water potential (e.g. Maherali *et al.*, 2004; Scoffoni *et al.*, 2011) at critical point and in relation with air embolism. In this context, it is important to note that leaf and soil water potentials are not necessarily correlated under water deprivation conditions (e.g. Bates & Hall, 1981; Gollan *et al.*, 1986). In addition, Ψ_{cr} is a characteristic that highly depends on the behaviour of the considered species with respect to water limitation conditions (see paragraph 2.4.2 regarding isohydric and unisohydric species).

Soil texture	Ψ_{ae} [MPa]	n	b
Sand	3.42 e-04	0.395	4.05
Loamy sand	1.74 e-04	0.410	4.38
Sandy loam	7.01 e-04	0.435	4.90
Silt loam	5.5 e-03	0.485	5.30
Loam	1.43 e-03	0.451	5.39
Sandy clay loam	8.43 e-04	0.420	7.12
Silty clay loam	1.43 e-03	0.477	7.75
Clay loam	3.53 e-03	0.476	8.52
Sandy clay	6.02 e-04	0.426	10.4
Silty clay	1.70 e-03	0.492	10.4
Clay	1.82 e-03	0.482	11.4

Table 1: Representative values for hydraulic parameters (Clapp & Hornberger, 1978): air matric potential (Ψ_{ae}), porosity (n), soil parameter (b).

The Australian Department of Environment and Primary Industries (DEPI, 2008) recommends the use of values between 0.05 and 0.07 MPa for critical soil water potential for crops in the semi-arid Shepparton Irrigation Region. Hensley and Deputy (1999) report the readings of tensiometers at water stress starting conditions for turfgrasses and landscape plants in Hawaii, differentiating between sandy soils and aggregated clays (Ψ_{cr} = 0.03 MPa) and non aggregated clays (Ψ_{cr} = 0.07 MPa). Gollan et al. (1986) compare Ψ_{cr} values for sunflower (0.07 MPa) and wheat (0.3 MPa). Finally, the value 0.03 was chosen for this thesis, in accordance with Laio et al. (2001), and taking into account the fact that the considered species (Pinus halepensis) presents a “water-saver” behaviour (see section 2.4.2).

Bare soil evaporation is modelled as occurring from a shallow superficial soil layer whose depth is z_{ss}, not higher than 15 cm. In HORAS, it is considered that this layer has the same properties as the entire effective root layer (depth z_e), and therefore the same soil moisture. Bare soil evaporation is computed as:

$$E = \min\left[H \cdot \left(\frac{z_{ss}}{z_e} \right) \cdot (1 - R), ET_o - E_i - T \right] \qquad [15]$$

4.3 WUE and LUE models

4.3.1 General conceptualization

The tested WUE and LUE models follow a tank-based scheme (Figure 23) similar to the one used for the HORAS model. Simulations are, again, performed with a daily time step, on a per unit ground area basis and equations are solved with finite difference approximations. The dynamics of vegetation biomass are in both cases modelled through a mass balance; in one case growth is based on transpiration (T) and takes into account the Water Use Efficiency (WUE) factor (Williams & Albertson, 2005; Istanbulluoglu *et al.*, 2012); in the other case carbon uptake is based on photosynthesis, simulated through the Absorbed Photosynthetically Active Radiation (APAR) and the Light Use Efficiency (LUE) factor (Arora, 2002; Polley *et al.*, 2011).

Both approaches consider respiration in order to estimate net primary production. Part of this total production is allocated to leaves, according to the maximum leaf biomass that can be sustained by the system. The modelled state variable is leaf biomass (B_l, kg DM m^{-2} vegetation cover; where DM denotes dry matter) from which leaf area index (LAI_{mod}, m^2 leaf m^{-2} ground) can be calculated by means of the specific leaf area (SLA, m^2 leaf kg^{-1} DM) and the fraction of vegetated area (f_t, m^2 vegetation cover m^{-2} ground), providing the possibility to compare models results with satellite products. Turnover, caused by leaf ageing, is then taken into account.

Real structural LAI changes more slowly than remotely sensed NDVI, which reflects chlorophyll and leaf angle adjustments before loss of structural tissues and leaf drop. In fact, Mediterranean summer drought is reported to induce a generalized decrease in chlorophyll, as a mechanism of protection (Kyparissis *et al.*, 1995). In particular, Aleppo pine showed a 25% reduction in chlorophyll content when a 30 month

water stress treatment was applied, maintaining soil water potential at -400 kPa (Baquedano & Castillo, 2006). For this reason, to compare model results with LAI_{NDVI}, it is advisable to scale LAI_{mod} by vegetation water stress, as in Sellers et al. (1996) and Williams and Albertson (2005), obtaining in this way LAI^*_{mod} (m^2 green leaf m^{-2} ground). Considering the properties of the models outputs and of the available satellite indexes, it appears suitable to compare LAI_{mod} with EVI, the latter being very responsive to structural LAI, and also LAI^*_{mod} with LAI_{NDVI}.

As in HORAS model, soil moisture in the effective root zone is the result of the balance between incoming precipitation (P) and leaf interception (I), the losses produced by evaporation from bare soil (E), transpiration (T) and the sum of soil leakage and runoff (L) (Figure 23).

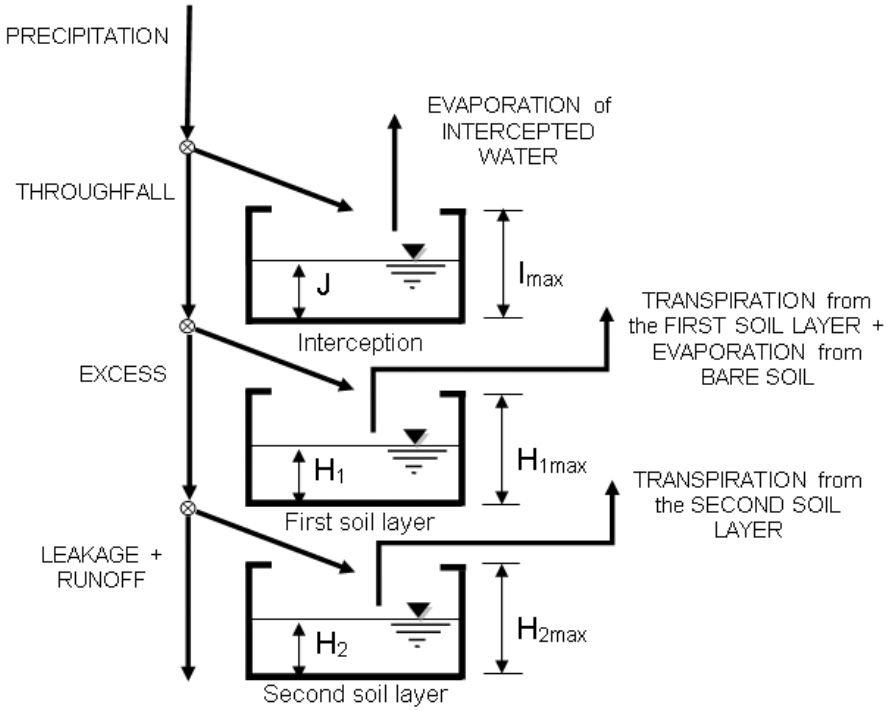

Figure 23: WUE and LUE vegetation models general structure.

The involved soil depth is divided into two layers: a shallow layer that is implicated in the processes of bare soil evaporation and superficial roots transpiration, and a second, underlying layer that provides soil moisture to deeper roots. Actual evapotranspiration (ET_o) is based on potential rate, corrected by a water stress function. Models are forced by daily inputs of precipitation and ET_o.

4.3.2 Carbon balance for WUE-model

Similar to Williams and Albertson (2005), the leaf biomass dynamics are modelled as:

$$\frac{dB_l}{dt} = \left(T \cdot WUE \cdot \rho_v \cdot \omega - \mathrm{Re}\right) \cdot \varphi_l - k_l \cdot B_l \qquad [16]$$

where B_l is the leaf biomass (kg DM m^{-2} vegetation cover) and k_l is leaf natural turnover factor. φ_l is fractional leaf allocation and *Re* is respiration, each described in section 4.3.5. ρ_v and ω are the density of water (Mg m^{-3}) and the conversion of CO_2 exchange to dry matter (kg DM kg^{-1} CO2), needed to convert the units. WUE (kg CO_2 kg^{-1} H_2O) is calculated with air diffusivities of CO_2 and H_2O vapour, ambient CO_2 concentration and saturated specific air humidity dependence as in Williams and Albertson (2005):

$$WUE = \frac{g_c\left(1-\alpha\right)C_a}{g_v\left(q^*-q\right)}\mu \qquad [17]$$

where g_c and g_v are air diffusivities of CO_2 and H_2O vapour (m^2s^{-1}), α is the ratio of intercellular to ambient CO_2 concentration, C_a is ambient CO_2 concentration (μmolCO_2 mol^{-1}air), q^* and q are saturated and actual specific humidity of air (kg H_2O kg^{-1}air), μ clears the units ($1.5 \cdot 10^6$ gCO_2 g^{-1}air).

This model is built on the hypothesis that water is the limiting factor for vegetative growth: the assumption made is that the control performed on transpiration by soil moisture can be shifted to growth, so that it results in growth itself being controlled only by water availability. Consequently, the very basis of this model makes it appropriate only for simulations in arid and semi-arid climate, excluding any environment where factors, other than water availability, control vegetation development.

4.3.3 Carbon balance for LUE-model

It has been hypothesised (Monteith, 1972; Monteith & Moss, 1977; Jarvis *et al.*, 1983) that there should be a strong positive relationship between plant biomass production by terrestrial vegetation and absorbed photosynthetically active radiation in ideal conditions (Medlyn, 1998). The proportionality between dry matter production and light absorption is known as light use efficiency (LUE; kg DM m^{-2} MJ^{-1}), and this relationship has been widely used in vegetation modelling (e.g. Knorr & Heimann, 1995; Ruimy *et al.*, 1999; Montaldo *et al.*, 2005). Stress conditions, such as water or nutrient deficit, tend to diminish LUE value (Green *et al.*, 1985; Li *et al.*, 2008) so that a correction factor has to be applied.

The second tested model simulated the leaf biomass (B_l, kg DM m^{-2} ground) as follows:

$$\frac{dB_l}{dt} = \left(LUE \cdot \varepsilon \cdot PAR \cdot FPAR - \mathrm{Re}\right) \cdot \varphi_l - \kappa_l \cdot B_l \qquad [18]$$

where ε takes into account the reduction in LUE due to stress sources. In this study, because of the semiarid climate, the water deficit was considered dominant over other causes of stress; hence ε is calculated as:

$$\varepsilon = 1 - \zeta \qquad [19]$$

where ζ is water stress obtained by equation [13]. As in the WUE-model, *Re*, φ_l and k_l are respiration, fractional leaf allocation and leaf natural decay factor respectively, and are described in paragraph 4.3.5. Monthly averaged Photosynthetically Active Radiation (PAR) was obtained from the incident global radiation provided by the World Radiation Data Centre using a constant ratio of 0.48 MJ (PAR) MJ^{-1} (global radiation) (McCree, 1972). The total fraction of incident PAR absorbed by the canopy (FPAR) was estimated with a Beer-Lambert law:

$$FPAR = 0.95 \cdot \left[1 - \exp\left(-k \cdot LAI_{\text{mod}}\right)\right] \qquad [20]$$

where *k* is the light extinction coefficient over foliage elements and LAI_{mod} is the leaf area per ground area.

4.3.4 Water Balance Terms

Water balance is performed daily for the two superimposed layers into which the effective root zone is divided, similar to Scanlon and Albertson (2003): a surficial layer, with thickness d_1 (mm) and water content H_1 (mm H_2O), and a deep layer, with thickness d_2 (mm) and water content H_2 (mm H_2O):

$$\frac{dH_1}{dt} = \left(P - I\right) - D - E - T_1 \qquad [21]$$

$$\frac{dH_2}{dt} = D - L - T_2 \qquad [22]$$

where *t* is time (d), *P* is precipitation, *I* is leaf interception, *D* is vertical water flux from the first to the second soil compartment, *L* is leakage + runoff, *E* is bare soil evaporation, *T1* and *T2* are plant transpiration from the superficial and the deep layer respectively, all with

units of mm d^{-1} per unit of ground area. The process of bare soil evaporation has access to the soil moisture of the surficial zone, while plants can use water from both zones, in proportion to the root density in each one. As in the simulations with HORAS, ponding is not considered because it was shown that in the study area this process is negligible (cf. section 4.2.3).

Interception follows:

$$I = \min\left(P \cdot f_t, I_{\max} \cdot f_t - J\right) \qquad [23]$$

where I_{max} is the maximum possible leaf water interception (mm d^{-1}), f_t is the fractional cover (% of vegetated soil) and J is the interception storage (mm), which is subjected to evaporation:

$$\frac{dJ}{dt} = I - \min\left(ET_o \cdot f_t, J\right) \qquad [24]$$

Vertical soil water flux (D) and leakage plus runoff (L) are calculated as "overflows" from the first and the second soil compartments respectively, as in the cascading bucket models: when water thickness of a soil layer exceeds the maximum storage capacity for that zone (H_{1max}, H_{2max}), the excess of water flows to the following soil layer (D, from layer 1 to layer 2) and either percolates out of the effective root depth or is transformed into runoff (L, when storage capacity of layer 2 is exceeded). Bare soil evaporation is simulated as:

$$E = ET_o \cdot f_b \cdot \beta_b\left(H_1\right) \qquad [25]$$

where $f_b = 1 - f_t$ is the bare soil fraction and β_b is the bare soil water limitation function.

Plant transpiration ($T=T_1+T_2$) is modelled taking into account the reduction of available energy due to evaporation of intercepted water:

$$T_1 = \left[ET_o \cdot f_t - \min\left(ET_o \cdot f_t, J \right) \right] \cdot \min\left(LAI_{\mathrm{mod}}, 1 \right) \cdot \beta_t\left(H_1 \right) \cdot r_1 \qquad [26]$$

$$T_2 = \left[ET_o \cdot f_t - \min\left(ET_o \cdot f_t, J \right) \right] \cdot \min\left(LAI_{\mathrm{mod}}, 1 \right) \cdot \beta_t\left(H_2 \right) \cdot \left(1 - r_1 \right) \qquad [27]$$

where LAI_{mod} is the simulated leaf area index, β_t is the water limitation function for trees and r_1 is the fraction of tree roots in the upper soil layer.

The soil water limitation function is:

$$\beta_j\left(H_i \right) = \begin{cases} 1 & \text{for } H_i \geq H_{i,cr} \\ \left(\dfrac{H_i - H_{i,\mathrm{lim}}}{H_{i,cr} - H_{i,\mathrm{lim}}} \right)^m & \text{for } H_{i,\mathrm{lim}} < H_i < H_{i,cr} \\ 0 & \text{for } H_i \leq H_{i,\mathrm{lim}} \end{cases} \qquad [28]$$

where subscript *j* (= *b* or *t*) indicates bare soil or tree land cover respectively, and it is linked to exponent *m* (= 1 for bare soil; = 3 for vegetation). Subscript *i* (= 1 or 2) refers to the soil layer involved. H_{lim} and H_{cr} are the water storages (mm) corresponding respectively to the wilting point and the critical point, below which transpiration is limited (Laio *et al.*, 2001). Water storage values are obtained multiplying soil depth (d_1 and d_2) by soil moisture. The power function proposed by Clapp and Horberger (1978) is used to obtain soil moisture (θ, m^3 H_2O m^{-3} soil) at specific soil states (see section 4.2.3).

4.3.5 Carbon Balance Terms

The carbon balance equations specific for each model tested are discussed in sections 0 and 4.3.3. In this section, the common terms for both models will be presented. Maintenance respiration (*Re*, kg DM m^{-2} d^{-1}) is calculated as in Sitch et al. (2003) based on tissue specific C:N ratios, air temperature, tissue biomass and phenology:

$$\mathrm{Re} = r \cdot \frac{C}{cn} \cdot \phi \cdot g\left(T\right) \qquad [29]$$

where *r* is tissue respiration rate, assumed to be 0.066 g C g^{-1} N d^{-1}, C is carbon, N is nitrogen, *cn* is the C:N ratio, variable between 40 and 80 in leaves (*cn* = 80 in pine needles), Φ is leaf phenological status, whose value is 1 for evergreen vegetation. *g(T)* is defined as:

$$g(T) = \exp\left[308.56 \cdot \left(\frac{1}{56.02} - \frac{1}{T + 46.02}\right)\right] \qquad [30]$$

where *T* is temperature (ºC).

Part of the daily net primary production (*NPP*, kg DM m^{-2}), namely $\left(LUE \cdot \varepsilon \cdot PAR \cdot FPAR - \mathrm{Re}\right)$ for the LUE-model, $\left(T \cdot WUE \cdot \rho_v \cdot \omega - \mathrm{Re}\right)$ for the WUE-model, is allocated to leaves through the fractional leaf allocation factor φ:

$$\varphi = 1 - \frac{LAI}{LAI_{\max}} \qquad [31]$$

where *LAI* is the simulated leaf area index within vegetated areas and LAI_{max} (m^2 leaf m^{-2} vegetated area) is the maximum LAI supported

by the system, considering the plant species and the type of environment. In the case of Mediterranean ecosystems, for example, LAI is the main component of water use regulation (Llorens *et al.*, 2011) and is therefore highly connected with average climatic conditions for each study site.

The assumption underlying this allocation scheme is that assimilated carbon is directly employed to allow structural growth. In fact, a considerable percentage of net canopy carbon assimilate is firstly allocated to a labile carbon pool, mainly comprised of non structural carbohydrates, rather then directly to structural NPP (e.g. Hoch *et al.*, 2003; Körner, 2003; Gough *et al.*, 2009). Future modelling efforts will be directed to include, even if in a simplified way, a reserve pool to better mimic the carbon assimilation processes.

Leaf area index within vegetated areas is simulated through the specific leaf area factor (*SLA*, m^2 leaf kg^{-1} leaf DM):

$$LAI = B_l \cdot SLA \qquad [32]$$

To obtain ground based leaf area index (LAI_{mod}, m^2 leaf m^{-2} ground) it is necessary to scale *LAI* by the vegetation fractional cover:

$$LAI_{\mathrm{mod}} = LAI \cdot f_t \qquad [33]$$

In addition, to make LAI_{mod} comparable with the *LAI* obtained from NDVI, average plant water stress of the previous 10 days ($\overline{\zeta}_{10}$) is taken into account as in Williams & Albertson (2005):

$$LAI^*_{\mathrm{mod}} = LAI_{\mathrm{mod}} \cdot \left(1 - \overline{\zeta}_{10}\right) \qquad [34]$$

This is because NDVI is influenced by leaf water content (Dawson *et al.*, 1998), due to changes in chlorophyll content, as discussed in section 3.2 and 6.2. Also, and subjected to soil type, it is possible that a change of soil colour occurs due to a change in soil moisture (cfr. 3.3). In this case, and depending on soil vegetation fractional cover, NDVI values might be further influenced by soil moisture, making the *LAI* values correction essential.

The water stress ζ is obtained as in Porporato et al.(2001):

$$\zeta\left(H_i\right)=\begin{cases} 0 & \text{for } H_i \geq H_{i,cr} \\ \left(\dfrac{H_{i,cr}-H_i}{H_{i,cr}-H_{i,\lim}}\right)^3 & \text{for } H_{i,\lim} < H_i < H_{i,cr} \\ 1 & \text{for } H_i \leq H_{i,\lim} \end{cases} \qquad [35]$$

where index *i* (= 1 or 2) identifies the shallower or the deeper soil layer.

Vegetation total water stress ζ is calculated as:

$$\zeta\left(H_1\right)\cdot r_1+\zeta\left(H_2\right)\cdot\left(1-r_1\right) \qquad [36]$$

5 Study area

The research site is a 20 km^2 Aleppo pine (Pinus halepensis Mill.) open forest in the Valdeinfierno catchment, south west of the Valdeinfierno reservoir, south east of Spain, in the province of Almeria (Figure 24 and Figure 25). The area is centred in 37º46'N, 2º00'O. Altitude is between 850 and 1350 m msl. The soil is a dolomitic lime.

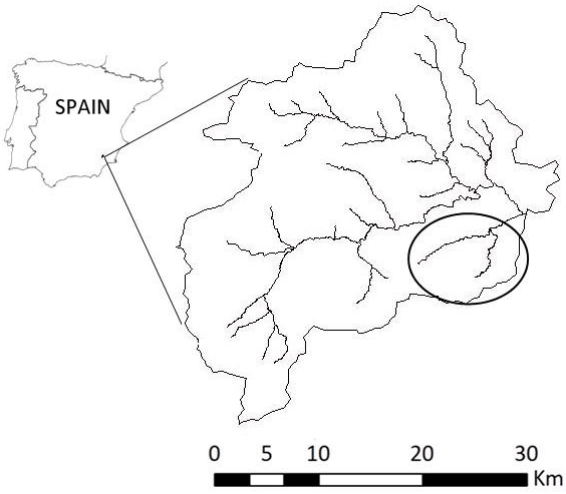

Figure 24: Location of the Valdeinfierno catchment within the Spanish territory and of the Aleppo pine forest within the catchment.

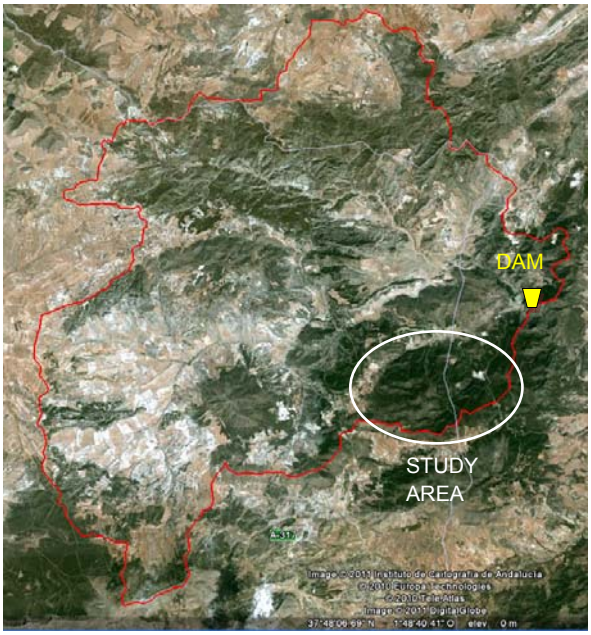

Figure 25: Satellite photography of the Valdeinfierno catchment (2011 Digital Globe; 2010 Tele Atlas; 2011 Instituto de Cartografía de Andalucía). The locations of the Valdeinfierno dam (yellow) and of the study area (white) are highlighted.

5.1 Precipitation data

The precipitation (P) records for the Valdeinfierno dam's weather station (1º 57' 51" W; 37º 48' 22" N) were analysed over the period January 1933 – June 2011. Rainfall occurs typically in autumn and spring and the average annual precipitation was 327 mm, having fluctuated between 99 mm (A.D. 1945) and 884 mm (A.D. 1989). In the considered period, anyway, the annual precipitation spans between 100 and 500 mm, if the abovementioned extremes are not considered (Figure 26). The most frequent value for annual precipitation lies in the interval 300 – 400 mm, to which the relative frequency of 0.35 is associated (Figure 27). The years with incomplete precipitation records are not taken into consideration in these statistics.

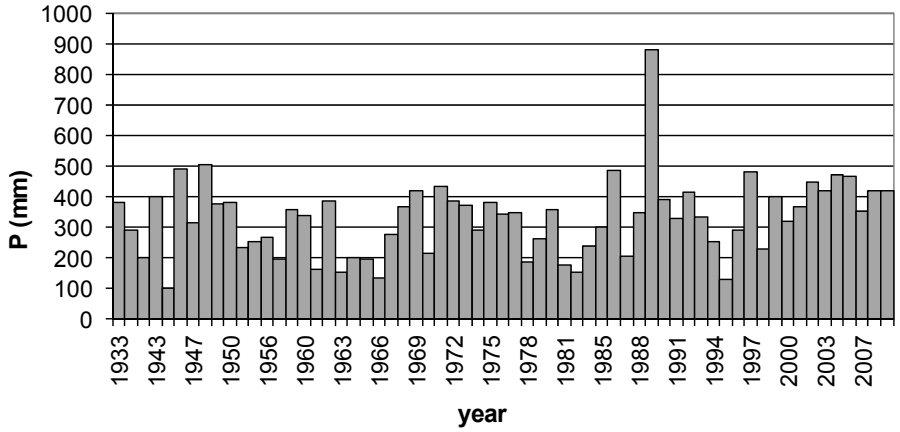

Figure 26: Annual precipitation (mm) for the years 1933 to 2010. Only the years with complete precipitation records are depicted.

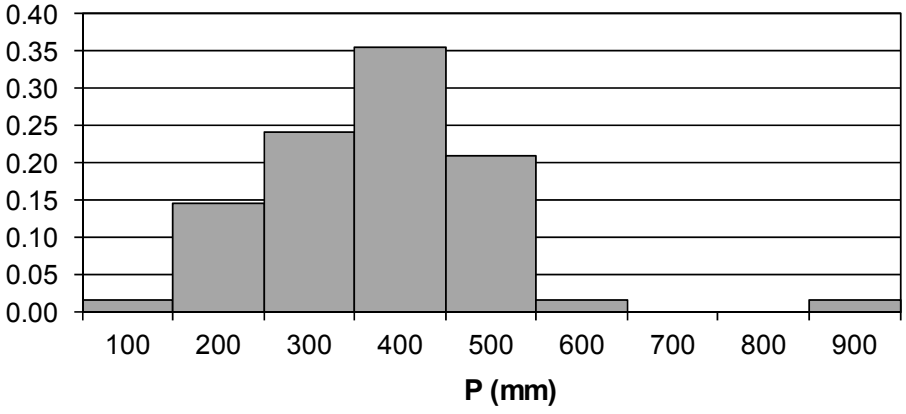

Figure 27: Relative frequency of the annual precipitation for the years 1933 to 2010.

As to the monthly records, a high variability can be noticed among them. The highest monthly precipitation was registered in October 1986 (250 mm/month). Peaks generally occur in spring and autumn and very low values are reported during summer months (Figure 28 and Figure 29). In particular, and averagely speaking, October and April are the rainiest months, with mean precipitation of 41 and 38 mm respectively.

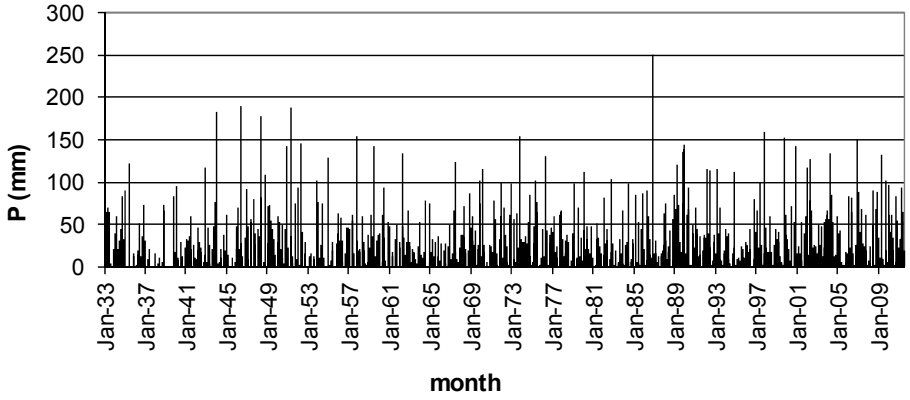

Figure 28: Monthly precipitation (mm) for the period January 1933 – June 2011.

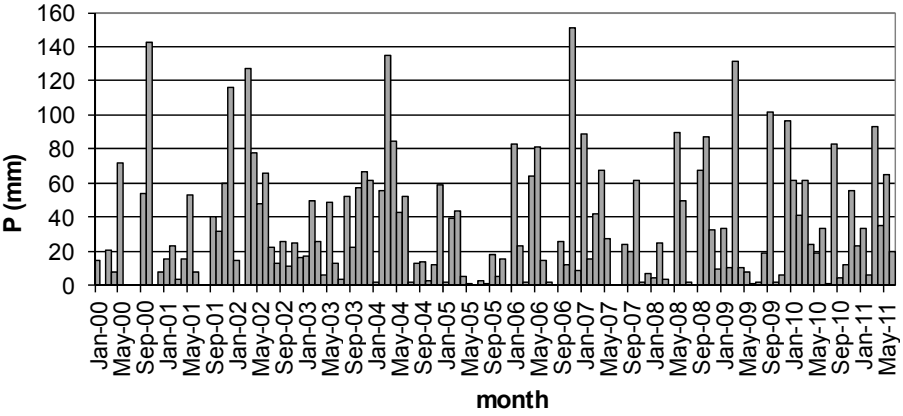

Figure 29: Monthly precipitation (mm) for the period January 2000 – June 2011, period considered for the vegetation simulations in chapter 7.

The driest months, on the other hand, are July and August, with 4 and 11 mm average precipitation (Figure 30). Also, when considering the maximum monthly precipitation (Figure 31), October and April show the highest records, with 250 and 190 mm respectively. The considerable difference between average and maximum values is due to the high inter-annual variability, with monthly records equalling zero at least once for each month of the year in the studied period. In fact, the

most frequent value for monthly precipitation lies between 0 and 20 mm (Figure 32) with a relative frequency value for this interval of 0.57.

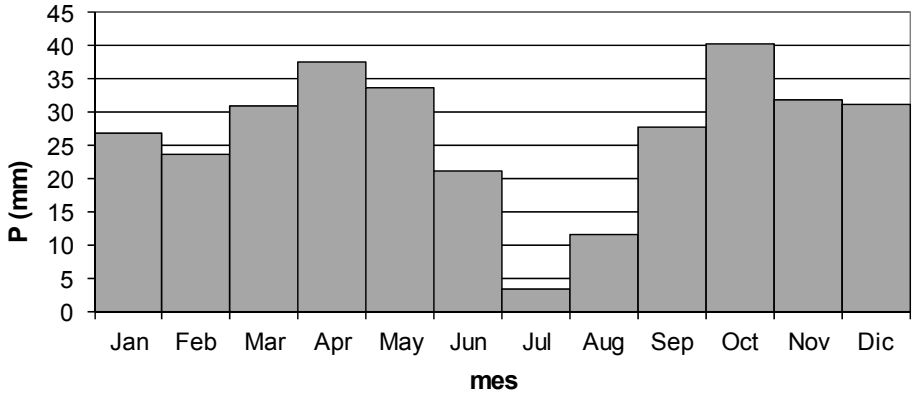

Figure 30: Mean monthly precipitation (mm).

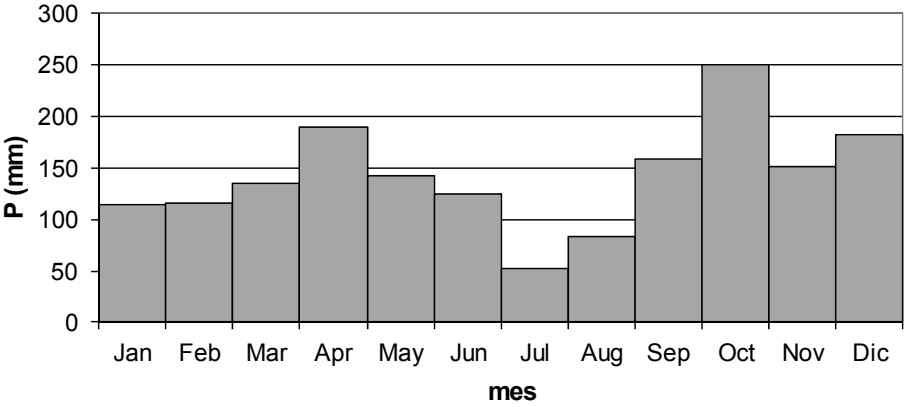

Figure 31: Maximum monthly precipitation (mm).

When studying vegetation, it is of greatest importance to consider, in addition to total and average precipitation amounts, the distribution of these volumes within each year. From now on, all those days with a precipitation record exceeding 0.4 mm will be regarded as rainy days (Latron, 2003), since values below this threshold are not considered

influential in the plant water uptake process. The month with the highest number of rainy days is April, with an average of 3.8 days; July is the month recording the lowest number of days with P > 0.4 mm, with an average of 0.6 days (Figure 33). In addition, July is the month that presents the lowest average precipitation volume per rainy day (3.3 mm), confirming that the most extreme drought conditions are reached during this month. October and September register the highest volumes per rainy day, with an average of 11.8 and 11.2 mm respectively (Figure 34).

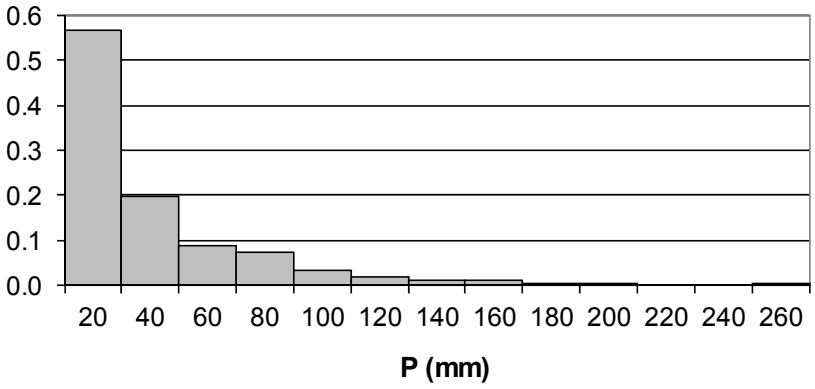

Figure 32: Relative frequency of the monthly precipitation.

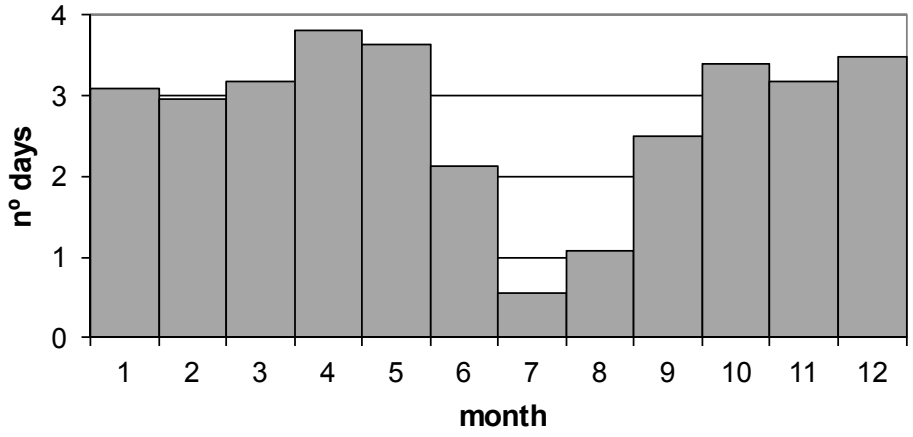

Figure 33: Average monthly number of rainy days (P > 0.4 mm).

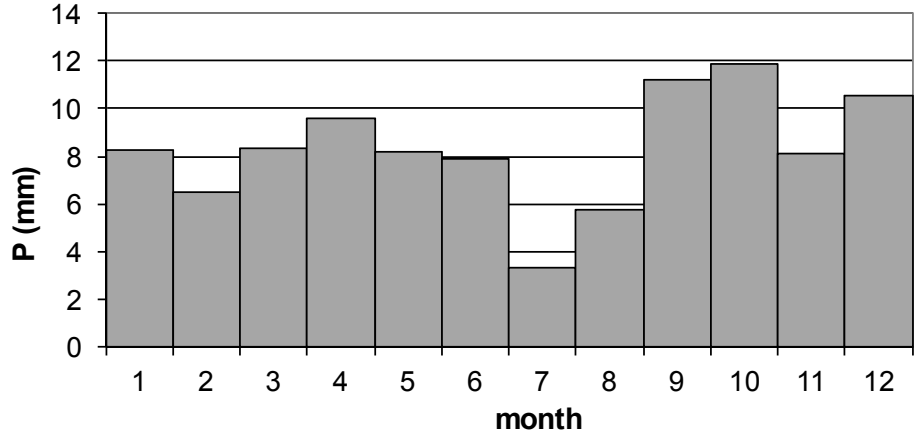

Figure 34: Average monthly precipitation volume (mm) per rainy day.

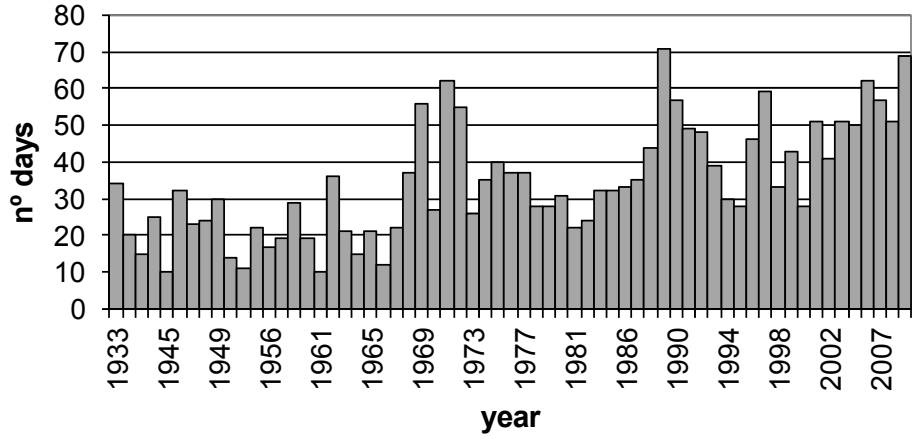

Figure 35: Number of rainy days (P > 0.4 mm) per year for the period 1933 to 2010. Only the years with complete precipitation records are considered.

In Figure 35 and Figure 36 the number of rainy days per year and the annual average precipitation volume per rainy day are depicted. A different behaviour of the years at the beginning and at the end of the series can be noted: a higher number of rainy days per year is registered for the last years with respect to the first years of the precipitation

record. On the other hand, a lower average volume per rainy day is calculated for the last years with respect to the first ones. Analysing separately the years before and after 1974, the average number of rainy days results 26 and 41 days/year, for the first and the second group respectively; the average precipitation volume is, on the other hand, 12.9 and 8.5 mm/rainy day respectively. From a Student's t-analysis, these differences between the average values are shown to be significant, with p-value < 0.025.

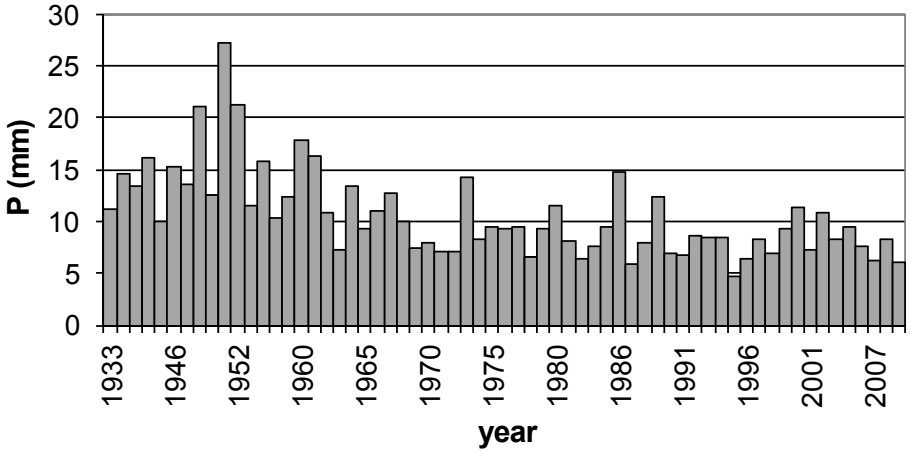

Figure 36: Average annual precipitation volume (mm) per rainy day for the period 1933 to 2010. Only the years with complete precipitation records are considered.

Another very important parameter, when dealing with vegetation, is the number of consecutive dry days. As for the definition of rainy days, the threshold considered is 0.4 mm, so that all those days with a precipitation record lower than 0.4 mm are considered dry days. In Figure 37, the number of consecutive dry days is depicted for each month from January 1933 to June 2011, with the exception of incomplete monthly records. The longest drought period registered was the one culminated in July 1945, with 192 consecutive dry days. Monthly values higher than the length of the month itself can be explained considering that if no precipitation is recorded at the end of one month,

the count continues with the following month's consecutive dry days. Averaging the length of dry periods for each month (Figure 38), August registers the highest value, with 55 days.

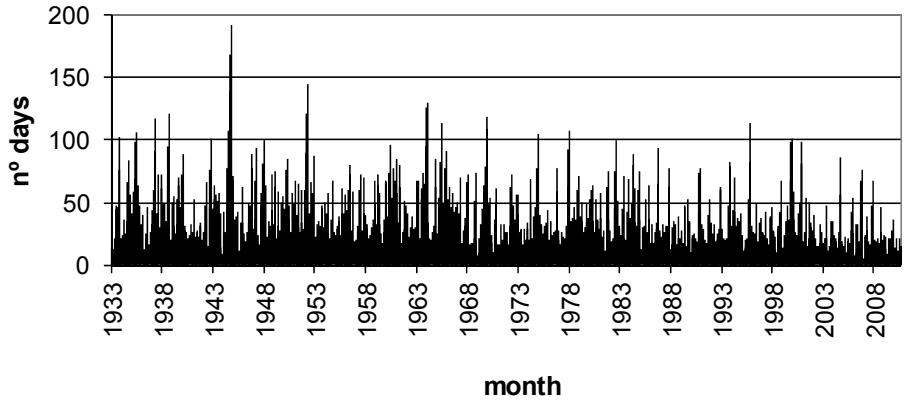

Figure 37: Number of dry (P < 0.4 mm) consecutive days.

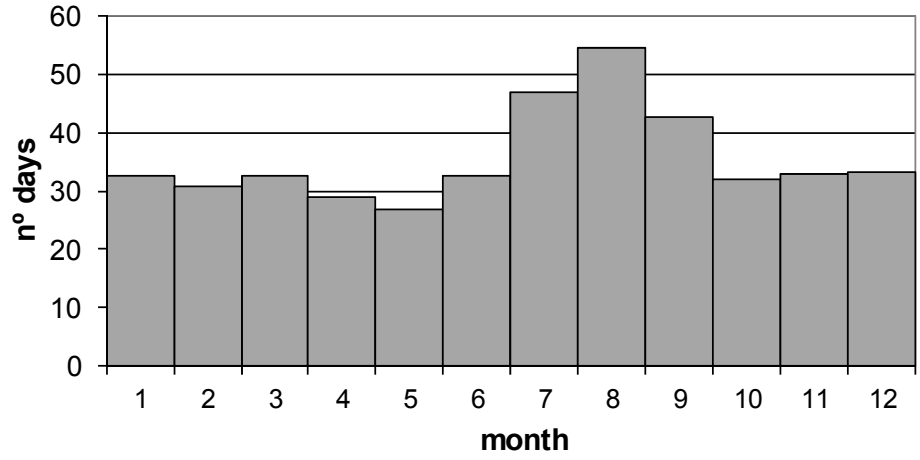

Figure 38: Average number of consecutive dry days (P < 0.4 mm) per month.

5.2 Temperatures, wind speed and reference evapotranspiration

The study site is characterized by an important annual variation in temperatures, with hot summers and cold winters. Mean monthly maximum air temperature ranges between 11ºC (December and January) and 31ºC (July and August), while mean monthly minimum temperature ranges between 1ºC (from December to February) and 15ºC (July and August) (Figure 39). The highest temperature recorded, since a weather station is active at Valdeinfierno dam, is 42ºC (July 1972) while the lowest recorded temperature is -13ºC (January 1985).

In Table 2, the average values of wind speed recorded by the Caravaca de la Cruz weather station, the nearest available station measuring this parameter, are reported. The annual average wind speed is 7 km/h (i.e. 1.94 m/s).

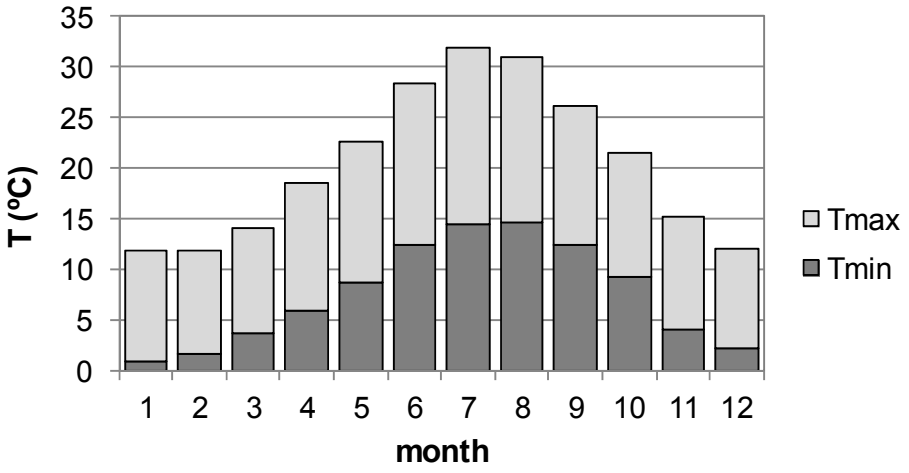

Figure 39: Average monthly values of maximum and minimum temperatures (ºC).

Month	Wind velocity (km/h)
January	11
February	12
March	6
April	1
May	4
June	7
July	8
August	5
September	9
October	4
November	7
December	9

Table 2: Average wind speed recorded by the Caravaca de la Cruz weather station (http://www.quetiempo.es/prevision/murcia/caravaca-de-la-cruz/**).**

The reference evapotranspiration was estimated thanks to the Hargreaves equation (Hargreaves & Samani, 1985):

$$ET_o = 0.0023 R_a \left(Temp + 17.8\right) \sqrt{Temp_{\max} - Temp_{\min}}$$

where ET_o is the reference evapotranspiration (mm/d); R_a is the water equivalent of the extraterrestrial radiation (mm/d), computed according to (Allen *et al.*, 1998); $Temp_{max}$, $Temp_{min}$ and $Temp$ are the maximum, minimum and average air temperature (ºC); 0.0023 is the coefficient originally proposed by Hargreaves and Samani (1985).

This equation is of easier application with respect to the FAO-56 Penman-Monteith equation (Allen *et al.*, 1998), only requiring air temperature values. Conversely, it does not take into consideration wind speed and relative humidity data, variables that considerably affect ET_o. For this reason, a local calibration of the equation's coefficient was sought, to increase the reliability of ET_o estimates.

Gavilán et al. (2006) published a study on the applicability of the Hargreaves equation and calibrated its coefficient using data from 86 weather station of the region of Andalusia. Considering the mean wind speed and the difference between maximum and minimum temperatures, they divided the weather stations into 4 groups, assigning to each group the most appropriate equation coefficient. From the results obtained by these researchers for stations near the study area, and with similar weather characteristics, the original coefficient 0.0023 is demonstrated to be suitable for using in the area considered in this study.

The average annual ET_o, estimated using the Hargreaves equation, is 1137 mm/year. In Figure 40, the average monthly precipitation is depicted. July exhibits the highest value (186 mm/month), while December the lowest one (30 mm/month).

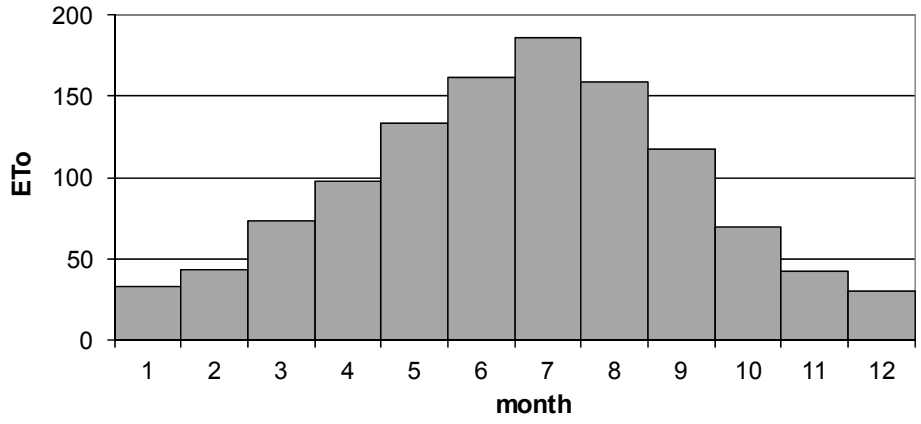

Figure 40: Monthly average reference evapotranspiration (ET_o) (mm/month).

5.3 Climate classification

The semiarid climate describes those climatic regions that receive precipitation below reference evapotranspiration, without this water deficit being so extreme as to define an arid climate. A more precise definition can be found in Köppen's work (1936).

Following Köppen climatic classification, to determine whether a region is subjected to semiarid climate it is necessary to establish a precipitation threshold (mm). This parameter is calculated by multiplying the average annual temperature (ºC) by 20, and by adding either 280 if the 70% or more of the annual precipitation occurs during the most sunny period of the year (from April to September in the northern hemisphere), or 140 if the 30% to 70% precipitation occurs in the same period, or 0 otherwise. If the annual precipitation is lower than the calculated threshold, and higher than the half of it, the climate is semiarid.

Following the described procedure, the semiarid character of the climate in the study area is demonstrated:

- Average annual temperature: 13.45ºC;
- Average temperature * 20: 269;
- Average precipitation in the period April to September: 135 mm;
- Average annual precipitation: 327 mm;
- % of precipitation during the sunny period, with respect to total annual precipitation: 41%;
- Precipitation threshold: 409 mm.

Considering that the average annual precipitation (327 mm) is lower than the calculated threshold (409 mm), and higher than half the threshold (204.5 mm), the semiarid character of the study area's climate is confirmed.

6 Satellite data

The remote sensing information used in this research was obtained from the data collected by the instruments aboard the MODIS Terra and Aqua satellites. Processed data are made openly available through online tools such as Reverb and GloVis. In particular, the satellite information used in this study is composed by the Normalized Difference Vegetation Index (NDVI), the Enhanced Vegetation Index (EVI), the Leaf Area Index (LAI) and the total Evapotranspiration (ET). The NDVI and EVI, both included in the products MOD13Q1 (NASA, 2012a) and MYD13Q1 (NASA, 2012c), are provided every 16 days at 250-meters spatial resolution; the LAI, included in the products MOD15A2 (NASA, 2012b) and MYD15A2 (NASA, 2012d), is provided every 8 days at 1000-meters spatial resolution; and lastly the ET data, included in the MOD16A2 product (Numerical Terradynamic Simulation Group, 2012), are provided every 8 days at 1000-meters spatial resolution.

Before they are made available to the public, the observations of the two MODIS satellites are filtered based on quality, cloud and viewing angle. A cloud-free, nadir view pixel with no residual atmospheric contamination is considered the best quality pixel, while cloud-contaminated pixels and extreme off-nadir sensor views are regarded as lower quality. Every 16 days, a single value per pixel from all the retained filtered data is extracted, and considered representative of each

pixel over the particular 16-day period. The technique employed to select the representative value depends on the number and quality of available observations. In the case of LAI and ET products, composite is made at 8-days timestep.

6.1 Data description

Satellite EVI, NDVI (e.g. Figure 41), LAI and ET were analyzed for the period 2000 – 2011 over the study area, averaging the spatial distributed data to obtain the evolution through time. All four products showed a marked seasonal quasi-sinusoidal behavior, but differences between them were noticed regarding the timing of peaks (Figure 42).

Satellite NDVI (e.g. Figure 41), EVI, LAI and ET were analyzed for the period 2000 – 2011 over the study area, averaging the spatial distributed data to obtain the evolution through time.

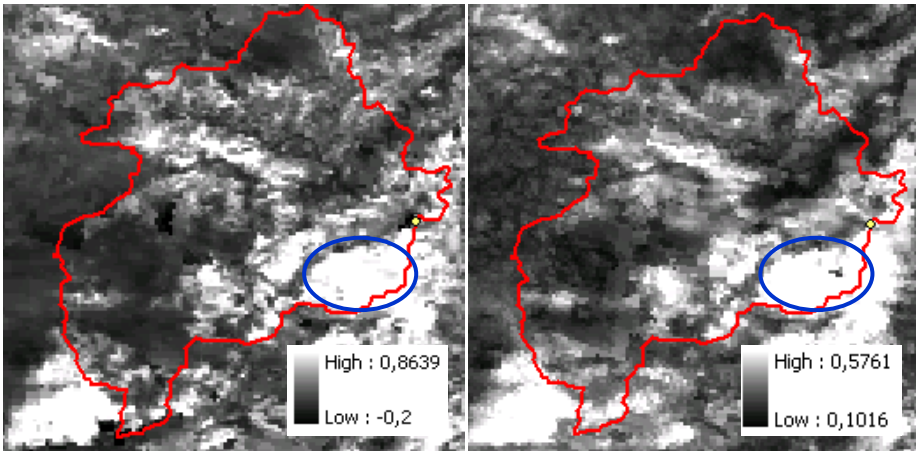

Figure 41: NDVI images referred to January 2001 (left) and June 2001 (right). The Valdeinfierno catchment is evidenced in red; in blue, the Aleppo pine area.

All four products showed a marked seasonal quasi-sinusoidal behaviour, but differences between them were noticed regarding the timing of peaks. EVI and LAI peaked around April and May, while minima were detected in December, even though the entire period from

September to February presented low values. As for the ET, maxima were registered in June – July and minima in December (Figure 42). The evapotranspiration data ranged between 0.1 and 1.8 mm/d, and were highly correlated with the ET_o (cf. section 5.2), being the Pearson coefficient 0.79.

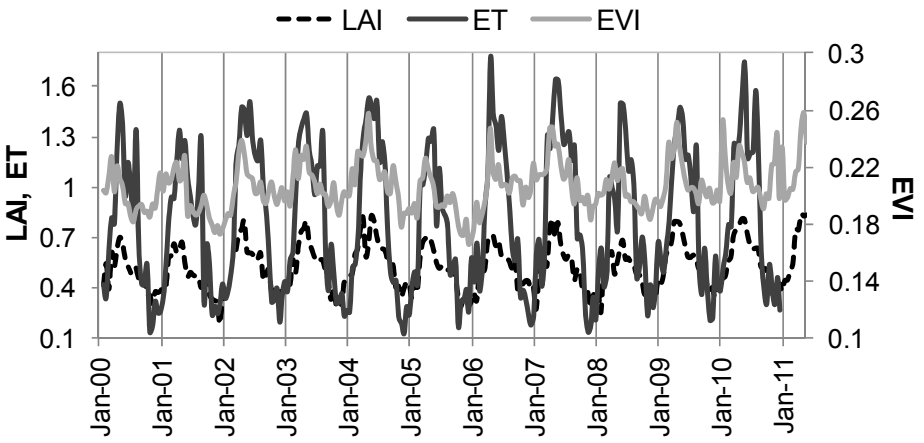

Figure 42: Evolution of LAI, ET (mm/d) and EVI as obtained from satellite data.

The NDVI was the only index that had a contrasting behaviour with respect to the others: two peaks were registered within each cycle, the highest one between November and February and a second, lower one in April – May. Minimum NDVI was recorded in August (Figure 43). The scatter plot of NDVI and EVI (Figure 44) suggests a low general correlation between the data. A t-distribution statistic test (95% confidence level) was performed, and the presence of a significant correlation between NDVI and EVI series rejected. However, when dividing the datasets into two groups, on one side data referring to months from April to September, and on the other side data referring to months from October to March, a significant correlation ($r = 0.66$) was found between the two indices for the former data group, while for the latter group's correlation was not statistically different from zero.

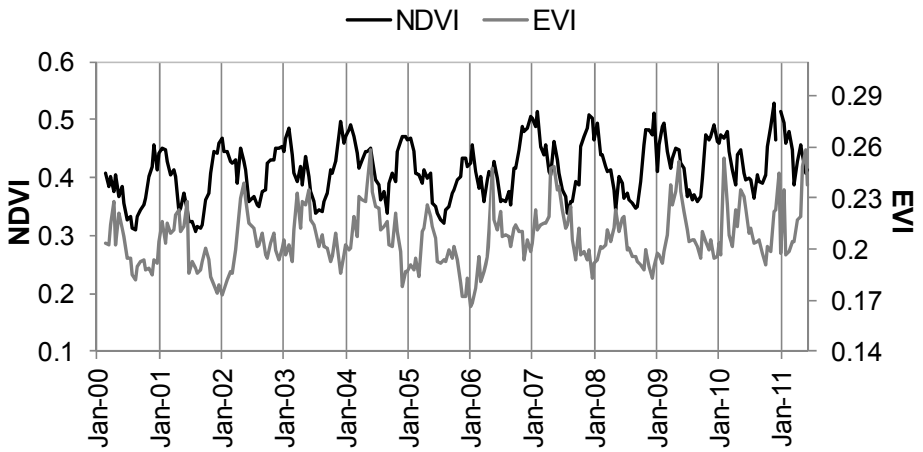

Figure 43: Evolution in time of NDVI and EVI, as obtained from satellite data.

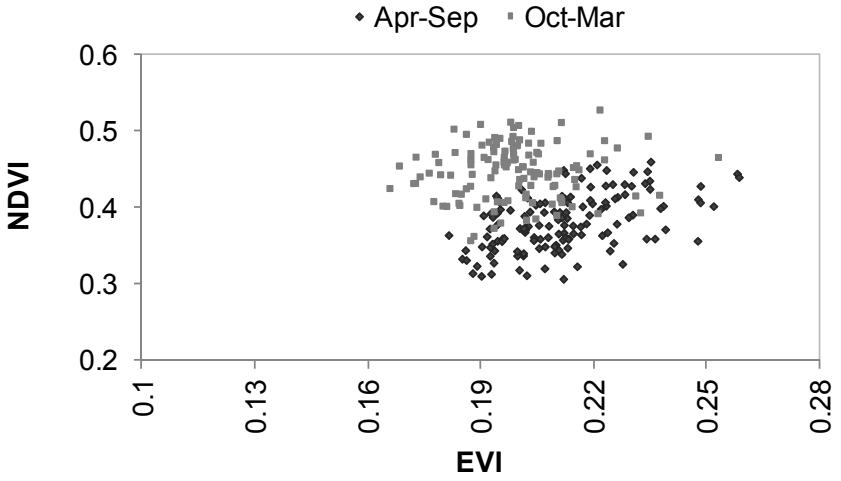

Figure 44: Scatter plot of NDVI with respect to EVI, as obtained from satellite data.

The ranges of variation for the NDVI and EVI were 0.3 – 0.5 and 0.16 – 0.26, respectively. Comparing the time series of these two indices with the respective month-by-month average calculated for the years 2000-2011 (Figure 46), some periods of low recorded values were

identified, in particular: summer-autumn 2000, summer-winter 2001 and summer 2005-spring 2006 for the EVI; summer-autumn 2000, summer-autumn 2001 and summer-winter 2005 for the NDVI. As for higher-than-average values, it is worth mentioning spring 2004 for both EVI and NDVI.

When fitting the EVI and NDVI data with a linear regression, an increasing trend over the years emerged in both cases (Figure 46 and Figure 46). To determine whether the trend is statistically significant or it cannot be differentiated from the null hypothesis of no trend in the data, the non-parametric Seasonal Kendall test was performed (Hirsch *et al.*, 1982). Assuming that a serial correlation occurs in the EVI and NDVI data, and considering that serial correlation violates the assumption of independence of data, an adjusted p-value was used (Hirsch & Slack, 1984). The significance level (α) to reject the null hypothesis was set on 0.025. The test was performed using the Computer Program for the Kendall Family of Trend Tests of the U.S Geological Survey (Helsel *et al.*, 2006). Kendall tau coefficient resulted 0.17 and 0.38, for EVI and NDVI data respectively. Only the NDVI growing trend was proven to be significant, with an adjusted p-value of 0.01. The trend identified in the EVI data, on the contrary, was shown to be equivalent to the null hypothesis.

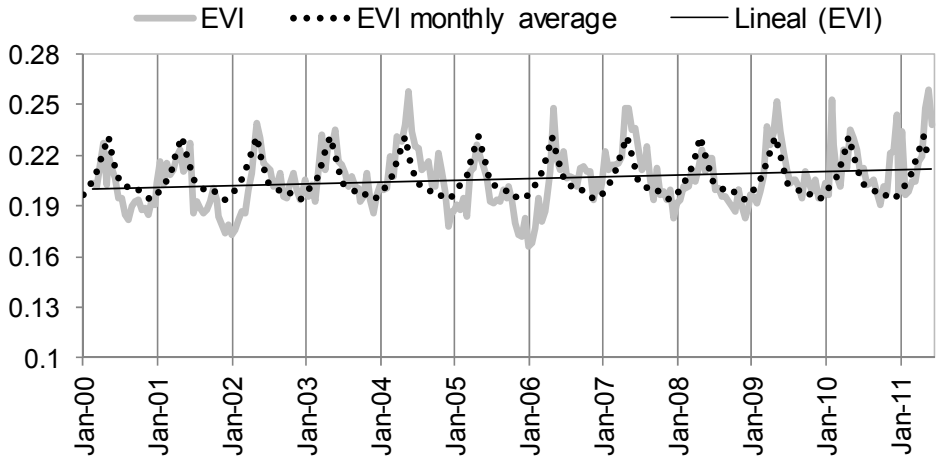

Figure 45: EVI series, with adjusted linear trend, compared to monthly average calculated for each month of the year for 2000 to 2011.

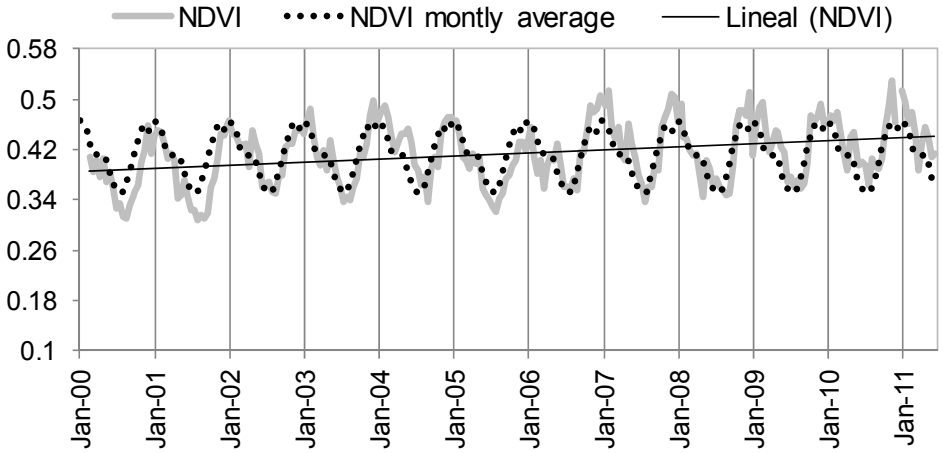

Figure 46: NDVI series, with adjusted linear trend, compared to monthly average calculated for each month of the year for 2000 to 2011.

The values of LAI provided in the MOD15A2 product, ranging between 0.2 and 0.8, appear to be very low compared to values reported in literature (Sabaté *et al.*, 2002; Sprintsin *et al.*, 2007; Vicente-Serrano *et al.*, 2010; Molina & del Campo, 2012) for the same species in similar climatic conditions. Molina and Del Campo (2012), for example, report values of LAI = 0.5 and forest cover = 16% for high-intensity thinning treatment in Aleppo pine forests. The vegetation in the study area is not as sparse as to justify similar LAI values. A field campaign in august 2012 obtained, for a plot in the study area, values of LAI ranging between 1 and 2, with the exception of few transects of sparser vegetation where the registered values were approximately 0.8. Even though field measurements restricted to a very short time period cannot be considered definitive proof of the unreliability of MODIS LAI product, they offer clues towards the rejection of these data in the study site. For this reason, and for what discussed in section 6.2, it was decided to reject this set of data and refer to EVI and NDVI for the estimation of vegetation biomass.

As for LAI_{NDVI} obtained from NDVI (cf. section 3.6.2), the parameters used in Beer's law for the study region were $NDVI_{can}$ = 0.9915; $NDVI_{back}$ = 0.0549 and k = 0.212 (Anselmi *et al.*, 2004). The resulting LAI differed

from MODIS MOD15A2 LAI product in timing – same differences as between MODIS NDVI and LAI data – and in range of variation, being LAI_{NDVI} higher in values and varying between 0.7 and 1.5 (Figure 47).

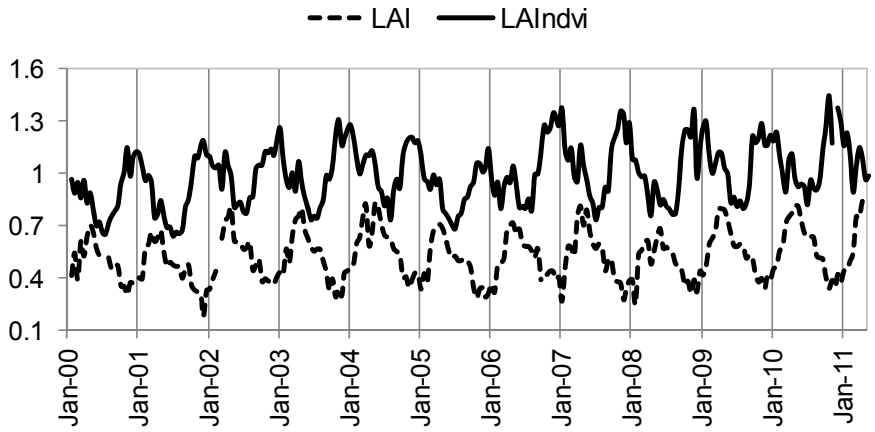

Figure 47: Evolution in time of LAI (MODIS MOD15A2 product) with respect to LAI_{NDVI}, obtained from NDVI data

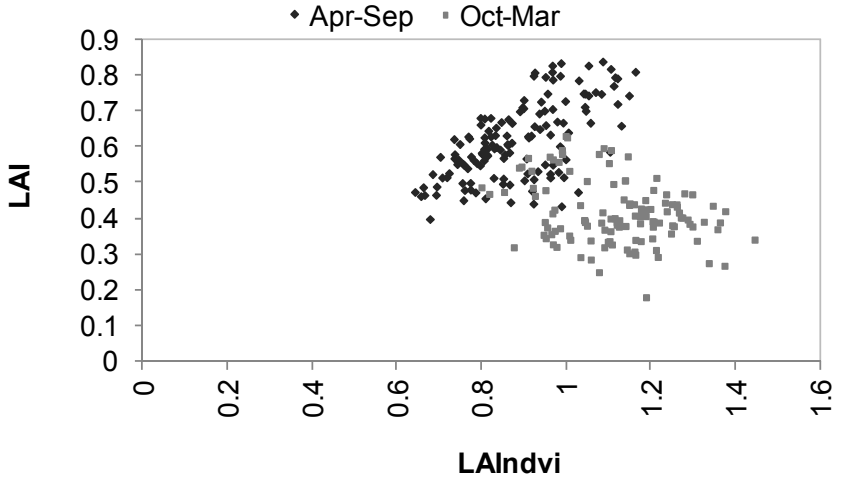

Figure 48: Scatter plot between LAI (MODIS MOD15A2 product) and LAI_{NDVI}, obtained from NDVI data.

The scatter plot (Figure 48) suggests the presence of two distinct groups of pairs of data. The total Pearson correlation coefficient is negative and statistically significant (r = -0.37), while dividing, as for NDVI and EVI, the datasets into two groups - April to September and October to March – the correlations result 0.63 and -0.29 respectively, both significantly.

6.2 Discussion

EVI has been proven to be generally highly influenced by vegetation structure, and in particular by LAI (Gao *et al.*, 2000; Huete *et al.*, 2002). This behaviour is confirmed by the satellite data used in this study: as depicted in Figure 42 and Figure 44, EVI exhibits peaks in April – May, followed by a decline trend that lasts until late autumn. The described rise and drop of the index correspond to the spring sprouting typical of Aleppo pine in the Spanish area (Weinstein, 1989; Pardos *et al.*, 2003) and the summer shedding of needles accumulated in the previous 1 - 3 years (García-Plé *et al.*, 1995; Borghetti *et al.*, 1998; Calatayud *et al.*, 2000; Muñoz *et al.*, 2003).

As far as LAI is concerned, the values extracted from MOD15A2 product are very low compared to values found in literature for the same species in similar environments (Sabaté *et al.*, 2002; Sprintsin *et al.*, 2007; Vicente-Serrano *et al.*, 2010; Molina & del Campo, 2012). A likely explanation was found on analyzing the data, where it was found that the land cover classification, on which the algorithm used to compute LAI is based, does not correspond to the actual vegetation. The area is classified partly as shrublands and partly as savannah. A similar problem was detected by Sprintsin et al. (2009) for the Yatir Aleppo pine forest located in an arid-semiarid climatic area. Nevertheless, considering the forest phenological cycle, the timing of maxima and minima appears to be correct. The product MOD16A2, which provides an estimation of ET, is derived from MOD15A2 LAI product. Having observed some inaccuracies in the hypothesis on which the latter index estimation is based, it is believed that also the former one could be affected by errors interesting its value. Particularly, the high correlation between the ET product and ET_o is suspect, considering the semi-arid

climate of the area, which determines water stress during the periods of highest ET_o.

As it is shown in Figure 44, NDVI reaches its annual maximum between November and February, when plants have completely recovered from summer drought and leaf chlorophyll content is high. Therefore, comparing EVI and NDVI series, it could appear that NDVI is shifted backwards, anticipating EVI. Analyzing more in depth the data, a second peak of NDVI is actually noticeable in correspondence with spring sprouting and EVI maximum. Hence, NDVI responds to different phenomena, recovery of pre-drought photosynthetic pigments level and growth of new shoots, with two distinct peaks. Similar behaviour was registered by Evrendilek and Gulbeyaz (2008) for Mediterranean forest in Turkey (Figure 49) even though in that case, probably due to lower time resolution, NDVI double peaks could not be appreciated and an apparent shift between the two indexes was recorded. This shift was registered in the mentioned research only for Mediterranean forest, while for other vegetation types in Turkey, like Warm Temperate vegetation or Mediterranean grassland and shrubland, the two indexes EVI and NDVI were synchronized.

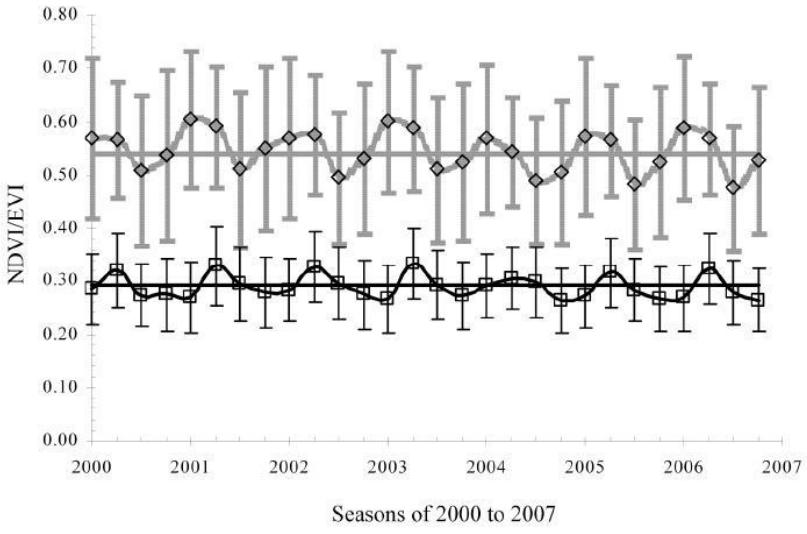

Figure 49: Time series MODIS NDVI (patterned curve) and EVI (solid curve) data of 2000 to 2007 for natural Mediterranean forest in Turkey (source: Evrendilek & Gulbeyaz, 2008).

When calculating LAI_{NDVI} from NDVI, the indirect dependence of NDVI on soil moisture (cf. section 3.2) for Mediterranean forest is transferred to the derived index, making the correction of model's results by water stress necessary, as described in section 4.3.5, to allow comparison with LAI_{NDVI}.

Overall, EVI and NDVI show a regular seasonal pattern. However, during some periods the values of the indexes clearly depart from the average trend, as described previously in section 6.1. These anomalies could be explained considering the precipitation records (Figure 50 and Figure 51); in fact there is a certain correspondence between the periods of lowest values of the two indexes and the periods of prolonged low precipitation. Only the drought corresponding to the period summer 2007-winter 2008 does not have a strong impact on the indexes' values. A possible explanation is that the 142.7 mm of precipitation accumulated during the 9 months from June 2007 to February 2008 were distributed quite uniformly during that period, preventing the soil from drying completely. Nonetheless, a lower-than-average value of spring maximum for EVI can be noticed and, as for NDVI, a drop is recorded in the same period.

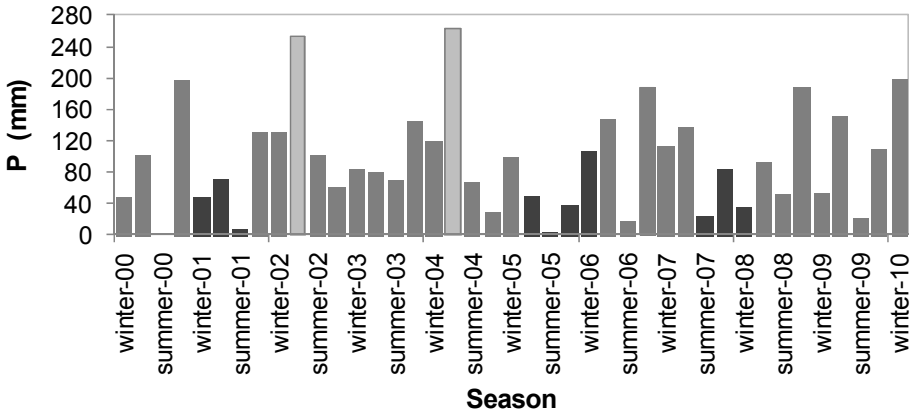

Figure 50: Seasonal precipitation (mm/season). Prolonged periods of low precipitation are evidenced in dark colours. In light colours, the rainiest seasons of the studied period.

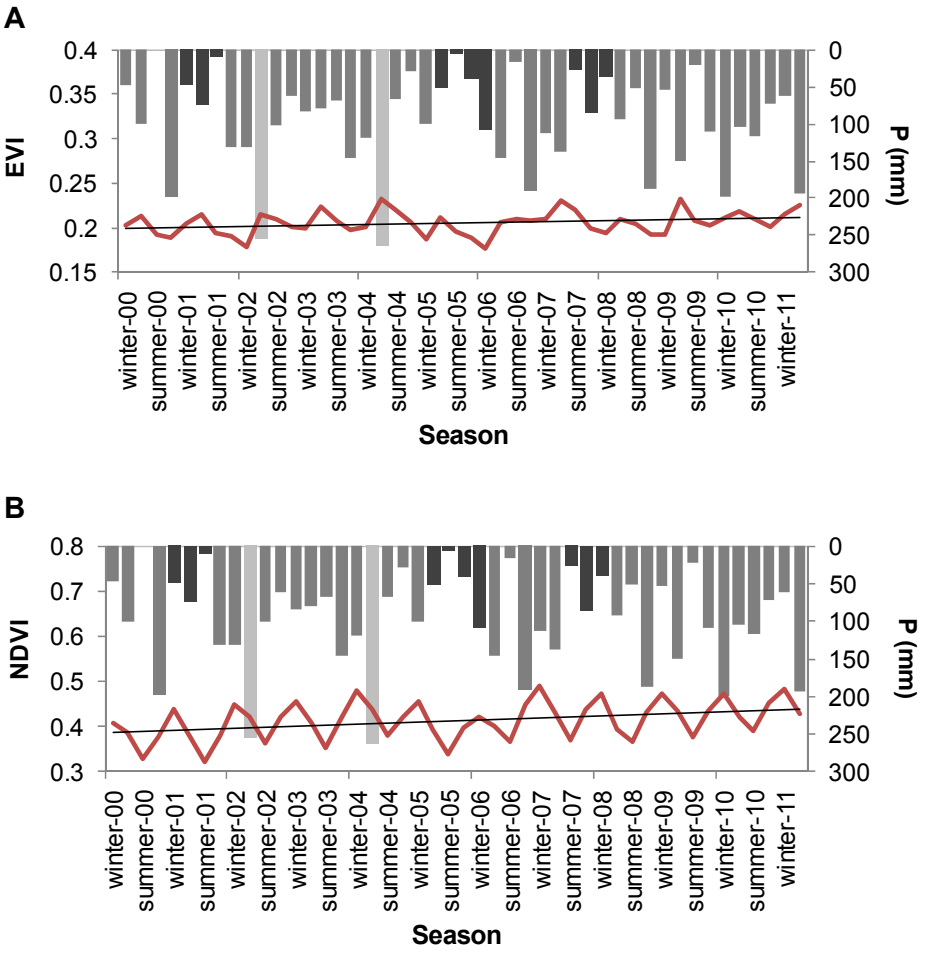

Figure 51: EVI (A) and NDVI (B) seasonal average values with adjusted linear trend, related to seasonal precipitation records (mm/season). Colour code is the same as in Figure 50.

As well as for low indexes' values, high values can also be linked to precipitation deviation from seasonal average. In fact, spring 2004 high precipitation rates result in high EVI and NDVI records because, it is believed, rain boosted the spring sprouting. With respect to the other rainy season during the studied period, spring 2002, no strong impact is detected on the two indexes. It has to be kept in mind, though, that the considered period is the growth season that follows a long drought

period (summer 2000 – summer 2001, with the only interruption of a strong precipitation event in October 2000). Vegetation is probably only mildly responding because in a recovery phase.

7 Results and discussion

In this chapter, the processes of implementation and calibration of the three selected models is described. The simulation results are analysed and compared with satellite data.

7.1 HORAS model

7.1.1 Model implementation and results

HORAS model requires precipitation and ET_o datasets as inputs. Precipitation and temperature records were supplied by the nearby Valdeinfierno weather station, while ET_o was calculated using the Hargreaves equation (Hargreaves & Samani, 1985) and temperature data (see section 5.2). The effective root depth is also necessary and was evaluated during a field campaign: a 900 mm layer of soil was estimated to be involved in the vegetation processes. Soil moisture at critical and wilting point were calculated through the Clapp and Horberger's equation (1978), taking into account the hydraulic parameters for loam (Ψ_{ae} = 1.43 e-03; φ = 0.451; b = 5.39. See section 4.2.3).

The model was calibrated maximizing the Pearson correlation coefficient (*r*) between the state variable R (relative foliar biomass; cf. section 4.2.1) and the EVI. The Pearson correlation coefficient between two sets of values, x and y, is defined as:

$$r = \frac{\sum_i \left(x_i - \bar{x}\right)\left(y_i - \bar{y}\right)}{\sqrt{\sum_i \left(x_i - \bar{x}\right)^2 \sum_i \left(y_i - \bar{y}\right)^2}} \qquad [37]$$

where $\bar{x}$ and $\bar{y}$ are the sample means of the two sets of values.

The maximization of the correlation was the only possibility to exploit the satellite information since R, while representing a foliar biomass and being therefore similar to what the EVI is sensitive to, cannot be assimilated with any physically measurable index.

Considering that the species growing on the study site is evergreen, the season-dependent leaf shedding coefficient (k_{se}) was set to zero. The parameters needing calibration in the dynamic vegetation equation (equation [7]) were four: the ratio between maximum net carbon assimilation and potential foliar biomass ($\alpha = A_{n,mx} / B_{pot}$), the maximum transpiration ratio (T_{mx}), the shape exponent (c) and the water stress-dependent leaf shedding coefficient (k_{ws}). Final values for these parameters can be found in Table 3.

Parameters	Description	Calibrated value
α	Ratio between maximum net carbon assimilation and potential foliar biomass [d^{-1}]]	0.0018
T_{mx}	Maximum transpiration ratio [mm d^{-1}]	5.5
c	Shape exponent	0.054
k_{ws}	Water stress-dependent leaf shedding coefficient	0.0035

Table 3: HORAS calibrated parameters' values.

After the calibration process, the correlation coefficient between R and EVI series was r = 0.39. In Figure 52, the comparison between the two indexes is depicted. It can be noticed that, as far as R is concerned, an annual cycle is not clearly present. Particularly, in the case of the two-year periods 2002-2003 and 2004-2005, the second year's growing season is barely recognisable: only a small peak appears in the overall descending trend of the variable. Also, it is highly noticeable a drop in simulated R, corresponding to the less accentuated decrease in EVI values during the period summer 2005 – spring 2006 (cf. section 6.1).

In Figure 53, the simulated ET and the satellite-deduced ET are depicted. Summer drought periods lead to a simulated ET almost equal to zero for up to 36 consecutive days during summer 2001 and summer 2005. Satellite-derived ET dataset, on the contrary, do not show such prolonged low values.

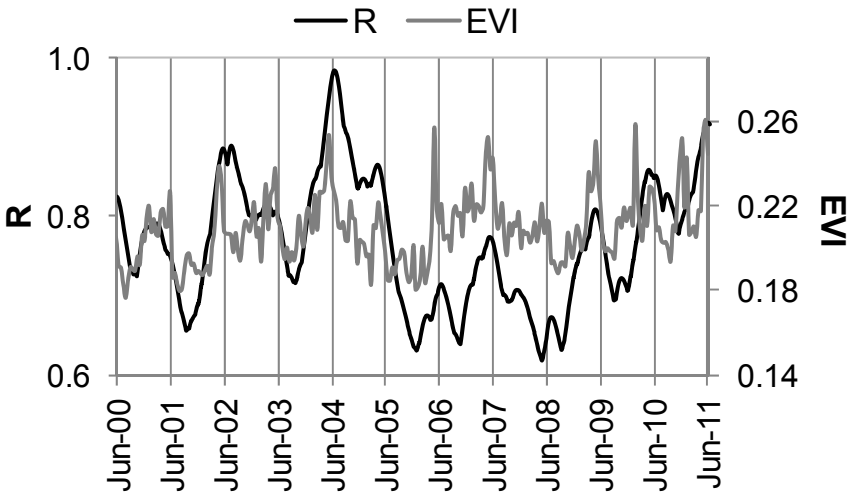

Figure 52: Results of the HORAS model: the simulated state variable R is compared with the EVI series.

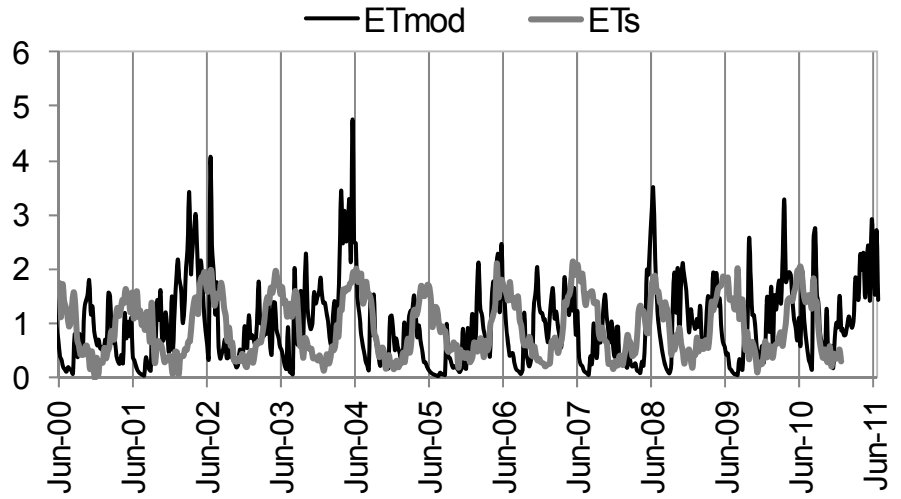

Figure 53: Simulated evapotranspiration (ETmod, mm) compared with satellite derived evapotranspiration (ETs, mm).

7.1.2 Discussion

The model was unable to reproduce the annual cycle of vegetation that is, on the contrary, evident in EVI and NDVI satellite data sets. However, it responded to vegetation annual maximum development (cf. section 6.2) with late-spring peaks in R values, more or less accentuated depending on the simulation year.

To investigate more in depth the problems that could underlie the poor results, the simulated evapotranspiration (ET_{mod}) was analysed. In particular, the numerous and long periods during which this variable has value close to zero were examined. Considering the model conceptualization, ET_{mod} will approach the value zero either down to the lack of available energy or due to the scarcity of soil moisture. As the study area is located in a semiarid region, and being the very low ET_{mod} relative to the summer period, simulated values of soil moisture close to the wilting point were the cause for the anomalous result. The different components of ET were analysed separately and, in particular, bare soil evaporation (E; Figure 54) and plant transpiration (T; Figure 55) were assessed.

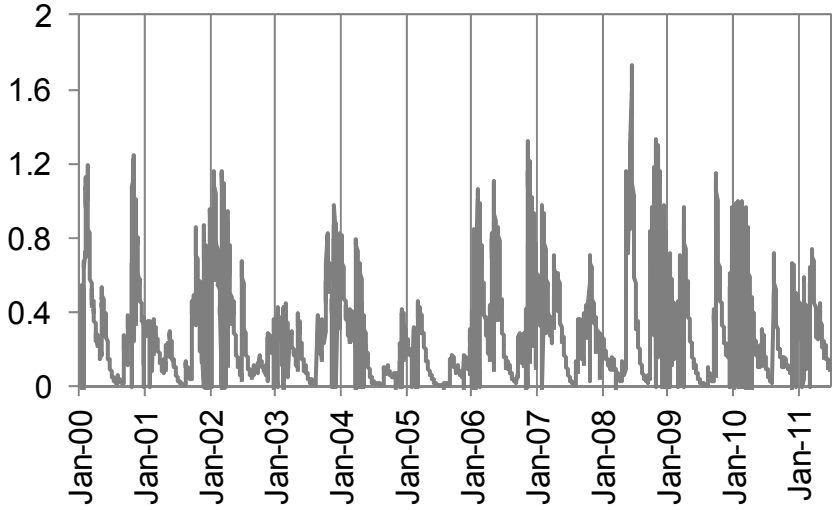

Figure 54: Simulated bare-soil evaporation E (mm d^{-1}).

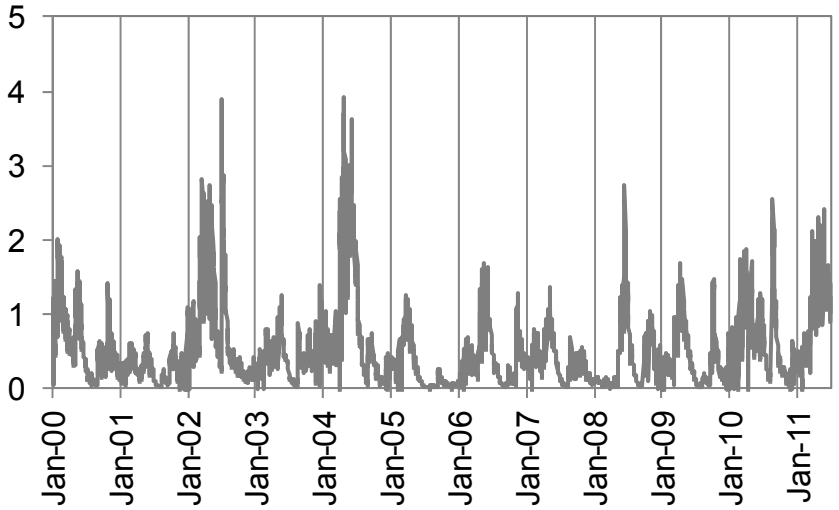

Figure 55: Simulated plant transpiration T (mm d^{-1}).

Considering the entire January 2000 – June 2011 study period, the average bare soil evaporation value was 0.3 mm d^{-1}, while the maximum

simulated value was 1.7 mm d^{-1}. As for transpiration, the average and maximum values were 0.5 and 3.9 mm d^{-1} respectively. On average, bare soil evaporation was responsible for the 31% of total ET, while transpiration was accountable for 56%. There is a disproportion between E and T values, considering that soil cover, simulated through the variable R, was on average 77%, leaving only 23% of the surface to bare soil evaporation processes. The reason for this inconsistency is that it is not correct to assume that the superficial soil layer involved in the E process has the same moisture content of the entire root soil depth. In fact, Wythers et al. (1999), from an analysis of silt loam, clay loam and sand loam soils under semiarid field conditions, ascertained that the soil moisture decrease due to bare soil evaporation was highly dependent on depth. Averaging on the 3 soil types, after a 14 days drought period E had the greatest influence on the upper 6 cm; after 51 days this influence was extended to the upper 10 cm. In addition, evaporation rate was not constant during the experiment, actually depending on time and therefore on soil moisture. For these reasons, to better simulate bare soil evaporation it would be important to introduce on one side an extraction function that depends on soil moisture as for vegetation transpiration, and on the other side to limit soil water loss to the moisture of a superficial soil layer that dries out if not recharged by precipitation.

Another aspect that should be taken into account when evaluating the HORAS vegetation model, is that the parameters involved are not directly relatable to natural processes, particularly the exponent c, so that calibration cannot be based on literature value ranges.

In light of what discussed, it was decided to abandon the HORAS model for the more literature-supported WUE and LUE models.

7.2 WUE and LUE models

7.2.1 Sensitivity analysis

To obtain an insight into the WUE- and LUE- models' functioning, and to assess which parameters mostly affect their performances, a general sensitivity analysis (GSA) (Hornberger & Spear, 1980) was performed on the two models. 8 parameters for each model were taken into account for the sensitivity analysis (Table 4), because either specific of the plant species and the study site or difficult to extrapolate from literature. The GSA was based on the Monte Carlo technique; parameters values were randomly sampled from uniform distributions within ranges based on literature estimations or field observations, and specified in Table 4. 60,000 independent sets of parameters were generated; for each of them, LAI^*_{mod} series (see section 4.3.5) was simulated and the objective function Root Mean Square Error (RMSE) calculated, contrasting model output with LAI_{NDVI}.

The RMSE, used to measure the difference between the *n* values predicted by a model ($\hat{y}$) and the *n* values actually observed (y) is defined as:

$$RMSE = \sqrt{\frac{\sum_i \left(y_i - \widehat{y_i}\right)^2}{n}} \qquad [38]$$

A threshold, identified by an RMSE value of 0.2, divided the parameters sets into two groups: behavioural parameters, which led to satisfactory simulations (RMSE below the threshold adopted), and non-behavioural ones, that produced non-acceptable results (RMSE above the threshold adopted). The threshold was chosen because considered a reasonable error, taking into account the models' potentiality. The analysis resulted in 3958 behaviours and 56042 non-behaviours for the WUE-model; 16893 behaviours and 43107 non-behaviours for the LUE-model. As in Medici et al. (2012), the cumulative probability distributions

of the two groups were obtained and the Kolmogorov-Smirnov two-sample test (KS) was used to evaluate the relative importance of each parameter contribution to the model simulation: the test statistic (KS index) is a measure of the maximum vertical distance between the cumulative probability distribution curves for the behaviours and non-behaviours. The larger the value of the KS index, the higher the importance of the considered parameter in determining the simulation result. The sensitivity analysis assessed that the parameter that most influences the WUE-model's outputs is LAI_{max}, with a KS index of 0.44, followed by I_{max} (KS = 0.31) and f_t (KS = 0.28). In the case of the LUE-model, the most influential parameter resulted to be d_1 (KS = 0.23), followed by the LAI_{max} (KS = 0.2) and d_2 (KS = 0.12). In Figure 56 the KS indexes are reported for each parameter of the models.

Parameter	Description	Min bound	Max bound	Sources*
LAI_{max}	Maximum LAI [m^2 leaf m^{-2} vegetation]	1	2	1, 2
SLA	Specific leaf area [m^2 leaf kg^{-1} DM]	1.5	2.5	3
ω	Conversion of CO_2 to DM [kg DM kg^{-1} CO_2]	0.4	0.7	4
LUE	Light use efficiency [kg C m^{-2} MJ^{-1}]	1.8	2.2	5
I_{max}	Maximum interception [mm d^{-1}]	0.5	5	6
r_1	Fraction of roots in upper soil layer [-]	0.1	0.4	7
d_1	Thickness of first soil layer [mm]	30	100	8
d_2	Thickness of second soil layer [mm]	500	1100	7
f_t	Vegetation fractional cover	0.7	1	7

Table 4: Range of parameters values considered for calibration and sensitivity analysis. The ω parameter is specific of the WUE-model and the LUE parameter is specific of the LUE-model; all the other parameters are common to both models.
*** References for calibration and sensitivity analysis ranges: 1. Ceballos and Ruiz de la Torre (1979); 2. López-Serrano et al. (2000); 3. Awada et al. (2003); 4. De las Heras et al. (2013); 5.Yuan et al. (2007); 6. Crockford and Richardson (1990); 7. Field campaigns; 8. Wythers (1999).**

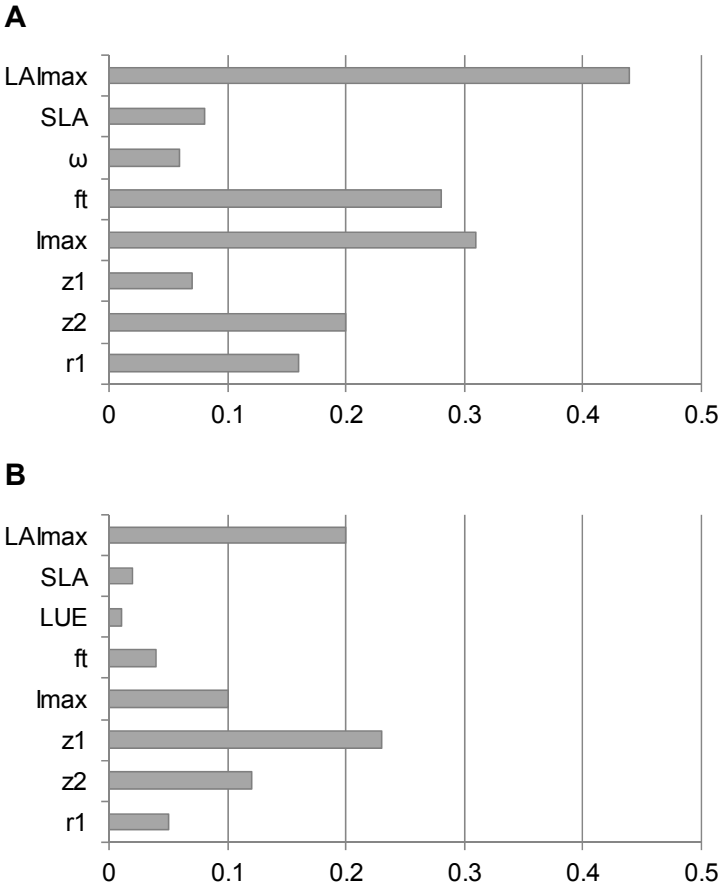

Figure 56: Graph of the KS indexes for the WUE-model's parameters (A) and the LUE-model's parameters (B).

To test the models' capability in reproducing the observed vegetation dynamics and their robustness, a General Likelihood Uncertainty Estimation (GLUE) (Beven & Binley, 1992) was performed, taking into account the behavioural sets of parameters and computing the 90% GLUE band, using the 5% and 95% percentiles as bounds. In this way, it was possible to calculate the likelihood-weighted distribution of the outputs corresponding to the accepted sets of parameters. The GLUE bounds are depicted in Figure 57. Considering the percentage of LAI_{NDVI} data included between the GLUE bands, 63% of the "observed" data were included within the WUE-model-associated GLUE bounds,

while 53% of them lie between the LUE-model-related bounds. Both models showed their lowest performances during autumn 2005 and from winter 2007 to spring 2008. In the first case, the recovery of LAI^*_{mod} after summer minimum was too slow compared to LAI_{NDVI} evolution; in the second case, there was a much stronger decline in LAI^*_{mod} values with respect to LAI_{NDVI} ones, starting in November and till April.

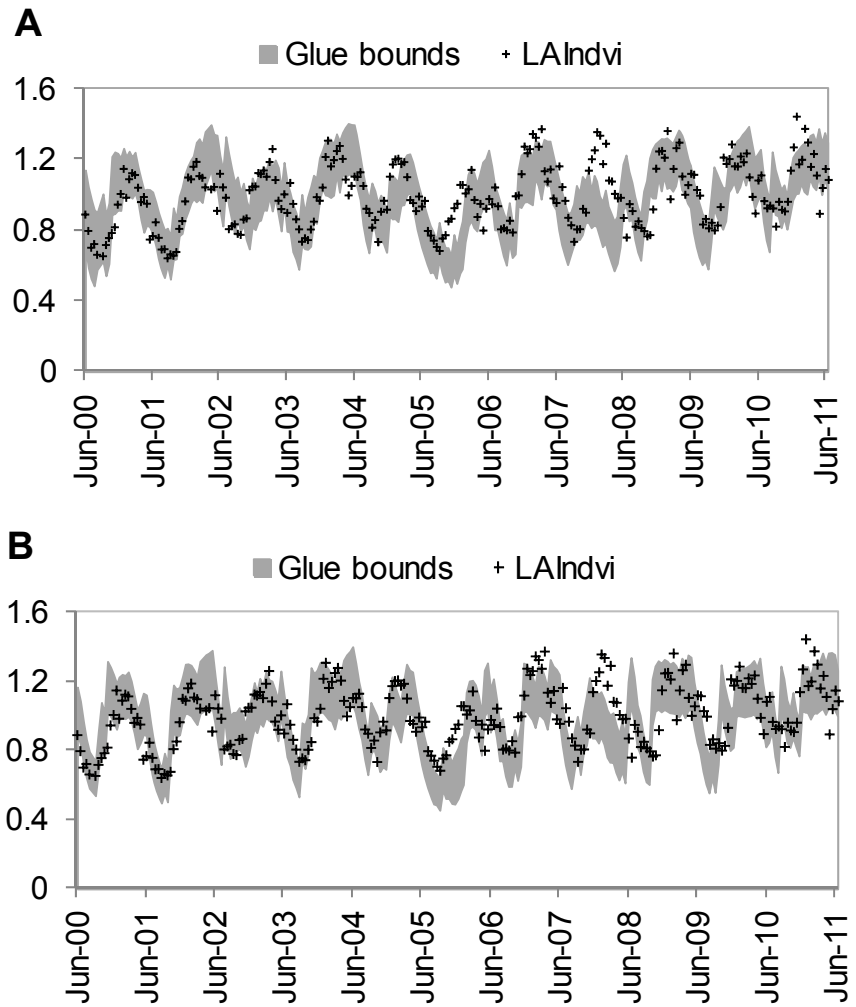

Figure 57: LAI_{NDVI}, as calculated from the satellite recorded NDVI, with the 90% GLUE band for the WUE-model (A) and the LUE-model (B).

7.2.2 Results

After evaluating models' sensitivity, the 8 parameters analysed in the sensitivity analysis were calibrated for each model. A genetic algorithm was used to contrast the simulated LAI^*_{mod} with LAI_{NDVI} and minimize the relative RMSE. Considering that the two models share the same hydrological structure and they calculate leaf area from leaf biomass in the same way, to ensure similar simulation conditions it was imposed that the parameters common to both models assumed the same final value. The same weight was associated to each model's objective function, while priority was given to parameters with higher ranking in the sensitivity analysis. A 4 months spin-up period was used, after which the system was independent from the initial conditions. The final values assigned to parameters are reported in Table 5.

Parameter	Description	Value	Sources*
LAI_{max}	Maximum LAI [m^2 leaf m^{-2} vegetation]	1.4	calib.
k_l	Leaf natural decay factor [d^{-1}]	0.00137	1, 2
SLA	Specific leaf area [m^2 leaf kg^{-1} DM]	1.6	calib.
I_{max}	Maximum interception [mm d^{-1}]	1	calib.
θ_{lim},θ_{cr}	Limit (lim), critical (cr) soil moisture [m^3 H_2O m^{-3} soil]	0.109, 0.256	calc.(3)
r_1	Fraction of roots in upper soil layer [-]	0.1	calib.
d_1,d_2	Thickness of soil layers [mm]	50, 950	calib.
Ψ_{ae}	Air entry matric potential for loam [MPa]	1.43E-03	3
Ψ_{lim}, Ψ_{cr}	Matric potential at limit (lim), critical (cr) points [MPa]	3, 0.03	4
n	Porosity [m^3 void m^{-3} soil]	0.451	3
b	Soil parameter for loam [-]	5.39	3
ω	Conversion of CO_2 to DM [kg DM kg^{-1} CO_2]	0.54	calib.
LUE	Light use efficiency [kg C m^{-2} MJ^{-1}]	2.1	calib.
f_t	Vegetation fractional cover	0.89	calib.

Table 5: Models parameters and constants. The ω parameter is specific of the WUE-model and the LUE parameter is specific of the LUE-model; all the other parameters and constants are common to both models. *Sources: 1. *Ceballos and Ruiz de la Torre* (1979); 2. *Calatayud et al*.(2000); 3. *Clapp and Hornberger* (1978); 4. *Laio et al.* (2001).

The application of the two dynamic vegetation models gave the results shown in Figure 60 to Figure 63, for the WUE-model, and in Figure 64 to Figure 69, for the LUE-model. Pearson correlation coefficient (*r*) between LAI_{mod} and EVI series was 0.45 for the WUE-model (Figure 58, Figure 61), and 0.57 for the LUE-model (Figure 64, Figure 67). When comparing LAI^*_{mod} and LAI_{NDVI}, *r* resulted 0.61 and 0.60 for the WUE- (Figure 59, Figure 62) and the LUE-model (Figure 65, Figure 68) respectively, while the RMSE was 0.181 in the first case and 0.162 in the second one. Two tailed t-distribution statistic tests were performed to verify the existence of statistically significant correlations between the considered variables (i.e.: LAI_{mod} vs. EVI and LAI^*_{mod} vs. LAI_{NDVI}, for both models). All correlations resulted to be significant, with $p<0.0001$ and considering 95% confidence level. Figure 70 shows the 11-year average of monthly LAI^*_{mod} and LAI_{NDVI}.

As far as ET was concerned (Figure 60, Figure 66), simulations and data provided by NASA presented the same seasonality, but two main differences could be identified: while satellite data did not show marked inter-annual changes in the peak values, both models presented significant differences between years, with highest annual maximum value in 2002 and lowest annual maximum value in 2005. In addition, simulations exhibited a relevant decay in ET values in August, when water stress reached its maximum values, while data processed from satellite information showed minor or no decline in the same period, fact that appears strange, considering the drought conditions of the study site during the summer period.

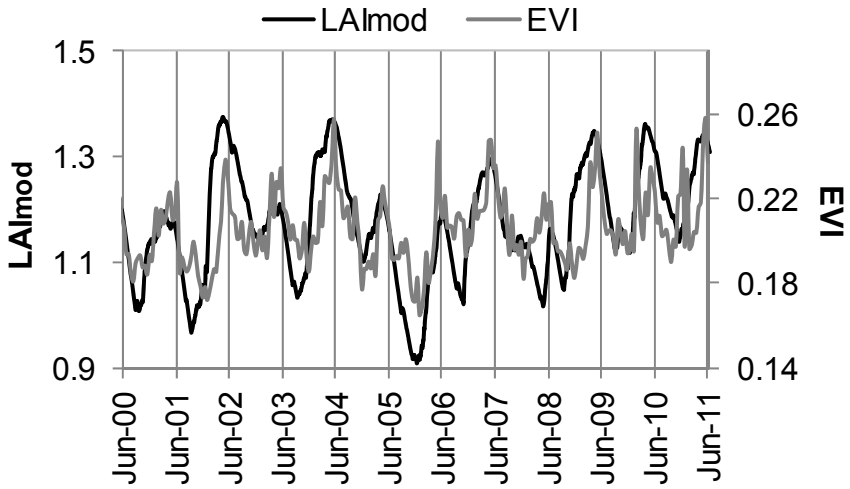

Figure 58: Evolution in time of LAI_{mod}, simulated by the WUE-model, and of EVI, extracted from satellite observations.

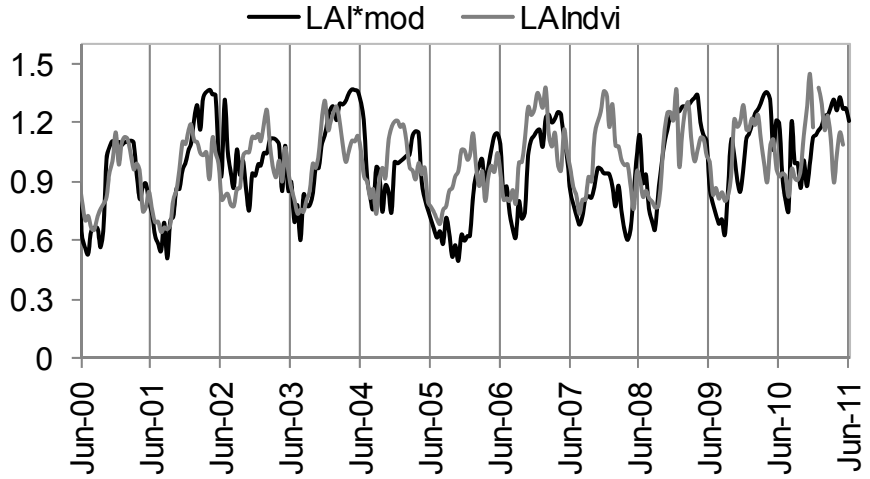

Figure 59: Evolution in time of LAI^*_{mod} (LAI_{mod} corrected by water stress), simulated by the WUE-model, and of LAI_{NDVI}, extracted from satellite observations.

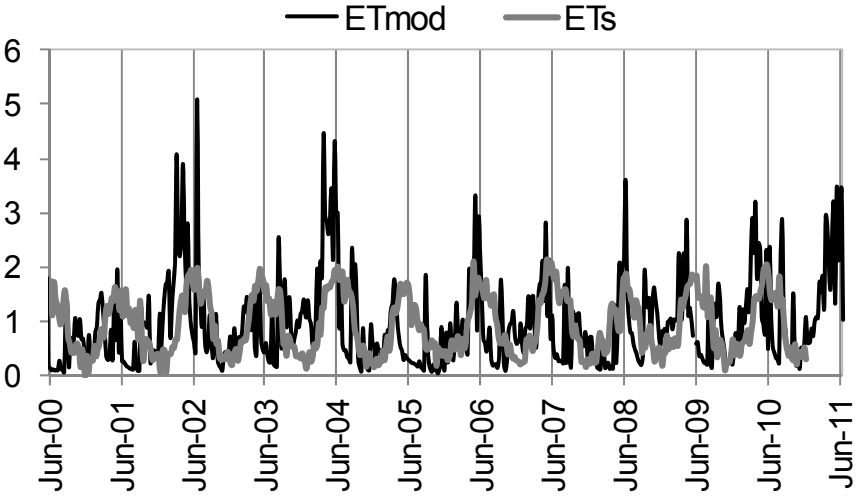

Figure 60: Evolution in time of ET_{mod} (mm/d), simulated by the WUE-model, and of ET_s (mm/d), provided by NASA.

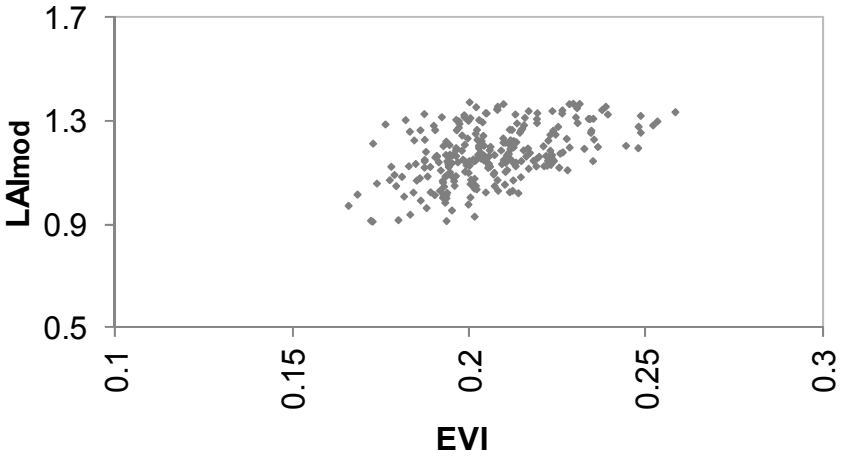

Figure 61: Scatter plot of LAI_{mod} vs. EVI. Results refer to WUE-model's simulations.

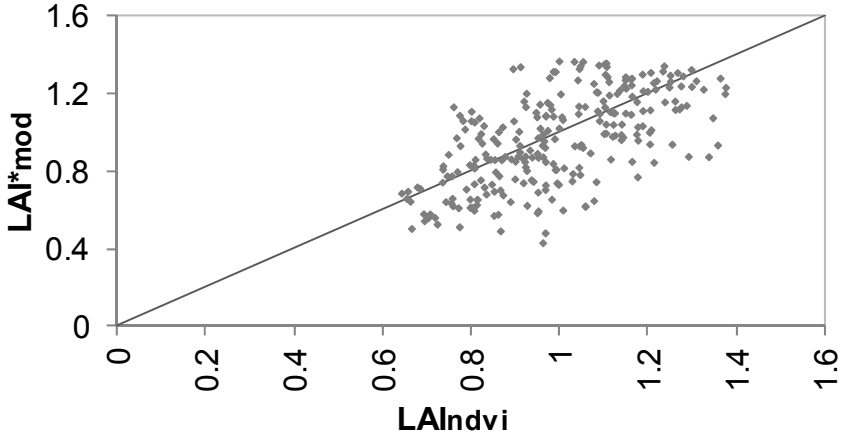

Figure 62: Scatter plot of LAI^*_{mod} vs. LAI_{NDVI}. Results refer to WUE-model's simulations.

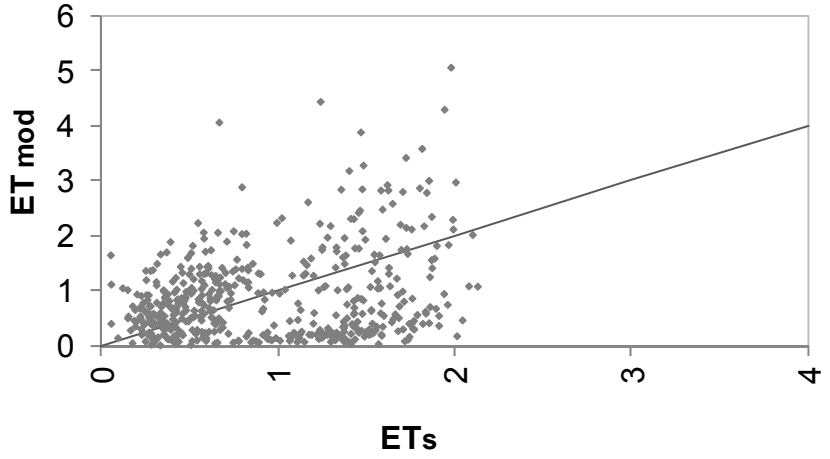

Figure 63: Scatter plot of ET_{mod} vs. ET_s. Results refer to WUE-model's simulations.

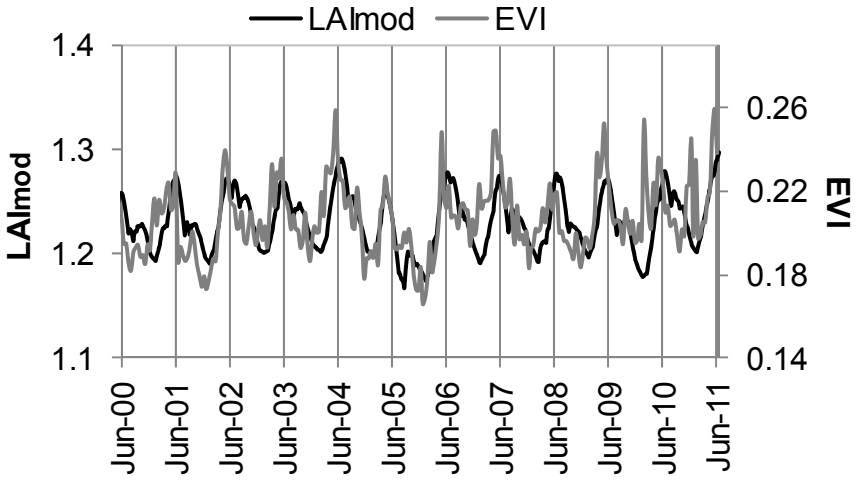

Figure 64: Evolution in time of LAI_{mod}, simulated by the LUE-model, and of EVI, extracted from satellite observations.

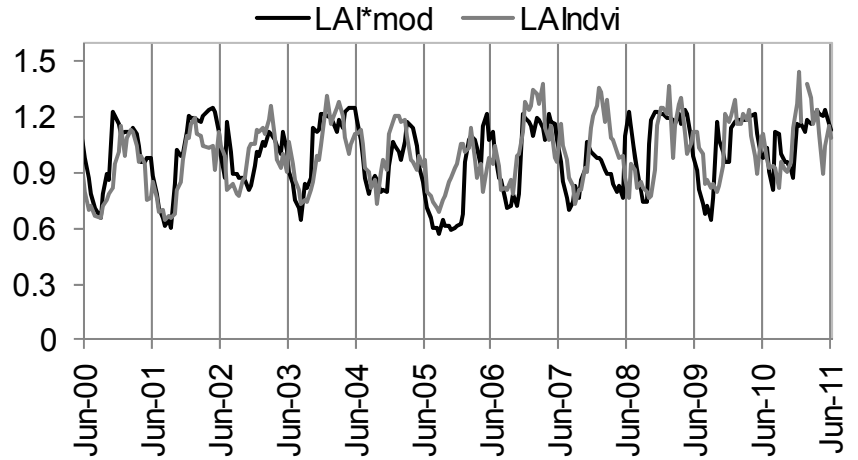

Figure 65: Evolution in time of LAI^*_{mod} (LAI_{mod} corrected by water stress), simulated by the LUE-model, and of LAI_{NDVI}, extracted from satellite observations.

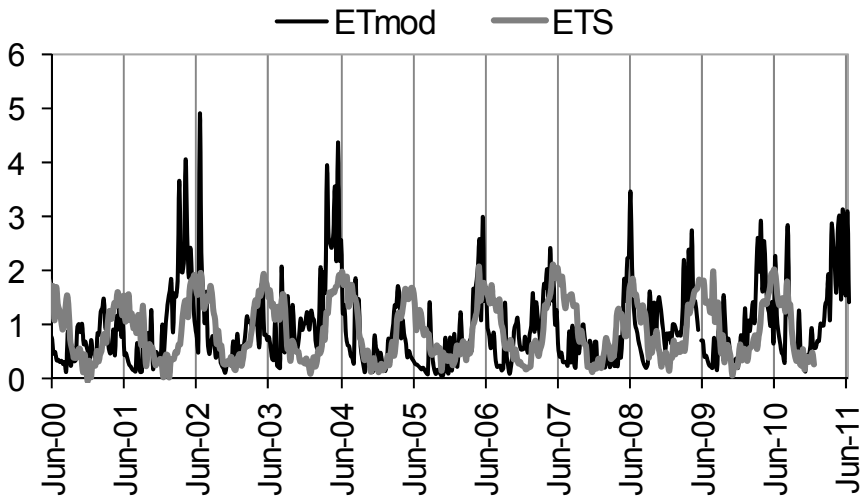

Figure 66: Evolution in time of ET_{mod} (mm/d), simulated by the LUE-model, and of ET_s (mm/d), provided by NASA.

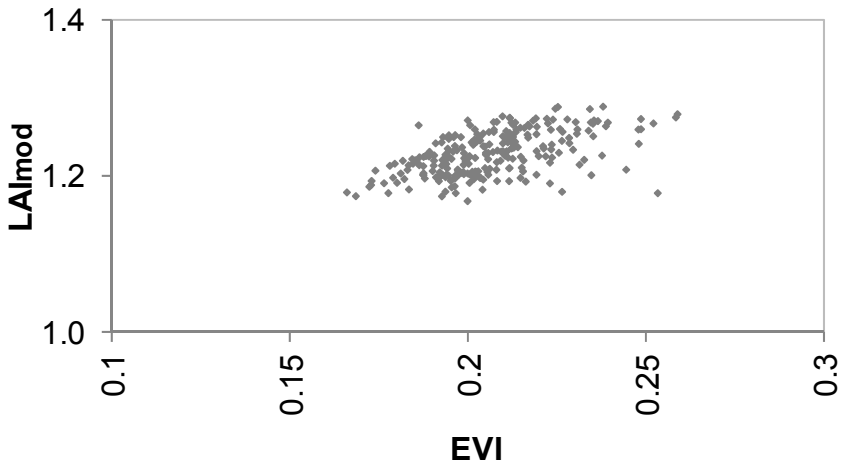

Figure 67: Scatter plot of LAI_{mod} vs. EVI. Results refer to LUE-model's simulations.

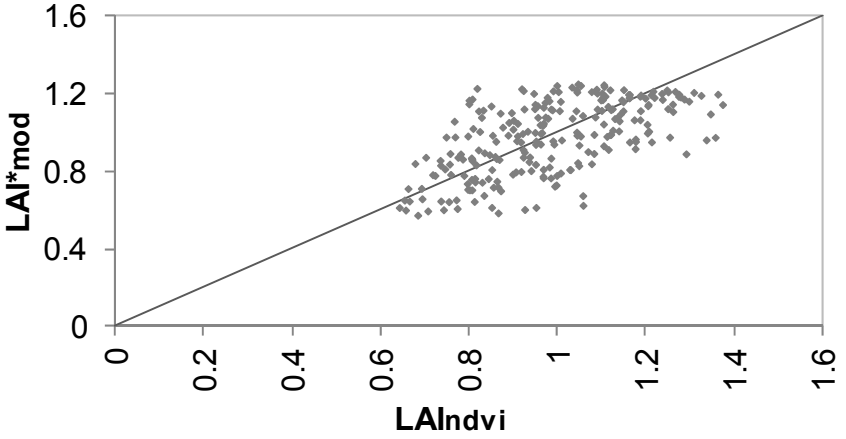

Figure 68: Scatter plot of LAI^*_{mod} vs. LAI_{NDVI}. Results refer to LUE-model's simulations.

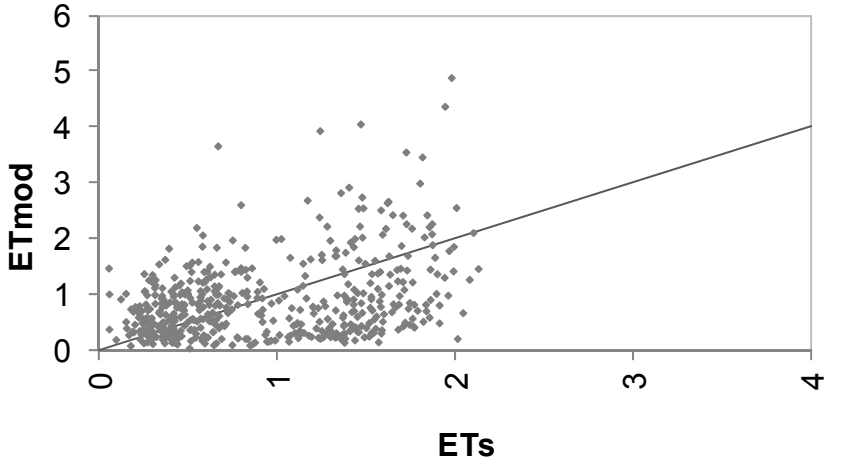

Figure 69: Scatter plot of ET_{mod} vs. ET_s. Results refer to LUE-model's simulations.

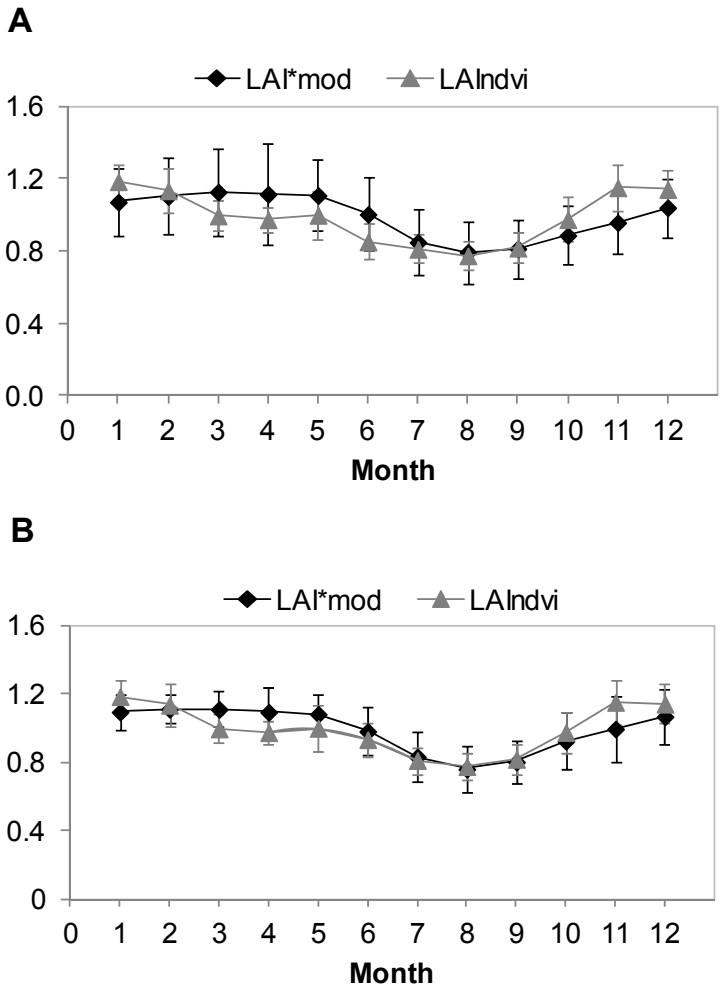

Figure 70: Satellite-derived LAI_{NDVI} and modelled LAI^*_{mod} averaged for each month of the year for 2000 to 2011, with bars indicating ±1 standard deviation, for the WUE-model (A) and for the LUE-model (B).

7.2.3 Discussion

The GSA and GLUE analysis provide the possibility of understanding the simulation capability of the models. In this case, they reveal quite a similar behaviour for the two models. A general good accordance of results with satellite data is found. Analyzing the two periods of poorest accordance between simulated LAI^*_{mod} of both

models and LAI_{NDVI}, i.e. autumn 2005 and autumn 2007 - spring 2008, it appears clear the link with the drought periods. As discussed in section 6.2, the low precipitation periods experimented by the study region are reflected in the satellite data, but the effect is not as marked as in the models simulations.

After the calibration, the models presented the same qualities and problems evidenced by the sensitivity analysis. As a whole, the LUE-model performed best, presenting the lowest RMSE and the best agreement with averaged LAI_{NDVI} at monthly timescale for amplitude and phase (Figure 70). Furthermore, the LUE-model has the capability to simulate vegetation dynamics in a wide range of environments, having the possibility to take into account different types of stress sources through a change in the formulation of ε (equation [19]), the LUE correction factor. Finally, it is a model that has been extensively used and therefore tested in literature. For these reasons, it is probably the best choice when looking for a parsimonious vegetation model to be coupled to a conceptual hydrological model.

8 Conclusions

Considering the important role of vegetation in the hydrological systems, appropriate vegetation modelling is crucial for ecological and hydrological applications. A well-performing model, which jointly simulates hydrological and vegetation processes, could become extremely useful to assess, among others, water resources, flood risk, vegetation cover and hill slope stability, particularly with a view to a possible future change in climatic conditions.

When initially approaching vegetation modelling, two basic issues had to be faced. The first question regarded how to choose the model and, particularly, which were the model characteristics to be sought, considering the research objectives. Secondly, having opted for satellite products as a means of comparison for models' results, and considering that vegetation indices supply indirect information, careful interpretation was needed to evaluate the implications of each remote-sensing product.

The following vegetation-related satellite products for a semi-arid region of Spain were analysed in order to assess their relation with vegetation state and development: NDVI, EVI, LAI and ET. The NDVI showed a strong dependence on soil moisture and leaf water content, explainable considering the impact of water-stress on chlorophyll content in Aleppo pine leaves and, possibly, a background soil colour change.

The EVI, on the other hand, proved to be well related to biomass dynamics and to leaf area index in particular. Both indices showed a regular seasonal pattern, even though prolonged periods of precipitation anomalies were reflected in the data as a departure from average trends of the indices themselves. In addition, the fact that these two indices were strongly influenced by different plant characteristics, which resulted not to be in phase in this particular environment, induced an apparent shift between the NDVI and the EVI time series. To be noted that a timing accordance between these indices is generally found in literature. The author is aware of only one literature example (Evrendilek & Gulbeyaz, 2008) of a similar behaviour in Mediterranean forest in Turkey. As for the LAI values provided by LP DAAC, they resulted to be too low with respect to field data and published ranges for the same species in similar climatic conditions. A possible explanation for this difference was found in the wrong land cover classification used by the algorithm that provides an estimation of this index, basing on satellite data. Lastly, the ET product appeared well correlated to reference evapotranspiration, surprisingly enough, considering the semiarid climate of the study area, which causes high water stress conditions during the periods of highest ET_o. In view of the fact that the MOD16A2 ET data are estimated employing land cover classification and LAI product, affected by error in this specific case, the reliability of the ET dataset itself was questioned. Consequently, it was considered opportune in this study to refer exclusively to EVI and NDVI as observational verification for subsequent modelling. Considering the characteristics of each index, as evidenced by the previous analysis, EVI was contrasted with modelled LAI_{mod}, while NDVI was related to water-stress affected LAI^*_{mod} values.

Three parsimonious vegetation models, namely the HORAS model, the WUE-model and the LUE-model, were then tested, in order to evaluate their capability to reproduce the information gathered from the satellite EVI and NDVI. The choice of the models was dictated by the quest for a simple conceptualization of the processes leading to vegetation growth, which could be suitably coupled with a hydrological model, and only requiring information commonly available in operational hydrological applications. The first model considered, HORAS, failed to

reproduce the annual vegetation cycle, probably due to a poor simulation of evaporation and transpiration processes. On the contrary, the latter two approaches, namely WUE-model and LUE-model, proved to be able to simulate reasonably well the vegetation dynamics and performed similarly, with the LUE-model achieving slightly better results, particularly during the periods of concurrent high available soil moisture and high ET_o. In these cases the WUE-model, linking growth to transpiration, overestimates vegetal biomass. This behaviour was confirmed through a General Likelihood Uncertainty Estimation (GLUE) applied in order to identify the bands of simulations generated by behavioural sets of parameters. Furthermore, considering that the WUE-model is specific for water limited environments only, while the LUE-model can be adapted to other types of ecosystems, the use of the latter is recommended when seeking a broadly applicable, simple vegetation model to be coupled with a conceptual hydrological model. Nonetheless, the WUE-model has proven to be a valid option when dealing with water-limited systems.

9 Future research lines

This thesis inevitably focused on a restricted range of topics, but there are several lines of research arising from this work that should be pursued in the near future.

Firstly, to better describe the spatial variations of vegetation within an hydrological catchment, considering changes of soil, plant species and weather conditions, the tested vegetation models should be implemented at a distributed level and coupled with a hydrological model.

As for remote-sensing data that may be helpful to assess hydrological-vegetation models performance, an interesting possibility is the soil moisture estimation. Two sensors are widely used in this sense: the Advanced Microwave Scanning Radiometer for Earth Observing System (AMSR-E) on-board NASA's Aqua satellite, and the Advanced SCATterometer (ASCAT) on-board the MetOp satellite. A good agreement of data derived from these sensors with in situ observed data has been reported in literature (Brocca *et al.*, 2011). Recently, another option has been made available by the ESA Soil Moistures and Ocean Salinity (SMOS) program, which as well provides surface soil moisture

maps. Data reflect moisture condition of just a few centimetre-deep soil layer and spatial resolution is approximately 40 km, making the data not directly available for basin-scale hydrological purposes. Nonetheless, well-performing models have been developed to estimate root-zone soil moisture from surface measurements (Manfreda *et al.*, 2012), and downscaling algorithms have been successfully applied to obtain 1 km resolution soil moisture maps (Piles *et al.*, 2011).

This research has focused on water as the only limiting factor affecting vegetation state and growth. However, semi-arid and arid ecosystems may be affected by other environmental stresses, particularly extreme temperatures (both high and low) and nutrient shortage, being the latter partially related to soil moisture itself. It may be necessary, in order to improve performance, to include the influence of these stress sources in the model conceptualization.

Finally, only forest ecosystems were considered. Yet, it is common for water-limited environments to exhibit herbaceous vegetation and open canopies. It should be therefore taken into consideration the potentiality for model improvement of an inclusion of conceptualized competition and succession processes.

10 Reference list

Abrol, I.P., Yadav, J.S.P. & Massoud, F.I. (1988) *Salt-affected soils and their management*, FAO.

AgSpecific (2012) How It Works. *http://www.agspecific.com/how-it-works/*.

Allen, R.G., Pereira, L.S., Raes, D., Smith, M. & others (1998) Crop evapotranspiration-Guidelines for computing crop water requirements-FAO Irrigation and drainage paper 56. *FAO, Rome*, **300**, 6541.

Allen, W.A., Gausman, H.W., Richardson, A.J. & Wiegand, C.L. (1970) Mean effective optical constants of thirteen kinds of plant leaves. *Applied Optics*, **9**, 2573–2577.

Allen, W.A. & Richardson, A.J. (1968) Interaction of light with a plant canopy. *Journal of the Optical Society of America*, **58**, 1023–1028.

American Society for Testing and Materials (2003) Reference Solar Spectral Irradiance.

Anselmi, S., Chiesi, M., Giannini, M., Manes, F. & Maselli, F. (2004) Estimation of Mediterranean forest transpiration and photosynthesis through the use of an ecosystem simulation model driven by remotely sensed data. *Global Ecology and Biogeography*, **13**, 371–380.

Arora, V. (2002) Modeling vegetation as a dynamic component in soilvegetation-atmosphere transfer schemes and hydrological models. *Reviews of Geophysics*, **40**, 1006.

Asner, G.P. (1998) Biophysical and biochemical sources of variability in canopy reflectance. *Remote Sensing of Environment*, **64**, 234–253.

Atwell, B., Kriedmann, P. & Turnbull eds., C. (2003) *Plants in action. Adaptation in nature, performance in cultivation.*, Macmillan Publishers Australia PTY LTD.

Awada, T., Radoglou, K., Fotelli, M.N. & Constantinidou, H.I.A. (2003) Ecophysiology of seedlings of three Mediterranean pine species in contrasting light regimes. *Tree Physiology*, **23**, 33–41.

Baquedano, F.J. & Castillo, F.J. (2006) Comparative ecophysiological effects of drought on seedlings of the Mediterranean water-saver Pinus halepensis and water-spenders Quercus coccifera and Quercus ilex. *Trees-Structure and Function*, **20**, 689–700.

Baret, F., Jacquemoud, S. & Hanocq, J.F. (1993) The soil line concept in remote sensing. *Remote Sensing Reviews*, **7**, 65–82.

Bates, L.M. & Hall, A.E. (1981) Stomatal closure with soil water depletion not associated with changes in bulk leaf water status. *Oecologia*, **50**, 62–65.

Bazzaz, F.A. (1979) The physiological ecology of plant succession. *Annual Review of Ecology and Systematics*, 351–371.

Beven, K. & Binley, A. (1992) The future of distributed models: model calibration and uncertainty prediction. *Hydrological Processes*, **6**, 279–298.

Borghetti, M., Cinnirella, S., Magnani, F. & Saracino, A. (1998) Impact of long-term drought on xylem embolism and growth in Pinus halepensis Mill. *Trees-Structure and Function*, **12**, 187–195.

Borowitzka, M.A. & Colmer, P.F. (1999) *Salt: an environmental stress. Plants in action. Adaptation in nature, performance in cultivation*, Macmillan Education Australia Pty Ltd, Melbourne, Australia.

Brocca, L., Hasenauer, S., Lacava, T., Melone, F., Moramarco, T., Wagner, W., Dorigo, W., Matgen, P., Martínez-Fernández, J., Llorens, P., Latron, J., Martin, C. & Bittelli, M. (2011) Soil moisture estimation through ASCAT and AMSR-E sensors: an intercomparison and validation study across Europe. *Remote Sensing of Environment*, **115**, 3390–3408.

Buermann, W., Wang, Y., Dong, J., Zhou, L., Zeng, X., Dickinson, R.E., Potter, C.S. & Myneni, R.B. (2002) Analysis of a multiyear global vegetation leaf area index data set. *Journal of Geophysical Research*, **107**, 4646.

Calatayud, V., Muñoz, C., Hernández, R., Sanz, M.J., Pérez Fortea, V., Soldevilla, C. & Sánchez, G. (2000) Seguimiento de daños en acículas de Pinus halepensis en localidades de Teruel y Castellón (España). *Ecología*, **14**, 129–140.

Carter, G.A. (1991) Primary and secondary effects of water content on the spectral reflectance of leaves. *American Journal of Botany*, **78**, 916–924.

Carter, G.A. (1993) Responses of leaf spectral reflectance to plant stress. *American Journal of Botany*, **80**, 239–243.

Cayrol, P., Chehbouni, A., Kergoat, L., Dedieu, G., Mordelet, P. & Nouvellon, Y. (2000) Grassland modeling and monitoring with SPOT-4 VEGETATION instrument during the 1997–1999 SALSA experiment. *Agricultural and Forest Meteorology*, **105**, 91–115.

Ceballos, Y. & Ruiz de la Torre, J. (1979) *Árboles y arbustos de la España peninsular*, ETSI Montes Publications, Madrid.

Ceccato, P., Flasse, S., Tarantola, S., Jacquemoud, S. & Grégoire, J.M. (2001) Detecting vegetation leaf water content using reflectance in the optical domain. *Remote Sensing of Environment*, **77**, 22–33.

Clapp, R.B. & Hornberger, G.M. (1978) Empirical equations for some soil hydraulic properties. *Water Resources Research*, **14**, 601–604.

Collins English Dictionary - Complete & Unabridged (2009) 10th Edition, HarperCollins Publishers.

Crockford, R.H. & Richardson, D.P. (1990) Partitioning of rainfall in a eucalypt forest and pine plantation in southeastern Australia: IV The relationship of interception and canopy storage capacity, the interception of these forests, and the effect on interception of thinning the pine plantation. *Hydrological Processes*, **4**, 169–188.

Curcio, J.A. & Petty, C.C. (1951) The near infrared absorption spectrum of liquid water. *Journal of the Optical Society of America*, **41**, 302–302.

Dawson, T.P., Curran, P.J. & Plummer, S.E. (1998) LIBERTY–modeling the effects of leaf biochemical concentration on reflectance spectra. *Remote Sensing of Environment*, **65**, 50–60.

Deering, D. (1978) Rangeland reflectance characteristics measured by aircraft and spacecraft sensors.

DEPI (2008) *Soil hydraulic parameters*. *Soil hydraulic properties*, Victoria, Australia.

Dingman, S.L. (2008) *Physical hydrology*, Prentice Hall Englewood Cliffs, NJ.

Dufour, A., Gadallah, F., Wagner, H.H., Guisan, A. & Buttler, A. (2006) Plant species richness and environmental heterogeneity in a mountain landscape: effects of variability and spatial configuration. *Ecography*, **29**, 573–584.

Eamus, D. (1999) *Soil-plant-atmosphere continuum*. *Plants in action. Adaptation in nature, performance in cultivation*, Melbourne, Australia.

Evans, J. (1999) *Leaf anatomy, light interception and gas exchange*. *Plants in action. Adaptation in nature, performance in cultivation*, Macmillan Education Australia Pty Ltd, Melbourne, Australia.

Evrendilek, F. & Gulbeyaz, O. (2008) Deriving vegetation dynamics of natural terrestrial ecosystems from MODIS NDVI/EVI data over Turkey. *Sensors*, **8**, 5270–5302.

Eykhoff, P. (1974) *System Identification-Parameter and State Estimation*, Wiley, New York.

Farjon, A. (2005) *Pines. Drawings and Descriptions of the genus Pinus*, Brill, Leiden.

Fourty, T. & Baret, F. (1997) Vegetation water and dry matter contents estimated from top-of-the-atmosphere reflectance data: a simulation study. *Remote Sensing of Environment*, **61**, 34–45.

Francés, F., Velez, J.I. & Vélez, J.J. (2007) Split-parameter structure for the automatic calibration of distributed hydrological models. *Journal of Hydrology*, **332**, 226–240.

Gamon, J.A., Field, C.B., Goulden, M.L., Griffin, K.L., Hartley, A.E., Joel, G., Peñuelas, J. & Valentini, R. (1995) Relationships between NDVI, canopy structure, and photosynthesis in three Californian vegetation types. *Ecological Applications*, **5**, 28–41.

Gao, X., Huete, A.R., Ni, W. & Miura, T. (2000) Optical–biophysical relationships of vegetation spectra without background contamination. *Remote Sensing of Environment*, **74**, 609–620.

García-Plé, C., Vanrell, P. & Morey, M. (1995) Litter fall and decomposition in a Pinus halepensis forest on Mallorca. *Journal of Vegetation Science*, **6**, 17–22.

Gavilan, P., Lorite, I.J., Tornero, S. & Berengena, J. (2006) Regional calibration of Hargreaves equation for estimating reference ET in a semiarid environment. *Agricultural water management*, **81**, 257–281.

Gigante, V., Iacobellis, V., Manfreda, S., Milella, P. & Portoghese, I. (2009) Influences of Leaf Area Index estimations on water balance modeling in a Mediterranean semi-arid basin. *Natural Hazards and Earth System Sciences*, **9**, 979–991.

Gill, A.M. & Allan, G. (2009) Large fires, fire effects and the fire-regime concept. *International Journal of Wildland Fire*, **17**, 688–695.

Gitelson, A.A., Viña, A., Arkebauer, T.J., Rundquist, D.C., Keydan, G. & Leavitt, B. (2003) Remote estimation of leaf area index and green leaf biomass in maize canopies. *Geophysical Research Letters*, **30**, 1248.

Glenn-Lewin, D.C. & Van der Maarel, E. (1992) *Patterns and processes of vegetation dynamics*. *Plant succession: theory and prediction* Population and community biology., Chapman and Hall, London.

Gobron, N. (2008) *Leaf area index (LAI)*. *Terrestrial essential climate variable for climate change assessment, mitigation and adaptation*, FAO.

Gollan, T., Passioura, J.B. & Rana Munns (1986) Soil water status affects the stomata conductance of fully turgid wheat and sunflower leaves. *Australian Journal of Plant Physiology*, **13**, 459–464.

Gough, C.M., Flower, C.E., Vogel, C.S., Dragoni, D. & Curtis, P.S. (2009) Whole-ecosystem labile carbon production in a north temperate deciduous forest. *Agricultural and Forest Meteorology*, **149**, 1531–1540.

Green, C.F., Hebblethwaite, P.D. & Ison, D.A. (1985) A quantitative analysis of varietal and moisture status effects on the growth of Vicia faba in relation to radiation absorption. *Annals of Applied Biology*, **106**, 143–155.

Lo Gullo, M.A. & Salleo, S. (1988) Different strategies of drought resistance in three Mediterranean sclerophyllous trees growing in the same environmental conditions. *New Phytologist*, **108**, 267–276.

Hargreaves, G.H. & Samani, Z.A. (1985) Reference crop evapotranspiration from temperature. *Applied Engineering in Agriculture*, **1**, 96–99.

Helsel, D.R., Mueller, D.K. & Slack, J.R. (2006) Computer program for the Kendall family of trend tests: US Geological Survey Scientific Investigations Report 2005–5275, 4 p.

Hensley, D. & Deputy, J. (1999) Using tensiometers for measuring soil water and scheduling irrigation. *Landscape*, **50**, 10.

De las Heras, J., Moya, D., López-Serrano, F.R. & Rubio, E. (2013) Carbon sequestration of naturally regenerated Aleppo pine stands in response to early thinning. *New Forests*, **44**, 457–470.

Hirsch, R.M. & Slack, J.R. (1984) A nonparametric trend test for seasonal data with serial dependence. *Water Resources Research*, **20**, 727–732.

Hirsch, R.M., Slack, J.R. & Smith, R.A. (1982) Techniques of trend analysis for monthly water quality data. *Water Resources Research*, **18**, 107–121.

Hoch, G., Richter, A. & Körner, C. (2003) Non-structural carbon compounds in temperate forest trees. *Plant, Cell & Environment*, **26**, 1067–1081.

Hornberger, G.M. & Spear, R.C. (1980) Eutrophication in Peel Inlet—I. The problem-defining behavior and a mathematical model for the phosphorus scenario. *Water Research*, **14**, 29–42.

Huete, A.R. (1988) A soil-adjusted vegetation index (SAVI). *Remote Sensing of Environment*, **25**, 295–309.

Huete, A.R., Didan, K., Miura, T., Rodriguez, E.P., Gao, X. & Ferreira, L.G. (2002) Overview of the radiometric and biophysical performance of the MODIS vegetation indices. *Remote Sensing of Environment*, **83**, 195–213.

Huete, A.R. & Jackson, R.D. (1988) Soil and atmosphere influences on the spectra of partial canopies. *Remote Sensing of Environment*, **25**, 89–105.

Huete, A.R., Jackson, R.D. & Post, D.F. (1985) Spectral response of a plant canopy with different soil backgrounds. *Remote Sensing of Environment*, **17**, 37–53.

Huete, A.R., Post, D.F. & Jackson, R.D. (1984) Soil spectral effects on 4-space vegetation discrimination. *Remote Sensing of Environment*, **15**, 155–165.

Hunt, E.R. & Rock, B.N. (1989) Detection of changes in leaf water content using near- and middle-infrared reflectances. *Remote Sensing of Environment*, **30**, 43–54.

IPCC (2007) *Climate Change 2007: Synthesis Report. Contribution of Working Groups I, II and III to the Fourth Assessment Report of the Intergovernmental Panel on Climate Change*, Core Writing Team, Pachauri, R.K and Reisinger, A. (eds.), Geneva, Switzerland.

Istanbulluoglu, E., Wang, T. & Wedin, D.A. (2012) Evaluation of ecohydrologic model parsimony at local and regional scales in a semiarid grassland ecosystem. *Ecohydrology*, **5**, 121–142.

Jackson, R.D. & Huete, A.R. (1991) Interpreting vegetation indices. *Preventive Veterinary Medicine*, **11**, 185–200.

Jajarmizadeh, M., Harun, S. & Salarpour, M. (2012) A review on theoretical consideration and types of models in hydrology. *Journal of Environmental Science and Technology*, **5**, 249–261.

Jarvis, P.G., Leverenz, J.W. & others (1983) Productivity of temperate, deciduous and evergreen forests. *Encyclopedia of Plant Physiology*, **12**, 234–280.

Jiménez-Muñoz, J.C., Sobrino, J.A., Mattar, C. & Franch, B. (2010) Atmospheric correction of optical imagery from MODIS and Reanalysis atmospheric products. *Remote Sensing of Environment*, **114**, 2195–2210.

Jordan, C.F. (1969) Derivation of leaf-area index from quality of light on the forest floor. *Ecology*, **50**, 663–666.

Kaufman, Y.J. & Tanre, D. (1992) Atmospherically resistant vegetation index (ARVI) for EOS-MODIS. *Geoscience and Remote Sensing, IEEE Transactions on*, **30**, 261–270.

Knorr, W. & Heimann, M. (1995) Impact of drought stress and other factors on seasonal land biosphere CO2 exchange studied through an atmospheric tracer transport model. *Tellus B*, **47**, 471–489.

Köppen, W. (1936) *Das geographisca system der climate*. *Handbuch der klimatologie, edited by: Koppen W, Geiger GC Gebr, Borntraeger*, pp. 1–44.

Körner, C. (2003) Carbon limitation in trees. *Journal of Ecology*, **91**, 4–17.

Kyparissis, A., Petropoulou, Y. & Manetas, Y. (1995) Summer survival of leaves in a soft-leaved shrub (Phlomis fruticosa L., Labiatae) under Mediterranean field

conditions: avoidance of photoinhibitory damage through decreased chlorophyll contents. *Journal of Experimental Botany*, **46**, 1825–1831.

Lacaze, B., Caselles, V., Coll, C., Hill, J., Hoff, C., De Jong, S. & Mehl, W. (1996) *DeMon: Integrated approaches to desertification mapping and monitoring in the mediterranean basin*, Space Applications Inst., Environmental Mapping and Modelling Unit, Italy.

Laio, F., Porporato, A., Ridolfi, L. & Rodriguez-Iturbe, I. (2001) Plants in water-controlled ecosystems: active role in hydrologic processes and response to water stress. II. Probabilistic soil moisture dynamics. *Advances in Water Resources*, **24**, 707–723.

Latron, J. (2003) Estudio del funcionamento hidrológico de una cuenca mediterránea de montaña. PhD thesis.

Lee, Y.J., Yang, C.M., Chang, K.W. & Shen, Y. (2011) Effect of nitrogen status on leaf anatomy, chlorophyll content and canopy reflectance of paddy rice. *Botanical Studies*, **52**, 295–303.

Leuzinger, S. & Hättenschwiler, S. (2013) Beyond global change: lessons from 25 years of CO2 research. *Oecologia*, 1–13.

Levitt, J. (1980) *Responses of plants to environmental stresses. Volume II. Water, radiation, salt, and other stresses.*, Academic Press.

Li, S.G., Eugster, W., Asanuma, J., Kotani, A., Davaa, G., Oyunbaatar, D. & Sugita, M. (2008) Response of gross ecosystem productivity, light use efficiency, and water use efficiency of Mongolian steppe to seasonal variations in soil moisture. *Journal of Geophysical Research*, **113**, G01019.

Lobell, D.B. & Asner, G.P. (2002) Moisture effects on soil reflectance. *Soil Science Society of America Journal*, **66**, 722–727.

López-Serrano, F.R., Landete-Castillejos, T., Martínez-Millán, J. & Cerro-Barja, A. (2000) LAI estimation of natural pine forest using a non-standard sampling technique. *Agricultural and Forest Meteorology*, **101**, 95–111.

Llorens, P., Latron, J., Álvarez-Cobelas, M., Martínez-Vilalta, J. & Moreno, G. (2011) *Hydrology and biogeochemistry of mediterranean forests*. *Forest Hydrology and Biogeochemistry* Ecological Studies., pp. 301–319. Springer.

Maherali, H., Pockman, W.T. & Jackson, R.B. (2004) Adaptive variation in the vulnerability of woody plants to xylem cavitation. *Ecology*, **85**, 2184–2199.

Le Maitre, D.C., Scott, D.F. & Colvin, C. (1999) Review of information on interactions between vegetation and groundwater. *Water SA*, **25**, 137–152.

Manfreda, S., Brocca, L., Moramarco, T., Melone, F. & Sheffield, J. (2012) A physically based approach for the estimation of root-zone soil moisture from surface measurements. *Hydrology and Earth System Science Discusssions*, **9**, 14129–14162.

Marshner, P. (2012) *Mineral nutrition of higher plants*, Third edition. Elsevier.

Martin, M.E. & Aber, J.D. (1997) High spectral resolution remote sensing of forest canopy lignin, nitrogen, and ecosystem processes. *Ecological Applications*, **7**, 431–443.

McCree, K.J. (1972) The action spectrum, absorptance and quantum yield of photosynthesis in crop plants. *Agricultural Meteorology*, **9**, 191–216.

McDowell, N., Pockman, W.T., Allen, C.D., Breshears, D.D., Cobb, N., Kolb, T., Plaut, J., Sperry, J., West, A. & Williams, D.G. (2008) Mechanisms of plant survival and mortality during drought: why do some plants survive while others succumb to drought? *New Phytologist*, **178**, 719–739.

McIntyre, S., Lavorel, S. & Tremont, R.M. (1995) Plant life-history attributes: their relationship to disturbance response in herbaceous vegetation. *Journal of Ecology*, **83**, 31–44.

Medici, C., Wade, A.J. & Francés, F. (2012) Does increased hydrochemical model complexity decrease robustness? *Journal of Hydrology*, **440-441**, 1–13.

Medlyn, B.E. (1998) Physiological basis of the light use efficiency model. *Tree Physiology*, **18**, 167–176.

Molina, A.J. & del Campo, A.D. (2012) The effects of experimental thinning on throughfall and stemflow: A contribution towards hydrology-oriented silviculture in Aleppo pine plantations. *Forest Ecology and Management*, **269**, 206–213.

Montaldo, N., Rondena, R., Albertson, J.D. & Mancini, M. (2005) Parsimonious modeling of vegetation dynamics for ecohydrologic studies of water-limited ecosystems. *Water Resources Research*, **41**, W10416.

Montaldo, N., Toninelli, V., Albertson, J.D., Mancini, M. & Troch, P.A. (2003) The effect of background hydrometeorological conditions on the sensitivity of evapotranspiration to model parameters: analysis with measurements from an Italian alpine catchment. *Hydrology and Earth System Sciences*, **7**, 848–861.

Monteith, J.L. (1965) Evaporation and environment. *Symposia of the Society for Experimental Biology*, **19**, 205–234.

Monteith, J.L. (1972) Solar radiation and productivity in tropical ecosystems. *Journal of Applied Ecology*, **9**, 747–766.

Monteith, J.L. & Moss, C.J. (1977) Climate and the efficiency of crop production in Britain [and discussion]. *Philosophical Transactions of the Royal Society B, Biological Sciences*, **281**, 277–294.

Mu, Q., Zhao, M. & Running, S.W. (2011) Improvements to a MODIS global terrestrial evapotranspiration algorithm. *Remote Sensing of Environment*, **115**, 1781–1800.

Muñoz, C., Pérez, V., Cobos, P., Hernández, R. & Sánchez, G. (2003) Sanidad forestal. Guía en Imágenes de Plagas, Enfermedades y Otros Agentes Presentes en los Bosques. *Mundi Prensa. Madrid*.

Myneni, R., Knyazikhin, Y., Glassy, J., Votava, P. & Shabanov, N. (2003) *User's Guide: FPAR, LAI (ESDT: MOD15A2) 8-Day Composite NASA MODIS Land Algorithm*, Boston University, Boston, MA.

Myneni, R.B., Ramakrishna, R., Nemani, R. & Running, S.W. (1997) Estimation of global leaf area index and absorbed PAR using radiative transfer models. *Geoscience and Remote Sensing, IEEE Transactions on*, **35**, 1380–1393.

NASA (2012a) *MOD13Q1 version-5*, LP DAAC, Sioux Falls, SD.

NASA (2012b) *MOD15A2 version-5*, LP DAAC, Sioux Falls, SD.

NASA (2012c) *MYD13Q1 version-5*, LP DAAC, Sioux Falls, SD.

NASA (2012d) *MYD15A2 version-5*, LP DAAC, Sioux Falls, SD.

Numerical Terradynamic Simulation Group (2012) *MOD16A2*, University of Montana, Missoula, MT.

Pardos, M., Climent, J., Gil, L. & Pardos, J.A. (2003) Shoot growth components and flowering phenology in grafted Pinus halepensis Mill. *Trees-Structure and Function*, **17**, 442–450.

Pasquato, M. (2011) Modelación dinámica y distribuida de la vegetación en climas semiáridos. Master Thesis.

Pate, M.A. (1999) *Strategies for surviving in fire-prone environments: seeders and resprouters*. *Plants in action. Adaptation in nature, performance in cultivation*, Macmillan Education Australia Pty Ltd, Melbourne, Australia.

Philip, J.R. (1966) Plant water relations: some physical aspects. *Annual Review of Plant Physiology*, **17**, 245–268.

Piles, M., Camps, A., Vall-Llossera, M., Corbella, I., Panciera, R., Rudiger, C., Kerr, Y.H. & Walker, J. (2011) Downscaling SMOS-derived soil moisture using MODIS visible/infrared data. *Geoscience and Remote Sensing, IEEE Transactions on*, **49**, 3156–3166.

Polley, H.W., Phillips, R.L., Frank, A.B., Bradford, J.A., Sims, P.L., Morgan, J.A. & Kiniry, J.R. (2011) Variability in light-use efficiency for gross primary productivity on Great Plains grasslands. *Ecosystems*, **14**, 15–27.

Porporato, A., Laio, F., Ridolfi, L. & Rodriguez-Iturbe, I. (2001) Plants in water-controlled ecosystems: active role in hydrologic processes and response to water stress. III. Vegetation water stress. *Advances in Water Resources*, **24**, 725–744.

Post, E. & Stenseth, N.C. (1999) Climatic variability, plant phenology, and northern ungulates. *Ecology*, **80**, 1322–1339.

Purevdorj, T.S., Tateishi, R., Ishiyama, T. & Honda, Y. (1998) Relationships between percent vegetation cover and vegetation indices. *International Journal of Remote Sensing*, **19**, 3519–3535.

Quevedo, D.I. (2010) Desarrollo de un modelo conceptual dinámico suelo-vegetación para zonas áridas y semiáridas. PhD thesis.

Quevedo, D.I. & Francés, F. (2008) A conceptual dynamic vegetation-soil model for arid and semiarid zones. *Hydrology and Earth System Science*, **12**, 1175–1187.

Raymond, C.A. & Schimleck, L.R. (2002) Development of near infrared reflectance analysis calibrations for estimating genetic parameters for cellulose content in Eucalyptus globulus. *Canadian Journal of Forest Research*, **32**, 170–176.

Renard, K.G., Lane, L.J., Simanton, J.R., Emmerich, W.E., Stone, J.J., Weltz, M.A., Goodrich, D.C. & Yakowitz, D.S. (1993) Agricultural impacts in an arid environment: Walnut Gulch studies. *Hydrological Science and Technology*, **9**, 145–190.

Renbuss, M.A., Chilvers, G.A. & Pryor, L.D. (1973) Microbiology of an ashbed. *Proceedings of the Linnean Society*, **97**, 302–310.

Robertson, G.P., Hutson, M.A., Evans, F.C. & Tiedje, J.M. (1988) Spatial variability in a successional plant community: patterns of nitrogen availability. *Ecology*, **69**, 1517–1524.

Robinson, S.A. (1999) *Photosynthesis in sun and shade. Plants in action. Adaptation in nature, performance in cultivation*, Macmillan Education Australia Pty Ltd, Melbourne, Australia.

Rock, B.N., Hoshizaki, T. & Miller, J.R. (1988) Comparison of in situ and airborne spectral measurements of the blue shift associated with forest decline. *Remote Sensing of Environment*, **24**, 109–127.

Rodriguez-Iturbe, I., D'odorico, P., Porporato, A. & Ridolfi, L. (1999) On the spatial and temporal links between vegetation, climate, and soil moisture. *Water Resources Research*, **35**, 3709–3722.

Rodriguez-Iturbe, I., Porporato, A., Laio, F. & Ridolfi, L. (2001) Plants in water-controlled ecosystems: active role in hydrologic processes and response to water stress. I. Scope and general outline. *Advances in Water Resources*, **24**, 695–705.

Rohde, A. (2007) Radiation transmitted by the atmosphere. *Global warming art project*.

Ruimy, A., Kergoat, L., Bondeau, A. & others (1999) Comparing global models of terrestrial net primary productivity (NPP): analysis of differences in light absorption and light-use efficiency. *Global Change Biology*, **5**, 56–64.

Sabaté, S., Gracia, C.A. & Sánchez, A. (2002) Likely effects of climate change on growth of Quercus ilex, Pinus halepensis, Pinus pinaster, Pinus sylvestris and Fagus sylvatica forests in the Mediterranean region. *Forest Ecology and Management*, **162**, 23–37.

Scanlon, B.R., Keese, K.E., Flint, A.L., Flint, L.E., Gaye, C.B., Edmunds, W.M. & Simmers, I. (2006) Global synthesis of groundwater recharge in semiarid and arid regions. *Hydrological Processes*, **20**, 3335–3370.

Scanlon, B.R., Levitt, D.G., Reedy, R.C., Keese, K.E. & Sully, M.J. (2005) Ecological controls on water-cycle response to climate variability in deserts. *Proceedings of the National Academy of Sciences*, **102**, 6033–6038.

Scanlon, T.M. & Albertson, J.D. (2003) Inferred controls on tree/grass composition in a savanna ecosystem: Combining 16-year normalized difference vegetation index data with a dynamic soil moisture model. *Water Resources Research*, **39**, 1224.

Scoffoni, C., McKown, A.D., Rawls, M. & Sack, L. (2011) Dynamics of leaf hydraulic conductance with water status: quantification and analysis of species differences under steady state. *Journal of Experimental Botany*, **63**, 643–658.

Sellers, P.J., Tucker, C.J., Collatz, G.J., Los, S.O., Justice, C.O., Dazlich, D.A. & Randall, D.A. (1996) A revised land surface parameterization (SiB2) for atmospheric GCMs. Part II: The generation of global fields of terrestrial biophysical parameters from satellite data. *Journal of Climate*, **9**, 706–737.

Sinclair, T.R., Schreiber, M.M. & Hoffer, R.M. (1973) Diffuse reflectance hypothesis for the pathway of solar radiation through leaves. *Agronomy Journal*, **65**, 276–283.

Sitch, S., Smith, B., Prentice, I.C., Arneth, A., Bondeau, A., Cramer, W., Kaplan, J.O., Levis, S., Lucht, W., Sykes, M.T. & others (2003) Evaluation of ecosystem dynamics, plant geography and terrestrial carbon cycling in the LPJ dynamic global vegetation model. *Global Change Biology*, **9**, 161–185.

Smith, E.L. (1936) Photosynthesis in relation to light and carbon dioxide. *Proceedings of the National Academy of Sciences of the United States of America*, **22**, 504.

Solovchenko, A. (2010) *Optical Screening as a Photoprotective Mechanism*. *Photoprotection in Plants* Springer Series in Biophysics., pp. 1–7. Springer Berlin Heidelberg.

Spiggest (2010) Rendered spectrum. *http://en.wikipedia.org/wiki/Color*.

Sprintsin, M., Karnieli, A., Berliner, P., Rotenberg, E., Yakir, D. & Cohen, S. (2009) Evaluating the performance of the MODIS Leaf Area Index (LAI) product over a Mediterranean dryland planted forest. *International Journal of Remote Sensing*, **30**, 5061–5069.

Sprintsin, M., Karnieli, A., Berliner, P., Rotenberg, E., Yakir, D. & Cohen, S. (2007) The effect of spatial resolution on the accuracy of leaf area index estimation for a forest planted in the desert transition zone. *Remote Sensing of Environment*, **109**, 416–428.

Teuling, A.J. & Troch, P.A. (2005) Improved understanding of soil moisture variability dynamics. *Geophysical Research Letters*, **32**, L05404.

Tucker, C.J. (1979) Red and photographic infrared linear combinations for monitoring vegetation. *Remote Sensing of Environment*, **8**, 127–150.

Tucker, C.J. (1980) Remote sensing of leaf water content in the near infrared. *Remote Sensing of Environment*, **10**, 23–32.

Tucker, C.J. & Sellers, P.J. (1986) Satellite remote sensing of primary production. *International Journal of Remote Sensing*, **7**, 1395–1416.

Turner, D.P., Urbanski, S., Bremer, D., Wofsy, S.C., Meyers, T., Gower, S.T. & Gregory, M. (2003) A cross-biome comparison of daily light use efficiency for gross primary production. *Global Change Biology*, **9**, 383–395.

Twomey, S.A., Bohren, C.F. & Mergenthaler, J.L. (1986) Reflectance and albedo differences between wet and dry surfaces. *Applied Optics*, **25**, 431–437.

Vicente-Serrano, S.M., Lasanta, T. & Gracia, C. (2010) Aridification determines changes in forest growth in Pinus halepensis forests under semiarid Mediterranean climate conditions. *Agricultural and Forest Meteorology*, **150**, 614–628.

Wardlaw, I.F. (1999) *Temperature: a driving variable for plant growth and development*. *Plants in action. Adaptation in nature, performance in cultivation*, Macmillan Education Australia Pty Ltd, Melbourne, Australia.

Weinstein, A. (1989) Geographic variation and phenology of Pinus halepensis, P. brutia and P. eldarica in Israel. *Forest Ecology and Management*, **27**, 99–108.

Whifield, D. (1999) *Water use efficiency of crops*. *Plants in action. Adaptation in nature, performance in cultivation*, Macmillan Education Australia Pty Ltd, Melbourne, Australia.

Whitmarsh, J. & Govindjee (1999) *The photosynthetic process. Concepts in Photobiology: Photosynthesis and Photomorphogenesis*, pp. 11–51. Kluwer Academic Publishers.

Williams, C.A. & Albertson, J.D. (2005) Contrasting short-and long-timescale effects of vegetation dynamics on water and carbon fluxes in water-limited ecosystems. *Water Resources Research*, **41**, W06005.

Woodward, F.I. & Williams, B.G. (1987) Climate and plant distribution at global and local scales. *Plant Ecology*, **69**, 189–197.

Woolley, J.T. (1971) Reflectance and transmittance of light by leaves. *Plant Physiology*, **47**, 656–662.

Wythers, K.R., Lauenroth, W.K. & Paruelo, J.M. (1999) Bare-soil evaporation under semiarid field conditions. *Soil Science Society of America Journal*, **63**, 1341–1349.

Yuan, W., Liu, S., Zhou, G., Zhou, G., Tieszen, L.L., Baldocchi, D., Bernhofer, C., Gholz, H., Goldstein, A.H., Goulden, M.L. & others (2007) Deriving a light use efficiency model from eddy covariance flux data for predicting daily gross primary production across biomes. *Agricultural and Forest Meteorology*, **143**, 189–207.

Zhao, D., Reddy, K.R., Kakani, V.G. & Reddy, V.R. (2005) Nitrogen deficiency effects on plant growth, leaf photosynthesis, and hyperspectral reflectance properties of sorghum. *European Journal of Agronomy*, **22**, 391–403.

Zwiggelaar, R. (1998) A review of spectral properties of plants and their potential use for crop/weed discrimination in row-crops. *Crop Protection*, **17**, 189–206.